The Provenance of, and Relationship Between, Methane and Halogens in Groundwater in Eastern Ontario

ALEXANDER LEMIEUX

Thesis submitted to the University of Ottawa in partial fulfillment
of the requirements for the degree of Master of Science

Department of Earth and Environmental Sciences
Faculty of Science
University of Ottawa

Abstract

The geology, hydrogeology, and groundwater geochemistry are described for an interface aquifer in Eastern Ontario exhibiting anomalously high proportions of iodine (I) as iodide (I^-) and dissolved methane (CH_4). The studied area is unique in that it shows a significant marine influence, attributed to the most recent Champlain Sea incursion 10 – 12 ka BP, which has implications for I and CH_4 enrichment. I and CH_4 in groundwater are found in high proportions in reducing fossil seawaters, which are typically observed in depressions in the bedrock surface that are overlain by thick layers of glaciomarine muds. I is released via microbial decomposition of marine phytoplankton into mud porewaters, where it is then leached to underlying groundwaters. ^{129}I and ^{14}C isotopic signatures of I and C compounds highlight the importance of allochthonous I and C sources in the Champlain Sea basin derived from glacial abrasion of the surrounding terrain and imported via glacial meltwater. CH_4 is microbial in origin, with marine phytoplankton from the Champlain Sea incursion and ancient terrestrial organic matter from an Early Wisconsinian interstadial period (60 – 75 ka BP) as the dominant substrates. A thermogenic CH_4 component was observed for areas underlain by the Billings shale unit. Both I and CH_4 originate at least partially from the same marine phytoplankton source within the muds, demonstrate similar controls on enrichment, and have a Spearman's rank coefficient of 0.62, indicating that the correlation between I and CH_4 in groundwater in the studied area is significant.

Résumé

La géologie, hydrogéologie et géochimie des eaux souterraines sont décrites pour un aquifère d'interface enrichi en méthane (CH_4) et en iode (I) sous forme d'iodure (I^-) dans l'est Ontarien. La région étudiée est unique, puisqu'elle démontre une influence marine attribué à l'invasion de la mer de Champlain il y a 10 – 12 ka BP, ce qui a des connotations importantes quant à l'enrichissement des eaux souterraines en CH_4 et en I. Des concentrations élevées de CH_4 et I sont observées dans les eaux marines fossiles réductrices dont la majorité se retrouvent dans les dépressions dans la surface du socle rocheux qui sont enfouies par d'épaisses couches de boues glaciomarines. I est enrichi dans les eaux de pore des boues par la décomposition microbienne de matière organique et ensuite lessivé dans l'aquifère sous-jacente. Les signatures isotopiques du ^{129}I et du ^{14}C soulignent l'importance des sources allochtones de I et de matière organique dans le bassin de la mer de Champlain provenant de l'érosion mécanique du terrain entourant et importées par le ruissellement glaciaire. Le CH_4 est d'origine microbienne, ayant comme substrat le phytoplancton marin datant de l'invasion mer de Champlain, ainsi que des sources de C terrestres provenant d'un interstade au Wisconsinien précoce, il y a 60 – 75 ka BP. La présence de CH_4 thermogénique est observée dans les endroits sous-tendus par l'unité Billings. Les composants proviennent (au moins en partie) de la même source de matière organique (phytoplancton marine), démontrent les mêmes contrôles pour l'enrichissement, et ont un coefficient de corrélation de Spearman de 0.62, illustrant un rapport important entre le CH_4 et I dans l'eau souterraine de la région étudiée.

Acknowledgements

Since this project initially began to take shape in 2015, I have received help, support, and encouragement from a great number of individuals without whom this thesis would not have been possible. Firstly, I would like my supervisors, Dr. Ian Clark and Dr. Stew Hamilton.

Ian, your knowledge, insight, and most of all enthusiasm for isotope geochemistry put me in a tremendous position to succeed. I learned a great deal from our conversations about geology, geochemistry, hockey (even though your choice in teams is quite poor), the great outdoors, and so much more. Being a part of the Multidisciplinary Applied Geochemistry Network (MAGNET) through your efforts and recommendation was one of the best things that could happen to a master's student.

Stew, you are the reason I decided to pursue hydrogeology as a profession. The amazing experience of working as part of the Ontario Ambient Groundwater Geochemistry Program (OAGGP) for two summers taught me many invaluable skills that will serve me for years to come. Your integrity and passion are infectious. I wish you the best of luck in your budding career as a bovine epidemiologist. I would also like to thank Jason Dyer, Courtney Rogerson, Neal McClenaghan for their help with summer 2016 field work. I could not have asked for a better group.

I would like to thank Tessa Di Iorio for her effort co-ordinating field work during the summer of 2015 and acting as a problem solver extraordinaire. Your attention to detail is admirable and I learned a lot from you. I would also like to thank the other South Nation Conservation Authority staff that made summer 2015 fieldwork possible: Angela, Marika, Saxon, Andrew and Thierry. A big thank you as well to Mike Melaney and Michaela for help with the 2016 field work.

Radiocarbon and ^{129}I analyses would not have been possible without the wonderful group of people in the AMS labs. Gilles, Sarah, Carley, Monika, Norm and Xiaolei, you guys are an amazing group that excels in teaching, problem-solving, and encouragement. I truly enjoyed every second of lab work with you all. Sarah and Gilles, your dedication to setting up the methane extraction line was staggering, and it made me realize the commitment you guys have towards students and the pursuit of knowledge.

To the G.G. Hatch Stable Isotope Lab: Paul, Wendy, Patricia, and Kerry, you were more than accommodating to whatever I needed for my research. The patience and kindness you show to everyone interacting with your lab does not go unnoticed.

Lisa, Hélène, and Carolyn, your help with anything related to uOttawa bureaucracy is very much appreciated. You guys make life so much less stressful as a grad student.

Mom and Dad, thank you for encouraging me every step of the way. Words cannot express how grateful I am for all the important life skills I have learned from you both and how much I appreciate your unwavering support. You make me proud to do what I do, inspired my curiosity for the world around me, and I owe all of this to you guys.

To the friends (new and old) who were always there for me and made grad school the best experience of my life, I would like to express my sincere gratitude. I learned something from each and every one of you and were the best support group a guy could ask for.

Finally, I would be remiss if I did not acknowledge the critical role of all the homeowners who participated in the groundwater studies. Your willingness to accommodate a group of strangers into your homes in the name of science truly embodies the spirit of Canadian hospitality.

I am truly lucky to be surrounded by so many amazing people throughout the course of grad school and look forward to what comes after. Thank you all.

Table of contents

List of Figures

List of Tables

List of Appendices

1 Introduction

1.1 Background

Geochemical analysis of shallow groundwaters (<200 mBGS) sampled from residential and monitoring wells in the central St-Lawrence lowlands region in Eastern Ontario by the Ontario Geological Survey (OGS) and South Nation Conservation Authority (SNCA) during the summers of 2012, 2013, and 2015 revealed problem areas with anomalously high concentrations of iodine (I) as iodide (I^-) up to 10 812 µg/L and dissolved methane (CH_4) concentrations regularly exceeding 2 mg/L (OGS, 2016).

For residents living within the affected areas, high concentrations of I and CH_4 in groundwater pose a potential health hazard. In Canada, 8.9 million people (30.3% of the total population) are reliant upon groundwater to satisfy their domestic water needs (Environment Canada, 2013), which highlights the importance of assessing the current state of these resources. I is an essential element for synthesis of thyroid hormones in the human body and an excess or deficiency can be harmful. Chronically high I intake above the proposed upper limit of 1 000 µg/day for adults can increase the risk of hyperthyroidism and goiter (WHO, 2007), and I-rich drinking water in China was shown to contribute to increased incidences of these health issues (Andersen et al., 2008). In China, a threshold I concentration of 150 µg/L in groundwater is used to define areas at risk of excessive I intake (China Ministry of Health, 2003), a guideline which is regularly surpassed in the study area. Although there is currently no drinking water limit for I in Canada (Health Canada, 2017) it is estimated that 15% of the Canadian population between the ages of 3 – 79 have an excessive I intake (Stats Canada, 2013) based on optimal urine concentrations of I required for nutritional sufficiency defined by the World Health Organization (WHO, 2007).

Elevated concentrations of CH_4 in groundwater pose an explosion hazard, as dissolved CH_4 in groundwater will degas to air. Once concentrations surpass 2 mg/L CH_4, the accumulation of CH_4 in unventilated areas such as well casings or plumbing conduits has the potential to surpass the lower explosive limit (LEL) of 4.4% (vol/vol) in air. The CH_4 concentrations observed in the

study area far exceed the limit established by the Province of Ontario for groundwater of 3L CH_4/m^3, which corresponds to approximately 2 mg CH_4/L (MOE, 2006).

The enrichment of I and CH_4 in groundwater in the study area is thought to be linked to glaciomarine muds deposited in the study area during a marine transgression in the Late Wisconsinian. The link between decomposition of organic matter in marine sediments with high concentrations of biophilic elements (such as I and Br) and CH_4 has been recognized in fore arc fluids (Dia et al., 1999; Muramatsu et al., 2001; Fehn et al., 2003). Because CH_4 and I have similar diffusion coefficients (Lide, 2005), they are expected to migrate together in solution.

1.1.1 Thesis objectives

The main objectives for this thesis are as follows:

a) Characterize the distribution of I and CH_4 in groundwater in the study area and evaluate the hydrogeochemical environments in which enrichment is favored.
b) Determine the mechanisms through which I and CH_4 are enriched in groundwater.
c) Trace the source of I and CH_4.
d) Investigate the potential relationship between CH_4 and I enrichment.

Objectives a), b), and c) are discussed in Chapters 2, 3, and 4 (respectively), while objective d) is discussed throughout the entirety of this document, with a definitive interpretation presented in the conclusion (Chapter 5).

1.1.2 Affiliations

Field work relevant to this thesis was conducted by the author during the summer of 2016 as part of the Ontario Ambient Groundwater Geochemistry Program (OAGGP), funded by the Ontario Geological Survey (OGS) and supervised by Dr. Stewart Hamilton, in conjunction with the South Nation Conservation Authority (SNCA), University of Guelph, and the University of Ottawa.

1.2 Study area

The studied area is situated in the St. Lawrence Lowlands region of southeastern Ontario at an average elevation of 70 mASL and lies 50 kilometres east of the City of Ottawa, along the southern shore of the Ottawa River (see Figure 1-1). With a combined population of 32 000 people in 2011 (Stats Canada, 2016), the studied area covers approximately 1 500 km^2 in 3 townships: Alfred, Plantagenet, and Clarence-Rockland, which are in turn part of the United Counties of Prescott and Russell. Villages within the study area are serviced primarily by water treatment plants that pump water from the Ottawa River. Outside of the serviced areas, residents obtain water from groundwater aquifers.

Eastern Ontario is part of the mixedwood plains ecozone, with a continental climate that results in warm to hot summers and cold winters. Annual precipitation from 1981 – 2010 averaged 943.3 mm/yr (Environment Canada, 2017), 23.7% of which was snow. Natural Resources Canada (NRCAN) estimates that 10% of precipitation that falls in Eastern Ontario enters groundwater aquifers (~94 mm annual recharge), with the rest being lost to evapotranspiration and surface water runoff (City of Ottawa, 2011). The average annual temperature is 6.4ºC, with the coldest month being January at an average temperature of -10.3 ºC and the hottest month being July, at an average temperature of 21 ºC (Environment Canada, 2017).

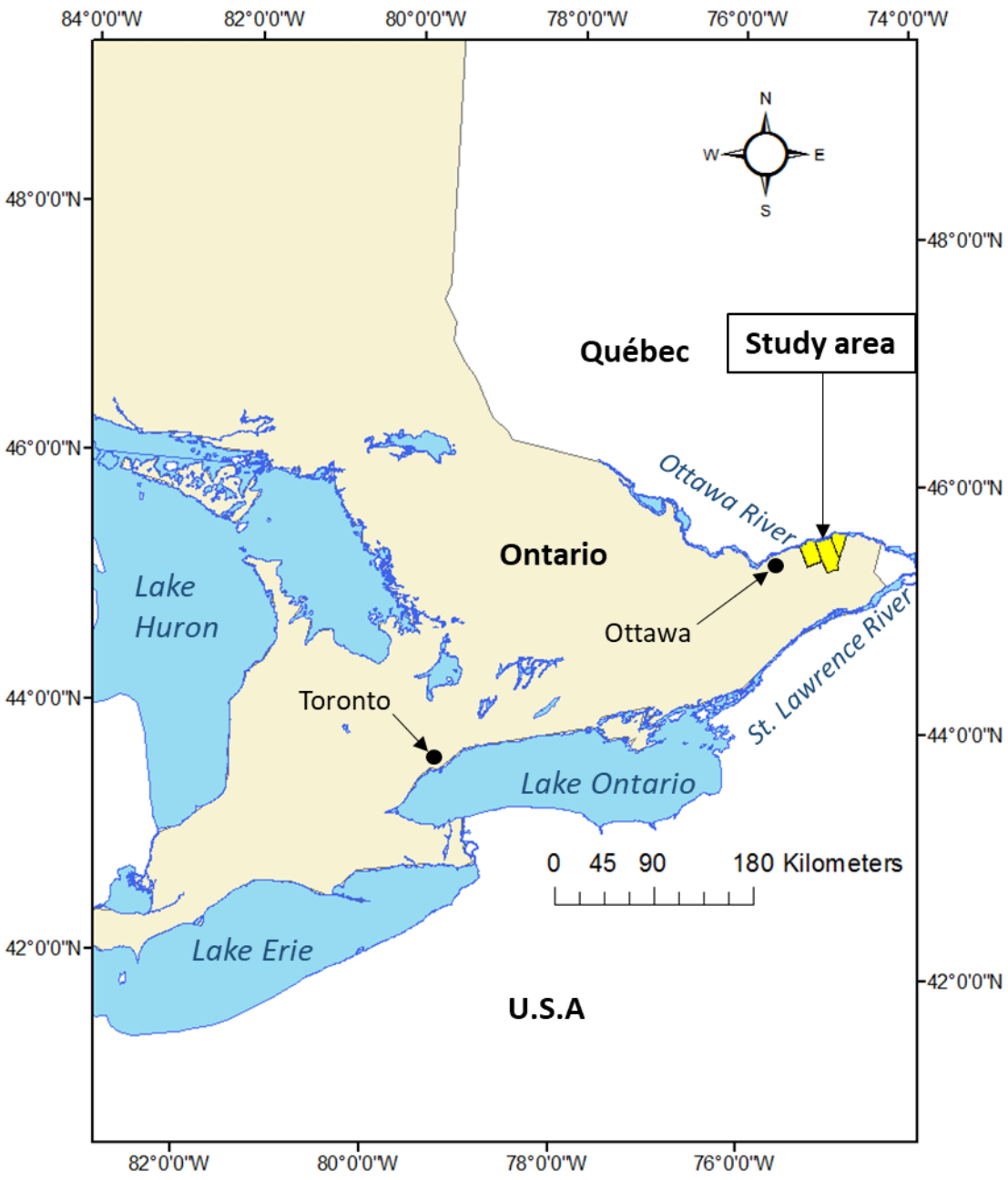

Figure 1-1. Location of study area.

1.2.1 Bedrock Geology

The study area is part of the Central St-Lawrence Platform geological province and consists of Paleozoic sedimentary rocks deposited during the Ottawa Embayment (which occurred from the Late Cambrian to Upper Ordovician Periods) that lie unconformably atop the

igneous and metamorphic Precambrian crystalline basement of the Canadian Shield (Armstrong and Dodge, 2007). Bedrock outcrops in the study area are rare, due to the thick layer of Quaternary sediments that overlies them. Precambrian rocks, such as metamorphic gneiss and marble with igneous dyke intrusions of pegmatite (Bélanger, 2008) are found in the northeastern portion of the study area, along the Ottawa River (Figure 1-2). These rocks formed during the Grenville Orogeny, a mountain-building event that occurred from 1.3 – 1.0 Bya.

Paleozoic sedimentary rocks in the area are comprised of sand- and dolostones (Upper Cambrian and Lower Ordovician in age), as well as interbedded limestones, siltstones, and shales (Middle to Upper Ordovician in age). Each unit is represented in the legend of Figure 1-2 in ascending order of deposition, beginning with the Covey Hill and Nepean Formations in the Upper Cambrian and ending with the Queenston Formation in the Upper Ordovician. The Covey Hill and Nepean Formations were deposited in the Upper (Late) Cambrian and are comprised mainly of feldspathic conglomerates to impure sandstones (Johnson et al., 1992). They, in turn, are unconformably overlain by the Lower Ordovician March and Oxford formations that make up the Beekmantown Group. The March Formation consists of interbedded sandstones and dolostones, while the Oxford Formation is comprised of fine-grained dolostone, shaly dolostone, and some sandstone (Johnson et al., 1992). The notable upward decrease in grain size in the Oxford is indicative of a progressive sea level rise throughout its deposition. Constantly fluctuating sea levels in the Early to Middle Ordovician resulted in the erosion of the Early Ordovician units (Bélanger, 2008).

Renewed transgression in the Middle Ordovician resulted in the deposition of the Rockliffe Formation, which is comprised of interbedded quartz sandstone and shale, with limestone in the upper portion of the unit (Johnson et al., 1992). Continually rising sea level is evidenced by the Ottawa Group, comprised of highly fossiliferous low-energy deposits of interbedded limestone and shale units that indicate continual deposition on a constantly deepening shelf (Johnson et al., 1992). Units from the Ottawa Group that are present in the study area include the Gull River, Bobcaygeon, Verulam, and Lindsay Formations. Finally, Upper Ordovician deposits are indicative of a continually deepening marine environment, as they are predominantly comprised of shales and siltstones, with interbeds of fine-grained limestone (Johnson et al., 1992). In the study area, these deposits are represented by the Billings, Carlsbad,

and Queenston formations. The Billings and Lindsay Formations have been identified as potential reservoirs of natural gas due to their high total organic carbon (TOC) contents ranging from up to 3 to 7% by weight, respectively (NRCAN, 2017).

The Paleozoic sedimentary rocks are flat-lying and undeformed, relative to the underlying Precambrian terrain of the Canadian Shield, due to the tectonically stable shallow shelf depositional environment in which they were deposited (Johnson et al., 1992). They are mostly unaffected by Paleozoic orogenic events. However, during the Late Mesozoic, the opening of the Atlantic Ocean produced block faulting, which would have resulted in the formation of the Ottawa-Bonnechere Graben (Johnson et al., 1992). The areas most severely affected by faulting are situated near the modern-day Ottawa River.

A notable feature of the bedrock topography is the presence of bedrock depressions, that play an important role in dictating the hydrogeological flow patterns within the study area. The location of these depressions is presented in Figure 1-3. Their significance will be further discussed in section 1.2.3.

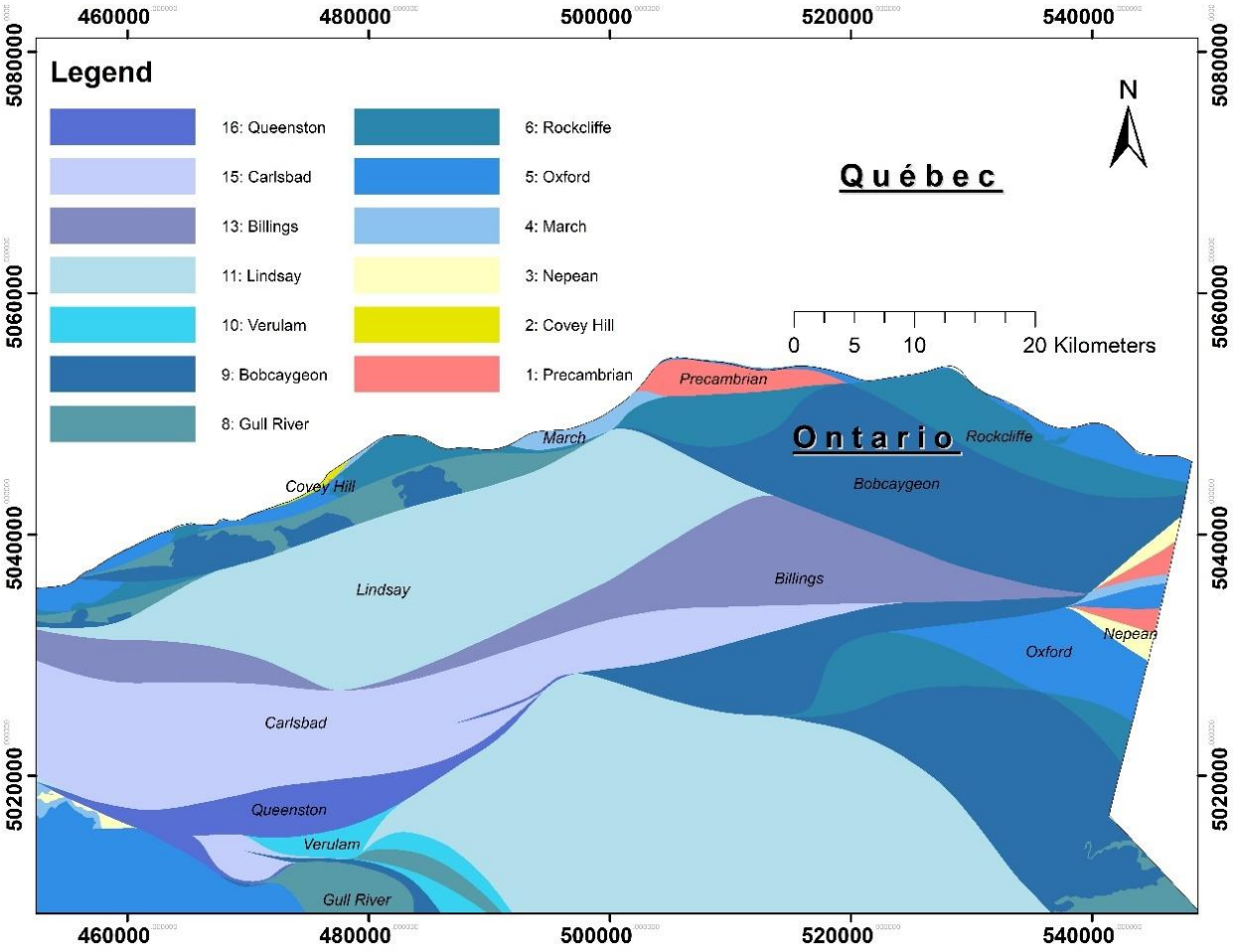

Figure 1-2. Bedrock geology in the study area. *Universal Transverse Mercator (UTM) co-ordinates provided using North American Datum 1983 (NAD83) in Zone 18N. Data obtained from OGS Miscellaneous Data Release MRD 219 (Armstrong and Dodge, 2007).*

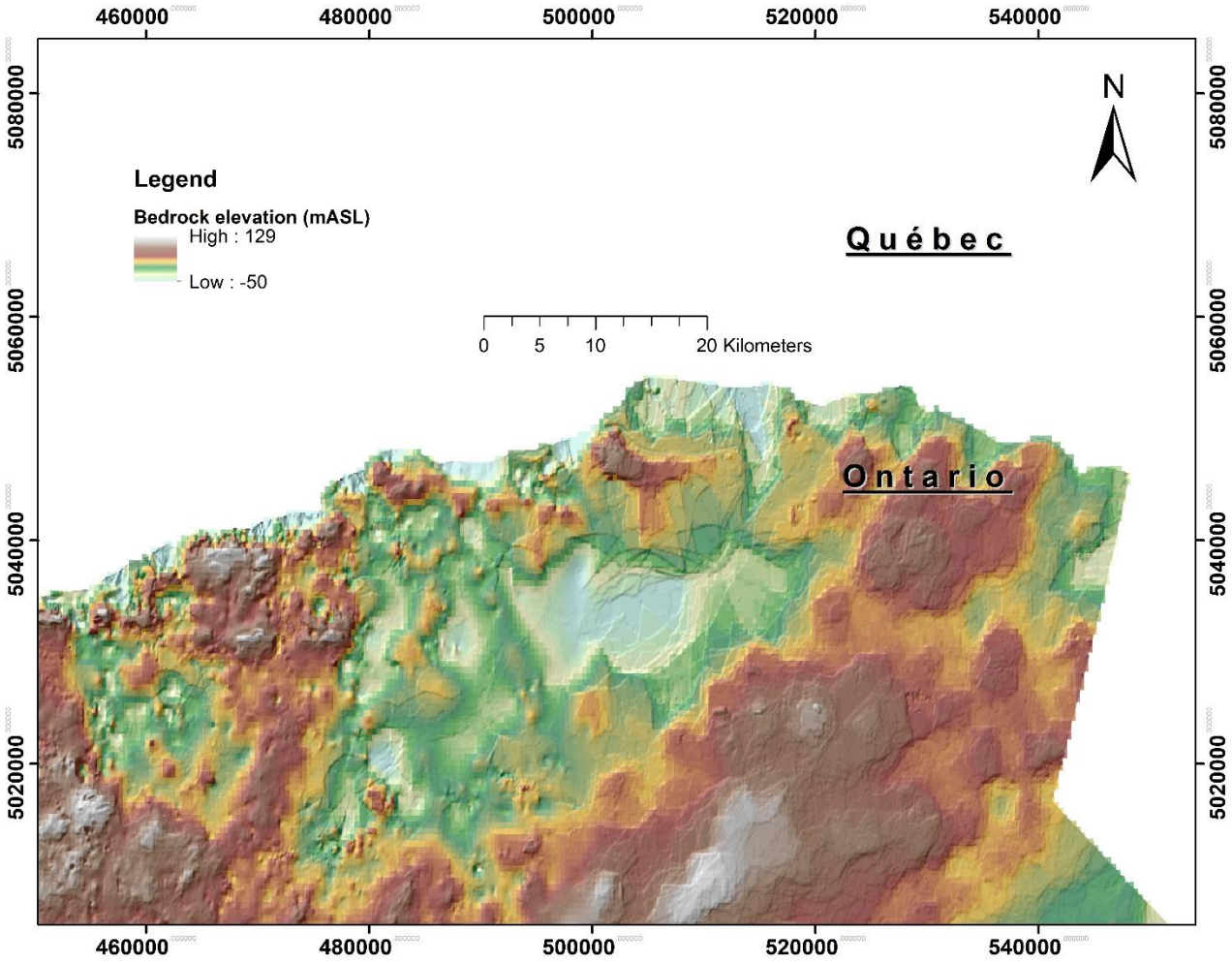

Figure 1-3. Bedrock topography in the study area. *Universal Transverse Mercator (UTM) co-ordinates provided using North American Datum 1983 (NAD83) in Zone 18N. Data obtained from OGS Miscellaneous Data Release MRD 207 (Gao et al., 2006).*

1.2.2 Surficial Geology and the Champlain Sea incursion

The surficial geology of the study area (presented in Figure 1-4) is heavily influenced by Quaternary glaciation, in particular the most recent Wisconsinian glacial episode, where the Paleozoic and Precambrian bedrock units were covered in till, subaqueous outwash deposits, glaciomarine muds, and nearshore sands. In the study area, sandy silt tills from the erosion of carbonates (also referred to as the Gentilly Till) are the most prevalent, due to the abundance of localized carbonaceous sedimentary rocks. The till is comprised of approximately 10% clasts (of the gravel size fraction), and 90% matrix, which consists of 40% sand, 50% silt, and 10% clay

(Sharpe, 1979). Interstadial deposits containing organic matter predating the Gentilly Till are present in the central St. Lawrence Lowlands, although there is no evidence from local well logs of the presence of these deposits in the studied area. The interstadial deposits are a heterogeneous group of fluvial, lacustrine, and paludal sediments that was deposited in two phases: a nonglacial fluvial episode, followed by a lacustrine and deltaic episode (Ochietti, 1989). This assemblage is referred to as the St. Pierre sediment, and is representative of the Les Becquets interstadial period that most likely occurred during the Early Wisconsinian, between 75 – 60 ka BP (Ochietti, 1989). Stratigraphic analysis coupled with radiocarbon (^{14}C) and thermoluminescence dating at a quarry in Pierreville, Québec (50 km north of the study area) revealed that the St. Pierre sediment also correlates with peat and organic-rich sands characterized by boreal-type pollen assemblages (Lamothe, 1989).

Following the most recent glacial maximum (23 ka BP) was the retreat of the Laurentide glacier, which began approximately 14 ka BP (Dyke et al., 2002). This retreat revealed an isostatically depressed landmass in the eastern Ontario region approximately 12.5 ka BP, after which a marine transgression occurred. The resulting inland sea is referred to as the Champlain Sea, which established its main basin in Eastern Ontario 12 ka BP (Parent and Ochietti, 1988) and submerged the study area for 2 ka (Fulton, 1987), with its level falling continuously due to the isostatic rebound of the continental crust (Rust and Romanelli, 1975). The Champlain Sea was comprised of a mixture between glacial meltwater, Pleistocene meteoric water, and seawater (Cloutier et al., 2010). The depositional sequence of Champlain Sea muds in the study area was described by Gadd (1986), who reported three mud units (presented from oldest to youngest): basal rhythmites, massive muds, and red-and-grey stratified mud. The Champlain Sea muds are underlain by subaqueous meltwater outwash deposits consisting of sand and gravel deposited during glacial retreat (Cummings et al., 2011), and overlain by nearshore sands. The entire sequence of mud and overlying sands was interpreted to be produced by deltaic offlap during regression of the Champlain Sea. Massive muds are the most abundant and widespread deposits, have an average thickness of approximately 10 meters with a maximum observed thickness of 90 meters (Charron, 1975) in the study area, and contain between 0.4-1% (w/w) organic matter (Laventure & Warkentin, 1965). Locally, the highest observed porewater salinities are observed in the massive muds and are thought to reflect the salinity of the Champlain Sea (Torrance, 1988).

During and after the regression of the Champlain Sea, the Ottawa River developed a complex channel system as it flowed over what was the floor of the Champlain Sea, reworking unconsolidated sediments (resulting in diamicton deposits) and washing away the nearshore deposits. Flow rates reached up to 100 000 m^3/s due to a combination of inflows from 3 000 km of melting ice margin, glacial Lake Agassiz, and the upper Great Lakes (Fulton, 1987). As flows gradually decreased, abandoned river channels exposed Precambrian and Paleozoic bedrock, in addition to poorly drained glaciomarine muds, upon which peaty deposits and wetlands formed. This occurred from approximately 10 – 4.7 ka BP, when the modern basin for the Ottawa River was established (Fulton, 1987).

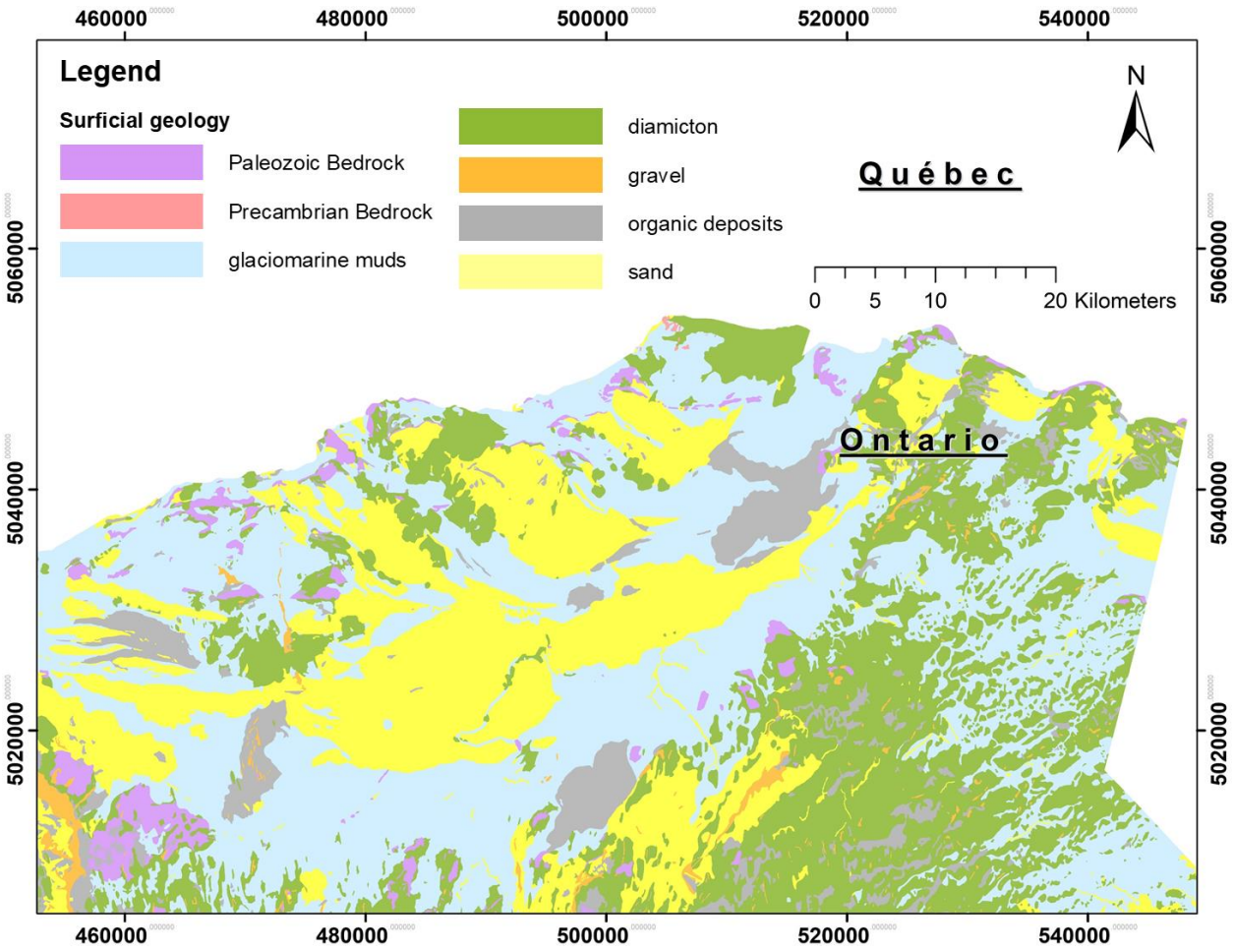

Figure 1-4. Surficial deposits in the study area. *Universal Transverse Mercator (UTM) co-ordinates provided using North American Datum 1983 (NAD83) in Zone 18N. Data obtained from OGS Miscellaneous Data Release MRD 128 (OGS, 2010).*

1.2.3 Hydrogeology and Groundwater Flow

The principal aquifer in the St-Lawrence lowlands is described as an interface, or contact aquifer (Cloutier et al., 2010; Montcoudiol et al., 2014). A layer of permeable till, subaqueous outwash sands and highly fractured bedrock comprise the interface aquifer and separate the overlying mud from the moderately fractured Paleozoic bedrock underneath. Geometric mean hydraulic conductivity for the interface flow (commonly exploited by domestic wells due to high yields) path of a similar aquifer in southwestern Québec is on the order of 7.8×10^{-4} m/s, whereas the conductivity for the intermediate and deeper flow paths ranges from 10^{-8} to 10^{-4} m/s, depending on the nature of the Paleozoic sedimentary rocks (Nastev et al., 2004). Hydraulic conductivities for the muds are lower, on the order of 10^{-10} to 10^{-8} m/s (Tavenas et al., 1983). Meteoric water recharges the system in topographically high areas where there is little to no mud and flows preferentially in the upper bedrock beneath the mud via the interface aquifer to topographically low areas. Charron (1975) noted that groundwater flow is controlled by bedrock topography in the study area due to the fact that the permeable interface zone is located at the contact between bedrock and surficial sediment deposits, and that the groundwater flow direction was generally from south to north. Depressions in the bedrock surface throughout the study area (Figure 1-3) represent the final feature of the flow system. These depressions contain fossil Champlain Sea waters which are confined above by a thick layer of overlying mud, and underneath by low-permeability bedrock (Cloutier et al., 2006). The system can be divided into 3 components: a hydraulically unconfined recharge area, a semi-confined transition area, and a confined lowland area, as shown by the conceptual model in Figure 1-5.

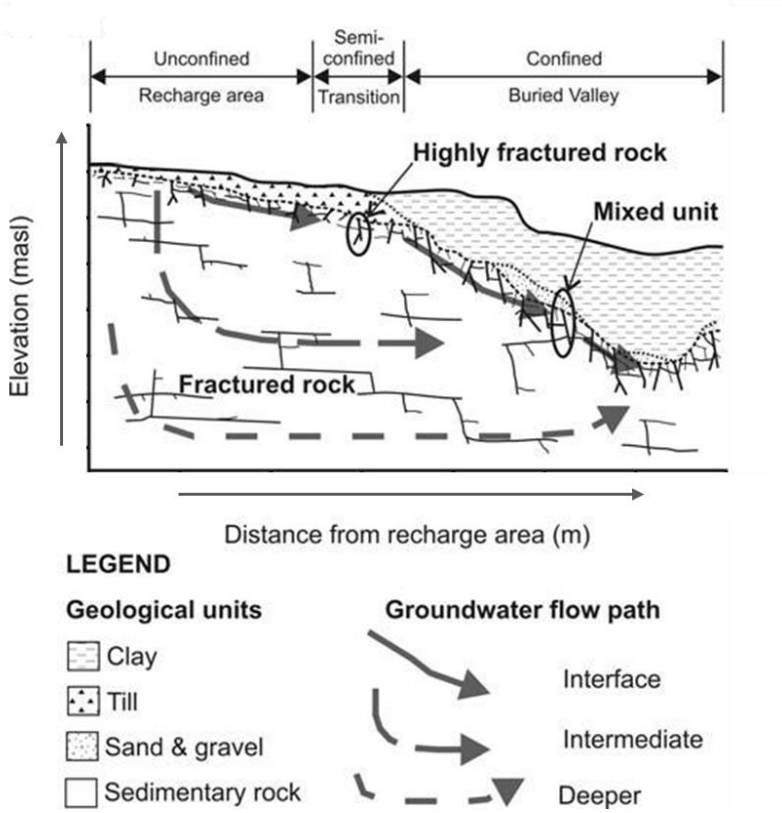

Figure 1-5. Conceptual model for groundwater flow. *Modified from Cloutier et al. (2010).*

A map of the groundwater potentiometric surface for the interface aquifer is presented in Figure 1-6. This map further illustrates the relationship between topography and groundwater flow in the study area and highlights stagnant zones with low hydraulic head values where lenses of fossil Champlain Sea water reside. Although flow regimes in the study area are predominantly horizontal as they travel through the continuous layer that constitutes the interface aquifer, solute diffusion from the low-permeability muds is non-negligible and can have profound impacts on water geochemistry, as demonstrated by Cloutier et al. (2006). Additionally, in a hydrogeological study of the St-Lawrence River Valley, Chapuis and Saucier (2013) concluded that the Champlain Sea muds are underdrained by groundwater ("leaky") aquifers, which collect small amounts of vertically seeping porewaters. Sauriol (2016) postulated that significantly higher proportions of groundwater recharge occur through Champlain Sea muds overlying esker aquifers in Eastern Ontario – however, there are no eskers observed in the studied area (Hinton et al., 2011; RRCA & SNC, 2008) and the dominant portion of recharge was assumed to occur in the topographically high areas presented in the conceptual model (Figure 1-5). This assumption is reflected by the potentiometric surface shown in Figure 1-6.

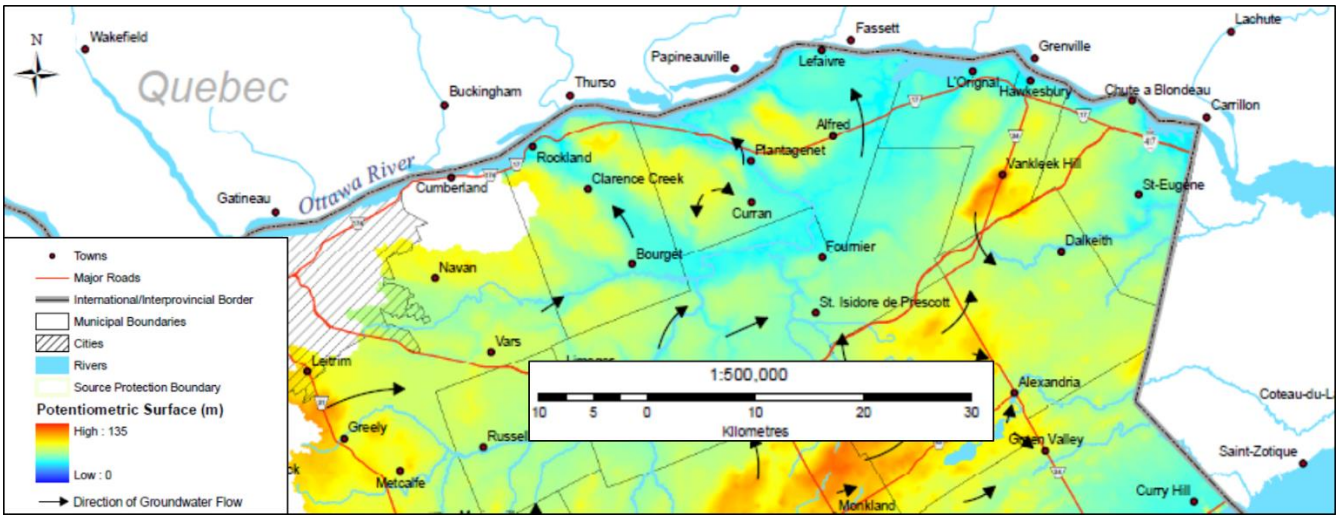

Figure 1-6. Groundwater potentiometric surface for the interface aquifer in the studied and surrounding areas. *Modified from Map 3-13 of the Source Protection Watershed Characterization Report (RRCA & SNC, 2008).*

1.3 Methods

Data for this study were collected during the summer of 2016 as part of the Ontario Ambient Groundwater Geochemistry Program (OAGGP), whose objective is to better understand regional trends in Ontario's groundwater systems by sampling water from domestic wells. Previous sampling was conducted in the study area during the summers of 2012, 2013, and 2015. However, isotopic data other than stable isotopes of water ($\delta^{18}O$ and $\delta^{2}H$) and tritium (^{3}H) was collected only during the 2016 iteration. As this represents the bulk of the subject matter discussed within this thesis, its unique sampling protocols will be covered in the most detail, and only results from the 2016 iteration will be presented in the text and appendices. For additional information regarding the methodology for previous iterations of the OAGGP sampling, the reader is encouraged to consult Freckelton and Hamilton (2012), Morton et al. (2013) and Di Iorio et al. (2015). Fifty-nine sites were sampled during the 2016 sampling program, 17 of which were dairy farms, as part of a collaborative thesis with Courtney Rogerson supervised by Dr. David Kelton of the University of Guelph investigating the relationship between high I in cow's milk and groundwater consumption for Eastern Ontario dairy herds (Rogerson et al., 2016). Only domestic wells exploiting the contact aquifer were chosen, and geological units represented by

groundwater samples include glacial sediments (n = 11), shales (n = 6), limestones (n = 41), and sandstone (n = 1).

1.3.1 Site Selection and Data Availability

Although this project was part of the OAGGP, the methodology for site selection differed from previous years. Rather than aiming for a homogenous spatial distribution of samples on a predefined grid, the 139 interface wells that had previously been sampled within areas overlain by contiguous thick marine sediments (CTMS, outlined in Figures 1-8 and 1-9) during the Eastern Ontario (2012), Township of Clarence-Rockland (2013) and Township of Alfred-Plantagenet (2015) iterations of the OAGGP were screened with respect to their I and CH_4 content. The intention was to return to a select few of these sites to collect an isotopic and inorganic geochemical sample suite. In the context of the studied area, CTMS is defined as overburden sediments of glaciomarine origin exceeding 20 meters (~65 feet) in thickness (Hamilton, 2015). Sites were chosen to represent the full spectrum of observed concentrations for I and CH_4. In areas prone to high I and CH_4 concentrations where no previously sampled sites existed, the cold-call protocol used by Hamilton et al. (2007) was employed to fill spatial gaps. Finally, a proximity analysis was carried out in ArcGIS to ensure that groundwater samples collected from dairy farms as part of concurrent work by Rogerson et al. (2016) were farther than 1 500 metres from proposed sample sites. Sample locations and IDs are illustrated in Figure 1-7.

The full hydrogeochemical dataset containing major, minor, and trace ion concentrations and station data for all field seasons (2012, 2013, 2015, 2016) is publicly available for download using the OGSEarth application from the Ontario Geological Survey website (https://www.mndm.gov.on.ca/en/mines-and-minerals/applications/ogsearth), as part of the Ontario Ambient Groundwater Geochemistry Program (OAGGP). All data from the 2016 field season (n = 59 samples) is presented in the Appendix or in the text of this manuscript.

Finally, three unoxidized glaciomarine mud samples were collected from Green's Creek, Gloucester (45˚28'00"N; 75˚34'35"W) and two samples from a farmer's field in Embrun, Ontario (45˚26'56"N; 75˚17'05"W) at an approximate depth of six meters below ground surface for stable and radioisotopic analysis of disseminated organic matter during the 2016 campaign

(see Figs. 1-7 & 1-8). Mud samples were dried at 60˚C for six days and powdered using a mortar and pestle prior to analysis.

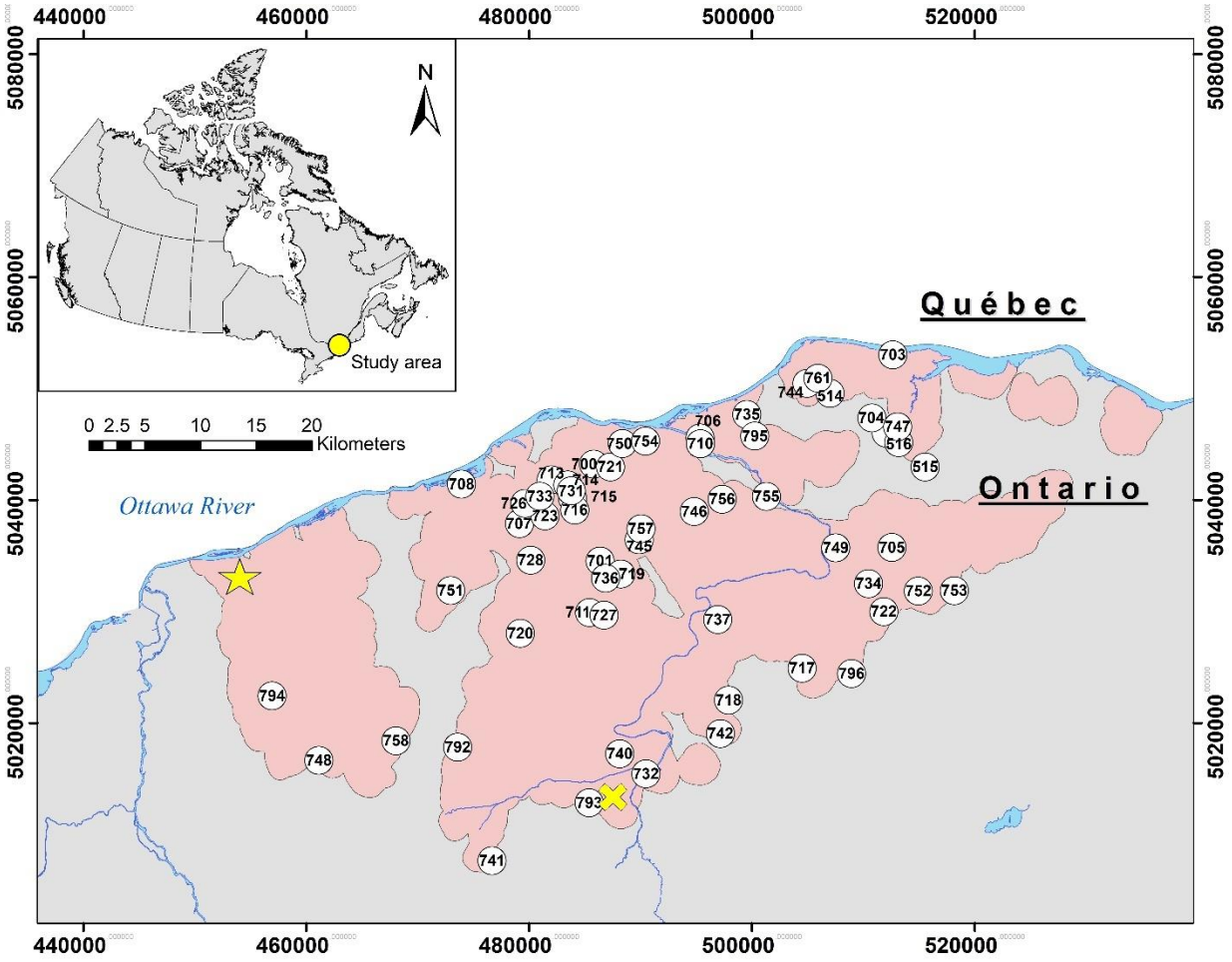

Figure 1-7. Location of groundwater sample sites (n = 59) relative to the distribution of Contiguous Thick Marine Sediment (CTMS), outlined in red. Star represents Green's Creek mud sample location, whereas X represents Embrun location. *Universal Transverse Mercator (UTM) co-ordinates provided using North American Datum 1983 (NAD83) in Zone 18N.*

1.3.2 Sampling Procedures

Interviews were conducted with homeowners during which historical water problems were discussed and a consent form was signed. Following this, a visual inspection of the well was carried out, and measurements such as GPS location, well collar stickup and static water level were recorded. Water was then purged through a manifolded group of PVC hoses with three distinct outlets (two of which were equipped with switch valves): one that led to a 121 L purge bucket, one led to a silicone rubber sampling hose, and a final one that led to a flow cell into which a YSI 6600 sonde connected to a YSI 650 multi-parameter display system instrument was inserted to record measurements of temperature (ºC), conductivity (µs/cm), pH, ORP (mV) and DO (mg/L). The YSI was calibrated daily, using a three-point calibration for pH (4, 7, and 10). DO was calibrated to 100% using water saturated air, and to 0% using a zero-oxygen calibration solution. Electrical conductivity was checked daily using a 1413 µs/cm solution, and ORP was checked weekly using ZoBell's solution (+240 mV). The temperature probe was not calibrated. Sampling began when temperature variations of groundwater were within a range of ± 0.1ºC and the other parameters measured by the YSI were judged to be stable.

Water was collected from each site in 14 separate sample bottles to be analyzed for metals (60 mL), anions (60 mL), mercury (60 mL), I/Br (60 mL), stable isotopes of water (^{18}O & ^{2}H; 125 mL), ^{3}H (250 mL), ^{129}I (500 mL), dissolved organic and inorganic carbon concentrations (DIC/DOC) and isotopes (3 x 40 mL), total Kjeldhal nitrogen (TKN) + NH_3 and NH_4 (45 mL), nitrate and nitrite (45 mL), CH_4 (1.2 L) and color (45 mL); this included a "spare" bottle (250 mL) for additional analyses, as required. All bottles excepting the CH_4 sample (600 mL of water in a 1.2 L bottle, see analytical methods section for explanation) were filled to the top with minimal headspace.

Excepting ^{129}I, CH_4 and DIC/DOC concentrations/isotopes, all bottles were acid-washed high-density polyethylene (HDPE). ^{129}I and CH_4 bottles were pre-baked borosilicate Wheaton bottles, and DIC/DOC bottles were amber glass vials with PTFE-rubber septa. These sample containers were chosen to minimize atmospheric exchange and degassing. At sites where there was significant exsolution of gas in the form of free bubbles, two 125 mL borosilicate Wheaton bottles were filled with the emitted gas (n = 19) using the inverted-bottle technique detailed in Lemieux et al. (2016), and two 500 mL borosilicate Wheaton bottles were filled with water after

it was passed through a 0.45 µm polyethersulfone high-capacity filter. The locations of these sampling sites are shown in Figure 1-8. All samples collected in Wheaton bottles were capped with butyl septa. The sample bottles for metals, anions, and mercury were each filled using a syringe and 0.45 µm polyvinylidene fluoride filter. For TKN + ammonia, I/Br, metal and mercury samples, 1:1 sulfuric acid, 0.2M nickel acetate, 1% HNO_3 and 2% HCl (respectively) were used as preservatives. For filtered ^{14}C DIC/DOC samples, 1 mL of a 5.8M silver nitrate solution was used as a preservative to precipitate Cl. Samples were refrigerated at ~4ºC in a dark area until analysis.

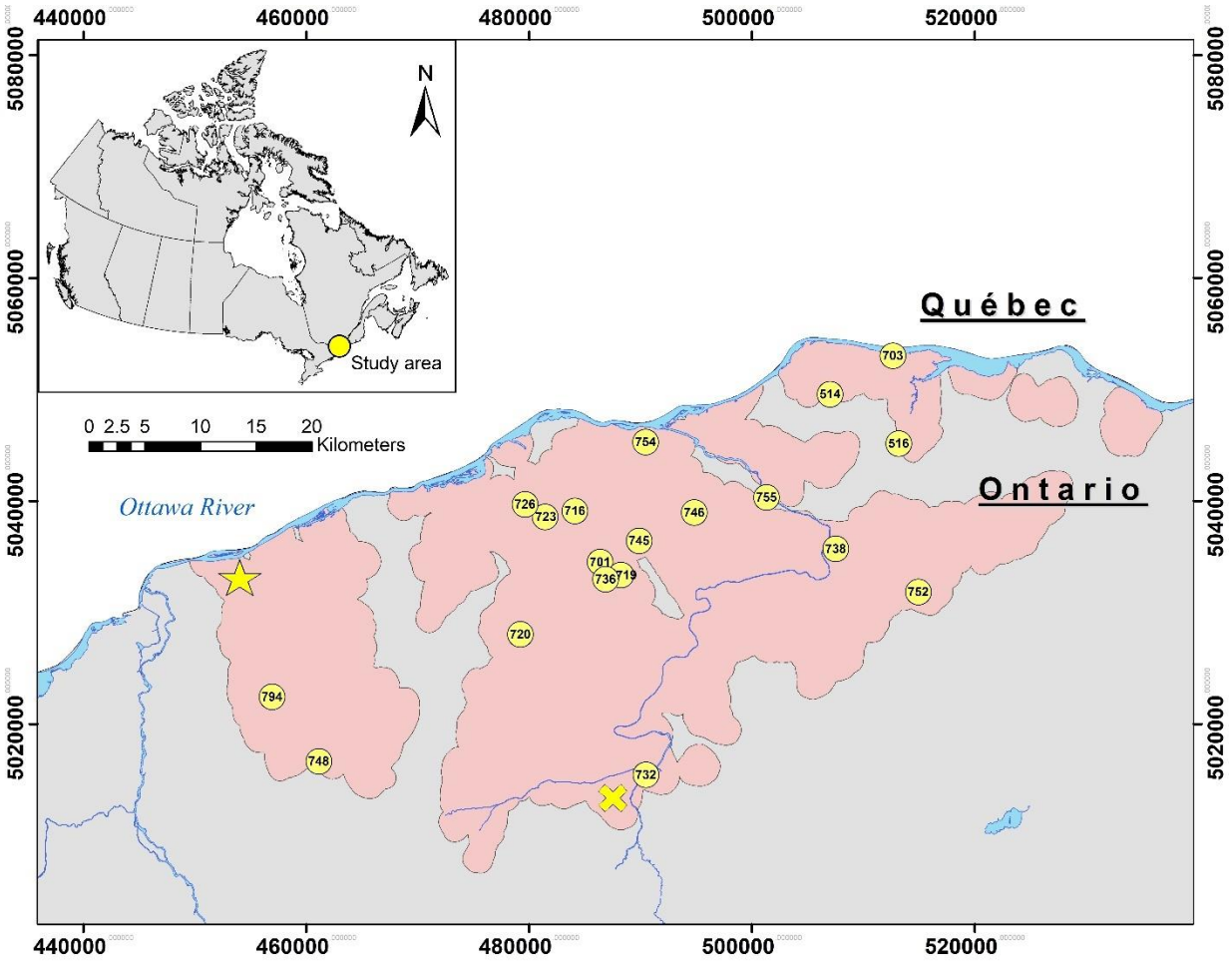

Figure 1-8. Location of collected gaseous phase samples (n = 19) relative to the distribution of Contiguous Thick Marine Sediment (CTMS), outlined in red. Star represents Green's Creek mud sample location, whereas X represents Embrun location. *Universal Transverse Mercator (UTM) co-ordinates provided using North American Datum 1983 (NAD83) in Zone 18N.*

1.3.3 In-field measurements

Alkalinity was measured on-site using a Hach® Model 1690001 digital titrator (10 mg – 4000 mg detection range) by titrating 1.6 N sulfuric acid into 100 mL of sample with an added indicator packet of bromocresol green. Titrated amounts were recorded at three endpoints: blue grey, violet grey and pink. Hydrogen sulphide (H_2S) content was also measured on site using a HACH model 2238-01 test kit (with an upper limit of 11.25 ppm) by preparing a blank of de-ionized water and comparing it, using a colour wheel, to a prepared sample. Hydrogen sulphide was not measured at sites where a distinctive rotten-egg odour was not observed.

1.2 L glass sample bottles (filled to 600 mL mark with sample) to be analyzed for CH_4 content were stored upside-down in a shaded area at room temperature for 24 hours before analysis. Gas concentrations (O_2, CH_4 and CO_2, recorded in ppm) in the headspace were then measured using an RKI Eagle 2 portable multi-gas meter, and water temperature was measured with the YSI sonde. CH_4 measurements were taken using two sensors: a low-level sensor capable of measuring from 0 to 50 000 ppm CH_4, and a high-level sensor capable of measuring up to 100% vol/vol CH_4. The low level CH_4 and CO_2 sensors were checked every day using 25 000 ppm CH_4 and 2.5% vol/vol CO_2 gas cylinders. The machine was also zeroed to air (0 ppm CH_4, 0% CO_2 and 21.9% O_2) during this process. The high-level CH_4 sensor was checked once a week using a 50% vol/vol CH_4 gas canister. In tandem with water temperatures, the concentration of gases within the headspace of the bottle were then used to estimate their aqueous concentrations (in ppm), using Henry's Law. These calculations are explained in detail by McIntosh et al. (2014).

Iodine (I) as iodide (I^-) and bromine (Br) bromide (Br^-) were measured within 5 days of sample collection, to minimize biases due to volatilization. I was measured with a Thermo Scientific™ Orion™ 9453BN iodide-selective electrode connected to an Orion™ Star A324 portable meter, while Br was measured with the Thermo Scientific™ Orion™ 9435BN bromide-selective electrode. The I meter was calibrated with 10, 1 000, and 10 000 ppb I standards, and the Br meter was calibrated with 0.5, 5 and 50 ppm Br standards prior to measurement. Measurements were corrected due to dilution from the nickel acetate preservative and the ionic strength-adjuster that was added just before measurement. Samples were stirred with magnetic

stir-bars during analysis, and measurements recorded after they stabilized (usually within 30 seconds).

1.3.4 Laboratory Techniques

Major and minor cation and anion concentrations were measured at Geoscience Laboratories (GeoLabs) in Sudbury, Ontario, Canada. Cations were analyzed by both inductively coupled plasma mass spectrometry (ICP-MS) using a Perkin Elmer Elan 9000 ICP-MS and inductively coupled plasma atomic emission spectrometry (ICP-AES) using a Teledyne Leeman Laboratories Prodigy ICP AES Radial View instrument. Anions were analyzed by Ion Chromatography (IC), using a dual-pump system ion chromatograph, Dionex model ICS-3000. Three IC methods were used: carbonate eluent, potassium hydroxide eluent, and dual analysis. Hg samples were analyzed by atomic fluorescence spectrometry, using a bromine/chlorine (BrCl) overnight digestion method. Overall method precision was determined with field and laboratory duplicate pairs using the method of Thompson and Howarth (1978).

Nitrate + nitrite, ammonia/ammonium, total Kjeldhal nitrogen (TKN) and organic nitrogen samples were analyzed by SGS analytical laboratories in Lakefield, Ontario, Canada within seven days of collection. Nitrate (NO_3^-) and nitrite (NO_2^-) were analyzed using a Dionex Ion Chromatograph and reported as ppm N. Ammonia (NH_3), Ammonium (NH_4^+) and TKN were analyzed using a Skalar Segmented Flow Autoanalyzer.

Stable oxygen and hydrogen isotopes of water were analyzed at Isotope Tracers Technologies (IT^2) in Waterloo, Ontario, whereas stable C isotope analysis occurred at the G.G. Hatch Stable Isotope Laboratory at the University of Ottawa. All stable isotopic data is reported using the standard δ-notation in parts per thousand (‰) relative to standards.

Stable isotope concentrations of water ($\delta^{18}O$ and δ^2H) were measured using a Picarro CRDS (Model L1102-i), which was calibrated using Vienna Standard Mean Oceanic Water (VSMOW), Standard Light Antarctic Precipitation (SLAP), and Greenland Ice Sheet Precipitation (GISP). These standards have $\delta^{18}O$ values of 0, -55.50 and -24.76‰ and δ^2H values of 0, -428.0 and -189.5‰ (respectively). Results are reported relative to VSMOW and have a precision of ±0.1‰ for $\delta^{18}O$ and ±0.6‰ for δ^2H.

For C isotopes of dissolved species in water ($\delta^{13}C$), samples were first run on an OI Analytical "TIC-TOC" analyzer (Aurora Model 1030) with a model 1088 autosampler to determine concentrations for organic/inorganic C (in ppm C). The "TIC-TOC" analyzer was interfaced to a Finnigan MAT Delta plus XP IRMS for analysis by continuous flow. Data was normalized using two different internal standards (KHP and sucrose). Analytical precision is ±2% for quantitative analysis, and ±0.2‰ for $\delta^{13}C$. $\delta^{13}C$ values are reported relative to the Vienna Pee Dee Belemnite (VPDB) standard.

For analysis of the collected glaciomarine mud, the samples were acidified using 1N HCl to remove carbonates and weighed into tin capsules with tungsten oxides (WO_3) and flash combusted at 1800˚C in an Elementar VarioEL Cube Elemental Analyser. Using ultrapure helium and a carrier, generated gases (CO_2, N_2, SO_2, H_2O) are separated using the "trap and purge method", then subsequently quantitatively measured with a thermal conductivity detector (TCD) with a precision of ±0.1%. The $\delta^{13}C$ isotopic composition of released CO_2 was measured using a DeltaPlus Advantage isotope ratio mass spectrometer, which was coupled to the EA with a ConFlo III interface. Precision of the isotopic analyses was ±0.2‰.

For C and H isotopes of CH_4 ($\delta^{13}C$ and $\delta^{2}H$), the gaseous components (N_2, O_2, CO_2, CH_4, and C_2-C_5 gases) of the gaseous phase were first analyzed quantitatively using a Gas Chromatograph Isolink (Agilent Technologies 7890A) system, with a precision of ±2 mol%. CH_4 was isolated from gaseous phase samples using the same GC Isolink (Agilent Technologies 7890A with combustion and pyrolysis furnaces) system interfaced via a Conflo 4 to a Delta V IRMS, manufactured by Thermo-Fisher. C isotopes were analysed after passing the CH_4 through a combustion furnace (kept at 1000˚C) and deuterium was analysed after passing CH_4through a pyrolysis furnace (kept at 1420˚C). Samples were normalized using the NGS1 and NGS2 international standards with $\delta^{13}C$ values of -29.11 and -44.84‰ and $\delta^{2}H$ values of -138 and -172‰ (respectively). C isotopes were reported relative to VPDB with a precision of ±0.2‰, and hydrogen isotopes were reported relative to VSMOW with a precision of ±2.0‰.

A carrier-addition method was used to extract I during a series of redox transformations for ^{129}I analysis. Two mg of NaI carrier with a $^{129}I/^{127}I$ ratio < 1.56×10^{-13} was added to a 200-mL aliquot of sample. The sample was acidified with 6M HNO_3 to pH = 2, and 1M $NaHSO_3$ was added to reduce all iodine (I) to iodide (I^-). The solution was vigorously shaken for 30 minutes

and left to stand for 16 hours. The following day, I was extracted into hexane by oxidizing it from I^- to I_2 using 6M $NaNO_2$. This extraction was repeated 3 times to ensure maximal collection of I. I was then back-extracted into distilled water. The resulting solution was acidified again using HNO_3 and heated to ~90ºC on a hot plate. Silver nitrate was added to precipitate the I as AgI, which was then dried overnight at 50ºC. Targets were prepared by mixing 1 to 2 mg of AgI with high-purity niobium powder, and pneumatically pressed into a stainless-steel cathode for analysis of ^{129}I at the Andre E. Lalonde AMS laboratory at the University of Ottawa using an HVE 3MV Tandetron. Measurements were normalized with respect to the ISO-6II reference material for which $^{129}I/^{127}I = (5.72 \pm 0.08) \times 10^{-12}$, by calibration with the NIST 3230 I and II standard reference material. Results are reported as $^{129}I/^{127}I$ ratio x 10^{-14} and are corrected for the amount of carrier added. Individual analyses are accompanied by their analytical uncertainty in Appendix F.

Enriched ^3H analysis was performed at the University of Waterloo Environmental Isotope Laboratory. ^3H values were measured by electrolytic enrichment (≥15x) with liquid scintillation counting (LSC). Samples with a specific conductivity exceeding 5 000 µs/cm were subject to azeotropic distillation. Results are reported in tritium units (TU), where 1 TU = 1 ^3H per 10^{18} ^1H, with a detection limit of 0.8 TU and a precision of ±0.5 TU.

Dissolved inorganic carbon (DIC), Dissolved organic carbon (DOC), organic C in mud and CH_4 gas extraction for ^{14}C analysis was performed at the Andre E. Lalonde AMS Laboratory. For DIC extractions, 85% phosphoric acid (H_3PO_4) was added to the sample, which was subsequently heated for one hour and sparged with helium to collect CO_2. DOC was extracted using a wet chemical oxidation (WCO) technique, where a sodium persulphate ($Na_2S_2O_8$) oxidant is added to the DIC-sparged sample in the presence of a silver nitrate ($AgNO_3$) catalyst. The solution is heated to 98ºC for at least an hour. Again, the headspace was evacuated with He to collect CO_2. CH_4 gas was combusted to CO_2, following methodology from Pack et al. (2015). Mud samples were pretreated using the acid-wash method outlined in Crann et al. (2017) and combusted in a Thermo Flash 1112 Elemental Analyser. In all extractions, CO_2 gas is purified in a vacuum line and trapped in a pre-baked 6 mm OD Pyrex breakseal containing a few grains of silver cobaltus and baked overnight at 200ºC. CO_2 was graphitized in an H_2 environment at 650ºC for three hours with -200 mesh reduced iron powder (CAS7439-89-6, P/N:

00737) as a catalyst. The prepared graphite samples were pressed into targets (aluminium target with copper backing pin) using a pneumatic press for ^{14}C analysis using the HVE 3MV Tandetron in the Andre E. Lalonde AMS Laboratories. DIC standards were IAEA-C2 and sodium bicarbonate, which contains no detectable ^{14}C. Internal kHP, salicylic acid, and citric acid standards were used for DOC analysis. CH_4 gas samples are uncalibrated, but processed blanks indicate minimal atmospheric contamination (< 0.05 pMC). Results are reported in percent modern carbon (pMC) relative to the Ox-II modern carbon standard (NIST SRM 4990C) and are normalized to a $\delta^{13}C$ value of -25‰ (relative to VPDB). ^{14}C ages are calculated as -8033ln(pMC) and reported in ^{14}C years BP (BP = AD 1950).

1.3.5 Quality Control

In addition to the 59 collected samples, nine quality control samples were submitted as part of the analyses discussed above: five standards, three duplicates, and one blank. Duplicates were taken from random locations, blanks were composed of ultrapure distilled and deionized water, and standards included various certified references materials and spiked standards.

The quality of chemical analyses was verified for each site by calculating the charge balance error (CBE). As per Freeze and Cherry (1979), aqueous solutions are electrically neutral due to the fact that positive charges from cations are balanced by the negative charges of anions. CBE is calculated using equation 1.1:

$$(1.1) \quad \% \text{ CBE} = \frac{\sum(z*m)cations - \sum(z*m)anions}{\sum(z*m)cations + \sum(z*m)anions} \text{ x } 100$$

Where z is the charge (eq/mol) and m is the molality (mol/kg) of the element in question. A positive CBE indicates cation excess, while a negative CBE indicates anion excess. Samples exhibiting a charge balance larger than ±10% were rejected from the final dataset. Of the 59 analyzed samples, the CBE was > ±10% for eight samples, all of which displayed an anion excess. These samples are 16-AG-703, 16-AG-705, 16-AG-707, 16-AG-734, 16-AG-736, 16-AG-753, 16-AG-755, and 16-AG-761. No sample exceeded a CBE of ± 16.66%.

1.4 References

Andersen, S., Guan, H.X., Teng, W.P., and Laurberg, P. (2008). Speciation of iodine in high iodine groundwater in China associated with goiter and hypothyroidism. *Biological Trace Element Research* 128: 95–103

Armstrong, D.K. and Dodge, J.E.P. (2007). Paleozoic geology of southern Ontario. *Ontario Geological Survey*, Miscellaneous Release—Data 219. ISBN 978-1-4249-4526-9.

Bélanger, R. 2008. *Urban Geology of the National Capital Area*. *Geological Survey of Canada*, Open File Report 5311. https://doi.org/10.4095/226165

Chapuis, R., and Saucier, A. 2013. A Leaky Aquifer below Champlain Sea Clay: Closed-Form Solutions for Natural Seepage. *Groundwater*, 51(6):960-967.

Charron, J.E. (1975). A study of groundwater flow in Russell County, Ontario. Environment Canada, Inland Waters Dir. Sci. Ser. No. 40, 26 pp.

China Ministry of Health 2003. Classification of areas with high iodine in water and endemic areas of goiter; China National Standard GB/T 19380-2003, p.1-2 [in Chinese with English abstract].

City of Ottawa. 2011. "Characterization of Ottawa's watersheds: an environmental foundation document with supporting information base". Retrieved online from: http://ottawa.ca/cs/groups/content/@webottawa/documents/pdf/mdaw/mdgy/~edisp/cap083402.pdf on July 19, 2017.

Cloutier, V., Lefebvre, R., Savard, M., Bourque, E., and Therrien, R. (2006). Hydrogeochemistry and groundwater origin of the Basses-Laurentides sedimentary rock aquifer system, St. Lawrence Lowlands, Québec, Canada. *Hydrogeology Journal*, 14(4): 573-590.

Cloutier, V., Lefebvre, R., Savard, M., and Therrien, R. (2010). Desalination of a sedimentary rock aquifer system invaded by Pleistocene Champlain Sea water and processes controlling groundwater geochemistry. *Environmental Earth Sciences*, 59(5): 977–994.

Crann, C.A., Murseli, S., St-Jean, G., Zhao, X., Clark, I.D., and Kieser, W.E. (2017). First status report on radiocarbon sample preparation at the A.E. Lalonde AMS Laboratory (Ottawa, Canada). *Radiocarbon* 59(3): 695–704.

Cummings, D. I., Gorrell, G., Guilbault, J. P., Hunter, J. A., Logan, C., Ponomarenko, D., and Sharpe, D. R. (2011). Sequence stratigraphy of a glaciated basin fill, with a focus on esker sedimentation. *Bulletin of the Geological Society of America*, *123*(7–8), 1478–1496.

Di Iorio, T., Lemieux, A.J. and Hamilton, S.M. 2015. Township of Alfred and Plantagenet groundwater study; in Summary of Field Work and Other Activities 2015, Ontario Geological Survey, Open File Report 6313, p.38-1 to 38-6. ISBN 978-1-4606-6803-0.

Dia, A. N., Castrec-Rouelle, M., Boulègue, J., and Comeau, P. (1999). Trinidad mud volcanoes: Where do the expelled fluids come from? *Geochimica et Cosmochimica Acta*, 63(7–8): 1023–1038.

Dyke, A.S., Andrews, J.T., Clark, P.U., England, J.H., Miller, G.H., Shaw, J., and Veillette, J.J. 2002. The Laurentide and Innuitian ice sheets during the Last Glacial Maximum. *Quaternary Science Reviews*, 21(1-3): 9-31.

Environment Canada. 2013. "Groundwater – Nature's Hidden Treasure". Retrieved online from: http://www.ec.gc.ca/water/en/info/publs/FS/e_FSA5.html on July 19, 2017.

Environment Canada. 2017. Ottawa Macdonald-Cartier International Airport Climate Station: Canadian Climate Normals 1981-2010. Retrieved online from: http://climate.weather.gc.ca/climate_normals/results_1981_2010_e.html?stnID=4337&autofwd=1on July 19, 2017.

Fehn, U., Snyder, G. T., Matsumoto, R., Muramatsu, Y., and Tomaru, H. (2003). Iodine dating of pore waters associated with gas hydrates in the Nankai area, Japan. *Geology*, 31(6): 521–524.

Freckelton, C.N. and Hamilton, S.M. 2012. Ambient Groundwater Geochemistry Project of the Ottawa–St. Lawrence River area; in Summary of Field Work and Other Activities 2012, Ontario Geological Survey, Open File Report 6280, p.37-1 to 37-7. ISBN 978-1-4606-0489-2.

Freeze, R.A., and Cherry, J.A. *Groundwater*. New Jersey: Prentice-Hall, 1979. Print. ISBN 978-0133653120

Fulton, R. (1987). Quaternary Geology of the Ottawa Region, Ontario and Quebec. *Geological Survey of Canada*, Paper 86-23**.** https://doi.org/10.4095/122374

Gadd, N.R. (1986). Lithofacies of Leda clay in the Ottawa basin of the Champlain Sea: Geological Survey of Canada Paper 85-21, 44 p. ISBN 0-660-12089-5.

Gao, C., Shirota, J., Kelly, R. I., Brunton, F.R. and van Haaften, S. 2006. Bedrock topography and overburden thickness mapping, southern Ontario; Ontario Geological Survey, Miscellaneous Release—Data 207. ISBN 1-4249-2550-9.

Hamilton, S.M., Brauneder, K. and Mellor, K.J. 2007. The Ambient Groundwater Geochemistry Project—southwestern Ontario; *in* Summary of Field Work and Other Activities, 2007, Ontario Geological Survey, Open File Report 6213, p.20-1 to 20-9.

Hamilton, 2015. Identifying areas of inferred risk of elevated iodine in groundwater in eastern Ontario. Unpublished Ontario Geological Survey report, 6 p.

Health Canada (2017). Guidelines for Canadian Drinking Water Quality—Summary Table. Water and Air Quality Bureau, Healthy Environments and Consumer Safety Branch, Health Canada, Ottawa, Ontario.

Hinton, M. J., Alpay, S., and Logan, C., 2011. Stop 1.2B. Hydrogeology; In: Deglacial history of the Champlain Sea basin and implications for urbanization. Russell, H.A.J., Brooks, G.R. and Cummings, D.I. (Editors), Joint annual meeting GAC-MAC-SEG-SGA, Ottawa, Ontario, May 25-27, 2011, Field Guide Book, p. 30-35. Geological Survey of Canada, Open File 6947

Johnson, M.D., Armstrong, D.K., Sandford, B.V., Telford, P.G., and Rutka, M.A. 1992. Paleozoic and Mesozoic Geology of Ontario. Geology of Ontario**;** *OGS Special Volume 4, Chapter 20.* Ministry of Northern Development and Mines, 2nd edition. ISBN 978-0772989765.

Laventure, R.S., and Warkentin, B.P. 1965. Chemical properties of Champlain Sea sediments. *Canadian Geotechnical Journal,* 2: 299-308.

Lamothe, M. (1989). A new framework for the Pleistocene stratigraphy of the Central St. Lawrence Lowland. *Géographie Physique et Quaternaire*, 43(2): 119–129.

Lemieux, A.J., Clark, I.D., Hamilton, S.M., Rogerson C.M. and Kelton, D.F., 2016. The provenance of, and possible relationship between, methane and halogens in groundwater in southeastern Ontario. Ontario Geological Survey Summary of Field Work and Other Activities, 2016, p. 33.1 to 33.7. ISBN 978-1-4606-8716-1.

Lide, D. (2005). *CRC Handbook of Chemistry and Physics (85th ed.), 2004–2005:* CRC Press, New York, NY, USA. ISBN 9780849304859

McIntosh, J., Grasby, S., Hamilton, S.M., and Osborn, S.G. 2014. Origin, distribution and hydrogeochemical controls on methane occurrences in shallow aquifers, southwestern Ontario, Canada. *Applied Geochemistry*, 50: 37-52.

Ministry of the Environment (MOE). 2006. *Technical Support Document for Ontario Drinking Water Standards, Objectives and Guidelines* (ODWSOG). Ontario Ministry of the Environment, Administrative Records, Government of Ontario, Canada. PIBS 4449e01.

Montcoudiol, N., Molson, J., and Lemieux, J.-M. (2014). Groundwater geochemistry of the Outaouais Region (québec, Canada): a regional scale study. *Hydrogeology Journal* 23: 377-396.

Morton, S.R., Di Iorio, T., Hamilton, S.M. and Robin, M.J.L. 2013. Development of an aquifer mapping tool, City of Clarence–Rockland, Ontario; in Summary of Field Work and Other Activities 2013, Ontario Geological Survey, Open File Report 6290, p.40-1 to 40-7. ISBN 978-1-4606-3107-2.

Muramatsu, Y., Fehn, U., and Yoshida, S. (2001). Recycling of iodine in fore-arc areas: Evidence from the iodine brines in Chiba, Japan. *Earth and Planetary Science Letters*, 192(4): 583–593.

Nastev, M., Savard, M.M. Lapcevic, P., Lefebvre, R., and Martel, R. 2004. Hydraulic properties and scale effects investigation in regional rock aquifers, south-western Quebec, Canada. *Hydrogeology Journal*, 12(3): 257-69.

Natural Resources Canada (NRCAN). "Ontario's shale and tight gas resources". Consulted April 2, 2018. Retrieved from https://www.nrcan.gc.ca/energy/sources/shale-tight-resources/17709

Ochietti, S. 1989. Quaternary geology of St. Lawrence Valley and adjacent Appalachian subregion. In: Fulton, R.J. (Ed.), Quaternary Geology of Canada and Greenland. Geology of Canada Series, No 1, pp. 350-389. ISBN 0-660-13114-5.

Ontario Geological Survey (OGS). Ambient Groundwater Geochemistry Data in GIS format. Consulted September 26, 2016. Retrieved from http://www.mndm.gov.on.ca/en/mines-and-minerals/applications/ogsearth/ambient-groundwater-geochemistry

Ontario Geological Survey. 2010. Surficial geology of southern Ontario; *Ontario Geological Survey*, Miscellaneous Release— Data 128 – Revised**.** ISBN 978-1-4435-2482-7 [zip file].

Pack, M.A., Xu, X., Lupascu, M., Kessler, J.D., and Czimczik, C.I. 2015. A rapid method for preparing low volume CH_4 and CO_2 gas samples for ^{14}C AMS analysis. *Organic Geochemistry*, 78: 89-98.

Parent, M., and Occhietti, S. (1988) Late Wisconsinian deglaciation and Champlain Sea invasion in the St. Lawrence Valley, Québec. *Géographie physique et Quaternaire*, 42: 215–246.

Raisin River Conservation Authority (RRCA) and South Nation Conservation (SNC). 2008. Raisin-South Nation Source Protection Region: Watershed Characterization Report. Consulted September 26, 2016. Retrieved from http://yourdrinkingwater.ca/page.php?id=68

Rogerson, C.M., Kelton, D.F., Hamilton, S.M., Lemieux, A.J. and Clark, I.D., 2016. The Investigation of Groundwater as a Source of High Milk Iodine levels in Eastern Ontario Dairy Herds. Ontario Geological Survey Summary of Field Work and Other Activities, 2016, p. 34.1 to 34.6. ISBN 978-1-4606-8716-1

Rust, B.R., and Romanelli, R., 1975, Late Quaternary subaqueous outwash deposits near Ottawa, Canada, p. 177–192, *in* Jopling, A.V., and McDonald, B.C., eds., Glaciofluvial and Glaciolacustrine Sedimentation: Society for Sedimentary Geology (SEPM) Special Publication 23.

Sauriol, J. (2016). Provenance of buried esker groundwater: the case of Vars-Winchester esker aquifer, Eastern Ontario, Canada. *Hydrogeology Journal*, *24*(1), 123–139.

Sharpe, D.R. 1979: Quaternary Geology of the Merrickville Area, Southern Ontario; Ontario Geological Survey, Report 180, 54p. Accompanied by Maps 2387, 2388, scale 1:50 000. ISBN 0-7743-3558-0.

Stats Canada. 2013. “Iodine status of Canadians, 2009 to 2011”.

Stats Canada. 2016. “Community profile – 2011 census”. Consulted December 14, 2017. Retrieved from http://www12.statcan.gc.ca/census-recensement/2011/dp-pd/prof/index.cfm?Lang=E

Tavenas,F., Leblond, P., Jean, P., and Leroueil, S. 1983. The permeability of natural soft clays. Part I: methods of laboratory measurement. *Canadian Geotechnical Journal*, 20: 629-644.

Thompson, M., and Howarth, R.J. (1978). A new approach to the estimation of analytical precision. *Journal of Geochemical Exploration* 9: 23-30.

Torrance, J.K., 1988, Mineralogy, pore-water chemistry, and geotechnical behaviour of Champlain Sea and related sediments, p. 259–275, *in* Gadd, N.R., ed., The Late Quaternary Development of the Champlain Sea Basin: Geological Association of Canada Special Paper 35, 312 p. ISBN 0-919216-35-8.

WHO. (2007). Iodine deficiency in Europe: A continuing public health problem. In M. Andersson, B. de Benoist, I. Darn- ton-Hill, & F. Delange (Eds.), (pp. 1–86). France: World Health Organization, UNICEF.

2 Characterization of I and CH_4 Distribution

2.1 Introduction

This section aims to characterize the distribution of iodine (I) as iodide (I^-) and methane (CH_4) exceedances with respect to the conditions observed in the present groundwater aquifer. Comprehensive hydrogeochemical studies have been carried out in geologically similar interface aquifers affected by the Champlain Sea invasion in the St. Lawrence Lowlands (Basse-Laurentides) region in the province of Québec (Cloutier et al., 2006; 2008; 2010; Montcoudiol et al., 2014; 2015), making the groundwater flow pathways and dominant geochemical processes relatively well known. In conjunction with previous work, the aim of this section is to describe the typical hydrogeological environment in which elevated concentrations of I and CH_4 are found. The characterization of the distribution of the components of concern in this study is a critical component, as it will allow the formation of informed hypotheses regarding the mechanism(s) for I and CH_4 enrichment, in addition to their potential sources within the aquifer system. The results discussed henceforth can be found in the hydrogeochemical dataset, presented in the Appendix.

2.1.1 I

I is a member of the halogen group of elements (column VII of the periodic table), has an atomic number of 53 and a molar mass of 126.9 g/mol. Within the range of pH and oxidative-reductive conditions found at the Earth's surface or within its oceans, it is present in three oxidation states, as iodide (I^-), iodate (IO_3^-), and gaseous iodine (I_2). The Eh-pH diagram for I speciation is presented in Figure 2-1 (also known as a Pourbaix diagram), along with Eh-pH values for collected groundwater samples in the study area. The conditions indicated in the diagram suggest that all I in the present groundwater system would be present as iodide (I^-). Because it is concentrated in many organisms within the marine environment, particularly primary producers such as phytoplankton or algae, it was described by Goldschmidt (1958) as a biophilic element. Significant reservoirs of I include recent marine sediments, sedimentary rocks,

soils and oceans (Fuge, 1986). The conditions for I enrichment in groundwater will be discussed in Chapter 3 of this thesis.

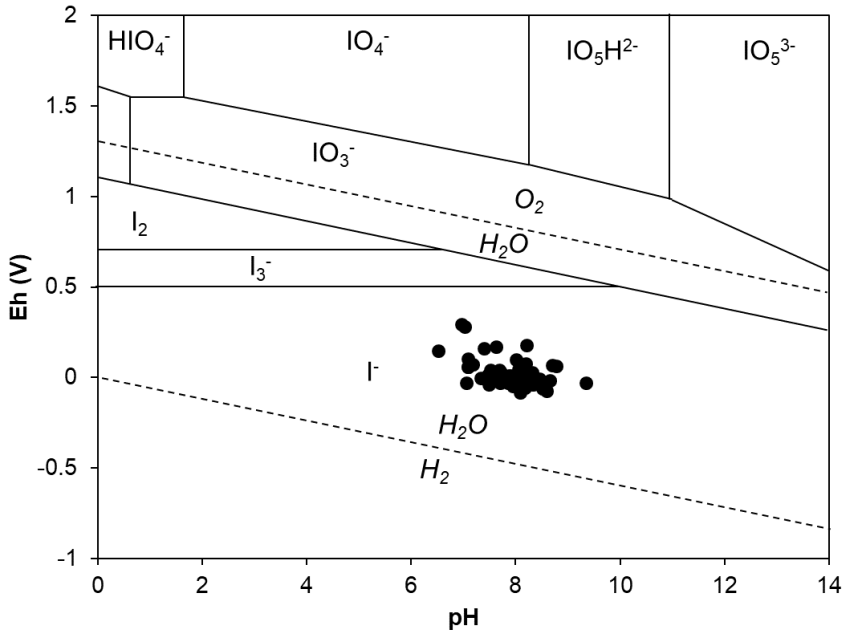

Figure 2-1. Pourbaix diagram with Eh-pH values for collected groundwater samples.

2.1.2 Methane

Methane gas (CH_4) is a reduced form of inorganic C found primarily in deep subsurface environments and is the main constituent in natural gas. It is generated via the anaerobic decomposition of organic matter through biological activity during diagenesis ("microbial" CH_4) or by the thermal decomposition of kerogen (referred to as catagenesis) as part of the post-mature stage of hydrocarbon production in sedimentary formations ("thermogenic" CH_4). Microbial methanogenesis commonly represents the last step in a series of reactions where O_2, NO_3^-, Mn^{4+}, Fe^{3+}, SO_4^{2-} and C compounds are used as terminal electron receptors in the oxidation of organic matter, based on the relative energy yield from reduction. Approximately 20% of the CH_4 gas reserves in the deep subsurface are estimated to be of microbial origin (Rice, 1993). The reduced nature of C in the CH_4 molecule makes it extremely unstable in oxidizing environments. In the atmosphere, it contributes to approximately 15% of the greenhouse effect

(Christiansen and Cox, 1995) while being present at low concentrations around 1800 ppb (IPCC, 2013). The nature of CH_4 in groundwater for the studied area will be discussed in Chapter 3.

2.2 Results and Discussion

2.2.1 Spatial distribution of components

Univariate analysis was conducted on the 59 samples collected during the summer of 2016 to elucidate the spatial trends for I and CH_4 enrichment in groundwater. The distribution of these components relative to bedrock topography and lithology, as well as the surficial geology, is presented in Figures 2-2 and 2-3. Qualitatively, it is apparent from these maps that extreme values of CH_4 (> 28 mg/L) and I (> 1 000 µg/L) are most typically observed in areas of low-lying bedrock topography, overlain by marine muds, and underlain by carbonate and shale bedrock units.

Due to the control bedrock topography exhibits on the groundwater flow in the study area (Charron, 1975), bedrock elevation was used as a proxy for distance from the recharge area (i.e. as bedrock elevation decreases, distance from the recharge area increases) in order to further explore the relationship of groundwater residence time with I and CH_4 enrichment. I concentrations in groundwater tend to increase as bedrock elevation decreases (Figure 2-4), implying that the highest concentrations would be observed in depressions in the bedrock surface. Also shown in Figure 2-4 is the positive relationship between I concentrations with respect to overburden (unconsolidated glacial sediment) thickness, which represents the combined thickness of the tills, subaqueous outwash deposits, glaciomarine muds, and nearshore sands. These relationships suggest that I is enriched in groundwater as it travels along the interface flowpath and residence times increase. Relationships between CH_4, bedrock topography, and overburden thickness, although somewhat present, are not particularly instructive. This suggests that while CH_4 may be enriched as groundwater travels along interface flowpaths, there may be other factors affecting its spatial distribution.

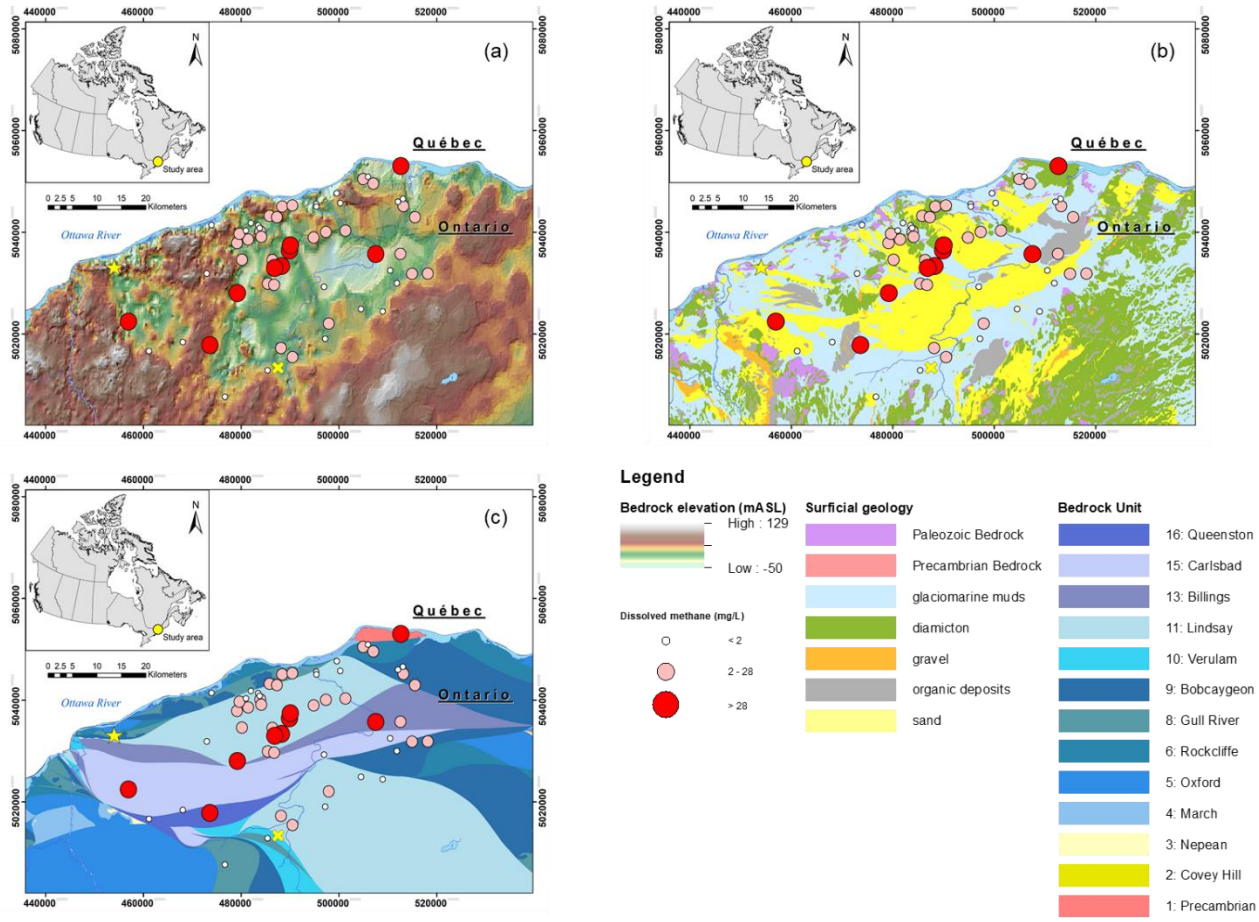

Figure 2-2. Location of groundwater samples and CH_4 concentrations relative to (a) bedrock topography, (b) surficial geology, and (c) bedrock lithology. Star represents Green's Creek site where mud samples were collected, whereas X represents Embrun sample site. Universal Transverse Mercator (UTM) co-ordinates provided using North American Datum 1983 (NAD83) in Zone 18N. *Map data acquired from OGS MRD 219 (Armstrong & Dodge, 2007), 207 (Gao et al., 2006) & 128 (OGS, 2010).*

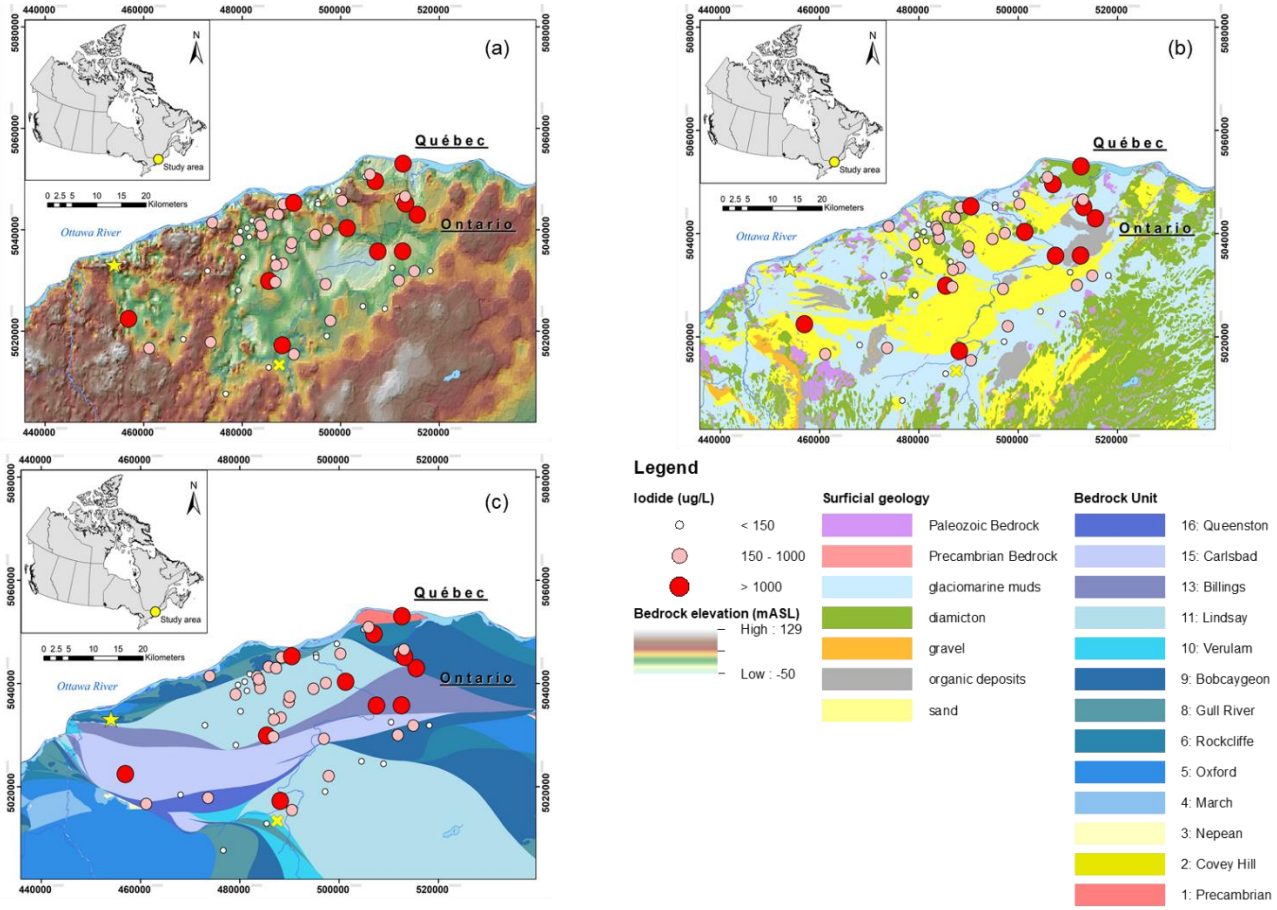

Figure 2-3. Location of groundwater samples and I concentrations relative to (a) bedrock topography, (b) surficial geology, and (c) bedrock lithology. Star represents Green's Creek site where mud samples were collected, whereas X represents Embrun sample site. Universal Transverse Mercator (UTM) co-ordinates provided using North American Datum 1983 (NAD83) in Zone 18N. *Map data acquired from OGS MRD 219 (Armstrong & Dodge, 2007), 207 (Gao et al., 2006) & 128 (OGS, 2010).*

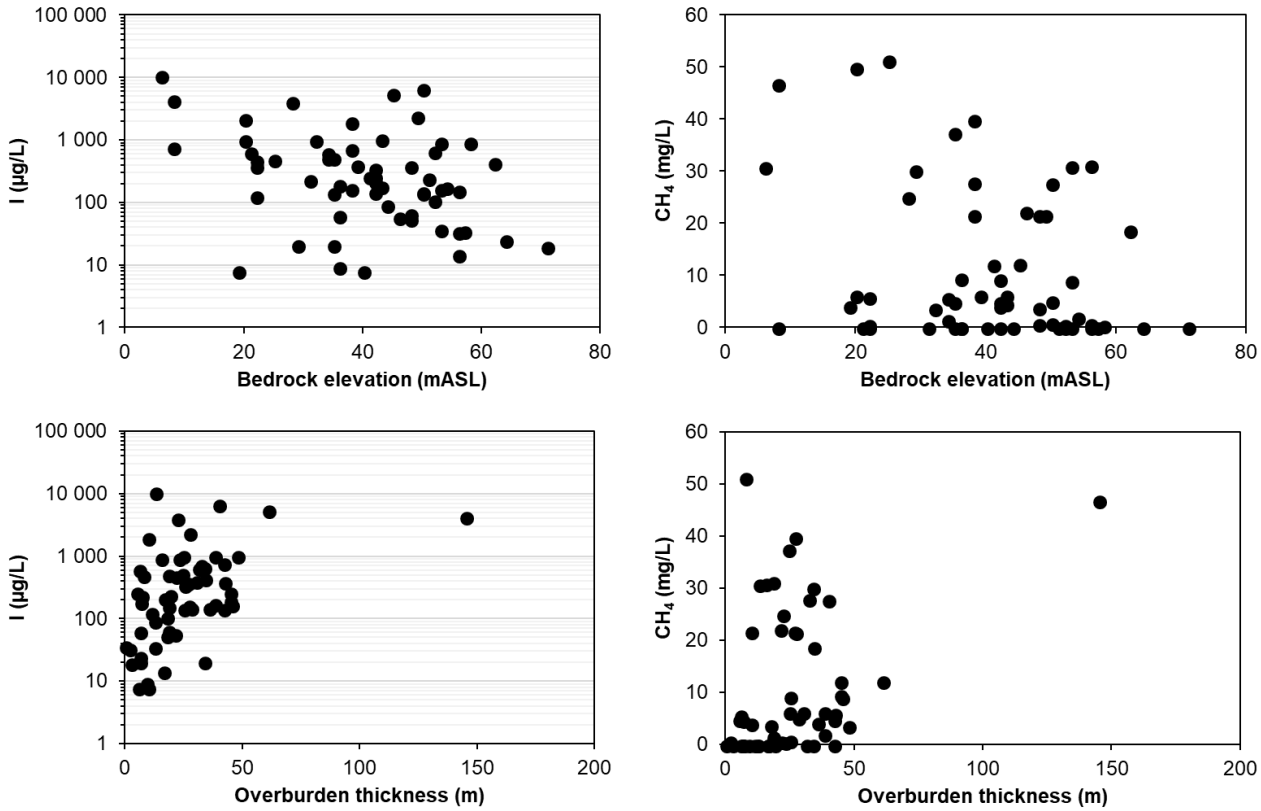

Figure 2-4. I and CH_4 concentrations relative to bedrock elevation and overburden thickness.

2.2.2 Relationship with salinization

A trend for increasing groundwater salinization as it travels along the interface flowpath was observed by Montcoudiol et al. (2015) and Cloutier et al. (2010) for analogous aquifers, where they demonstrated that groundwater geochemical facies progressed from Ca-HCO_3 to Na-HCO_3, Na-HCO_3-Cl and finally Na-Cl with increasing distance from the recharge areas. The main groundwater processes driving the transition from Ca-HCO_3 to Na-HCO_3 are ion exchange ($Ca^{2+}\leftrightarrow 2Na^{+}$) with the glaciomarine muds and subsequent carbonate dissolution due to the loss of Ca and Mg from solution from ion exchange, whereas the evolution of Na-HCO_3 to Na-Cl groundwater groups is mainly attributed to mixing with fossil Champlain Sea water (Cloutier et al., 2010).

The boxplots presented in Figure 2-5 demonstrate that the enrichment of I and CH_4 is concurrent with the transition from Ca-CO_3 to Na-Cl type groundwaters, with median values

below drinking water limits (< 150 µg/L I, < 2 mg/L CH_4) for Ca-HCO_3 (n = 6) groundwaters, intermediate concentrations in Na-HCO_3 (n = 14) and Na-HCO_3-Cl (n = 27) groundwaters, and most extreme values (> 1 000 µg/L I, > 28 mg/L CH_4) in Na-Cl (n = 12) groundwaters. It is important to recognize that this trend is more apparent for I, whereas CH_4 exhibits extreme values (> 28 mg/L) in Na-HCO_3 and Na-HCO_3-Cl waters in addition to Na-Cl waters.

Comparing the halide ratios attained in Na-Cl type waters, it is possible to observe that the Cl/Br ratio is similar to that of seawater, representative of remnant Champlain Sea water (table 1). However, considering the Cl/I and Br/I ratios, it appears that they are far below what would be expected if all I in the system were derived from seawater. In fact, Cl/I and Br/I ratios suggest that the fossil seawater has been enriched in I by a factor of approximately 150. The mechanism and source for this enrichment shall be further discussed in Chapters 3 and 4 of this thesis.

Table 1. Comparison of observed halide ratios with seawater values

Ratio	Average observed value	Seawater[1]
Cl/Br	290	288
Cl/I	1 900	300 000
Br/I	8	1 200

[1] values from Fabryka-Martin et al. (1991)

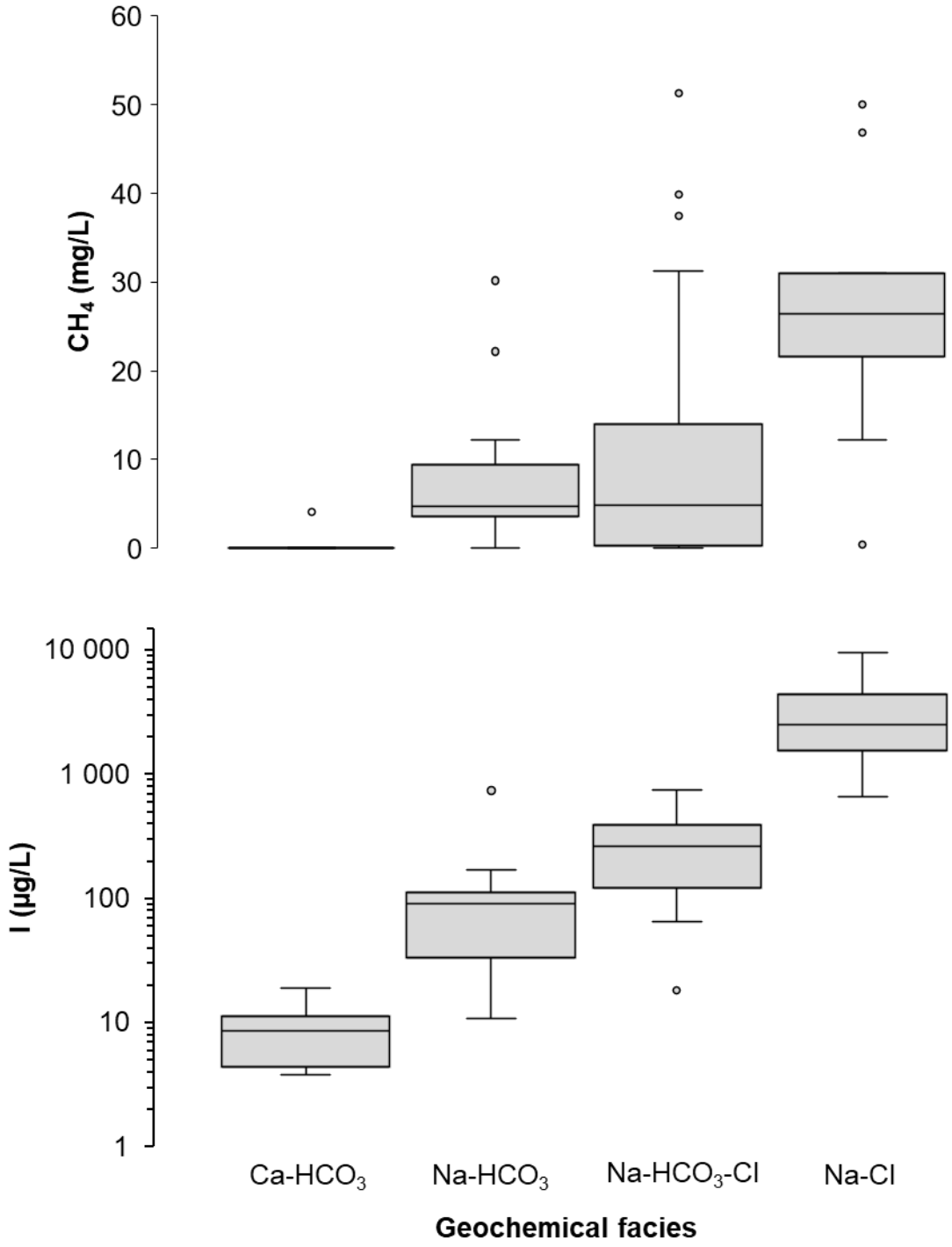

Figure 2-5. Box-and-whisker plots representing I and CH_4 concentrations relative to the four different groundwater geochemical facies observed: Ca-HCO_3, Na-HCO_3, Na-HCO_3-Cl, and Na-Cl.

2.2.3 Significance of bedrock lithology

I and CH_4 concentrations were compared to the representative geological unit sampled, which include limestone (n = 41), unconsolidated glacial and glaciomarine sediment (n = 11), shale (n = 6), and sandstone (n = 1) units. The box-and-whisker plots are shown in Figure 2-6. The highest median concentrations of I and CH_4 are observed in samples from shale units (27.9 mg/L and 1 544 µg/L, respectively), in addition to the largest interquartile ranges. Comparing the proportions observed for samples derived from limestone and glacial sediment units, they appear similar for I, whereas higher values of CH_4 appear to be observed in limestone units.

While high I in groundwaters has been correlated to bedrock lithology in groundwaters sampled from shale (Lu et al., 2015; Hamilton et al., 2015), limestone, and carbonate-rich glacial sediments (Fuge and Johnson, 1986; Fuge, 2005; Voutchkova et al., 2014), evidence has been presented in this manuscript suggesting that I is enriched in groundwater as distance from recharge areas increase. In the central portion of the study area, the primary limestone (Lindsay Formation) and shale (Billings, Carlsbad and Queenston Formations) units sampled correspond spatially with areas of low bedrock topography, indicating that perhaps the distribution of I in groundwater may depend more on bedrock topography rather than lithology. This highlights the importance of the distribution of glaciomarine muds, which increase in thickness as bedrock elevations decrease. The interpretation presented here agrees with results from Cloutier et al. (2006) for a similar interface aquifer in Québec, where they demonstrated that bedrock lithology does not control major ion chemistry, and instead attributed geochemical variations to hydrogeological conditions associated with surface sediments.

The trends presented in Figure 2-6 for CH_4 indicate that concentrations are significantly higher in samples derived from limestone and shale units. This could be indicative of the presence of a thermogenic CH_4 component in groundwater in areas underlain by the Lindsay and Billings formations, which have been identified as potential natural gas source units (NRCAN, 2017). The presence of a thermogenic CH_4 component could potentially explain the less significant relationships observed between CH_4 enrichment and other spatial parameters. Significantly increasing CH_4 concentrations during the transition from Ca-HCO_3 to Na-Cl type groundwaters (Figure 2-5) are likely indicative of CH_4 enrichment processes that are independent of bedrock lithology and related to the glaciomarine muds overlying the aquifer. Thus, the CH_4

pool may represent the concurrence of two different CH_4 sources in the aquifer: natural gas and CH_4 derived from microbial activity in the glaciomarine muds.

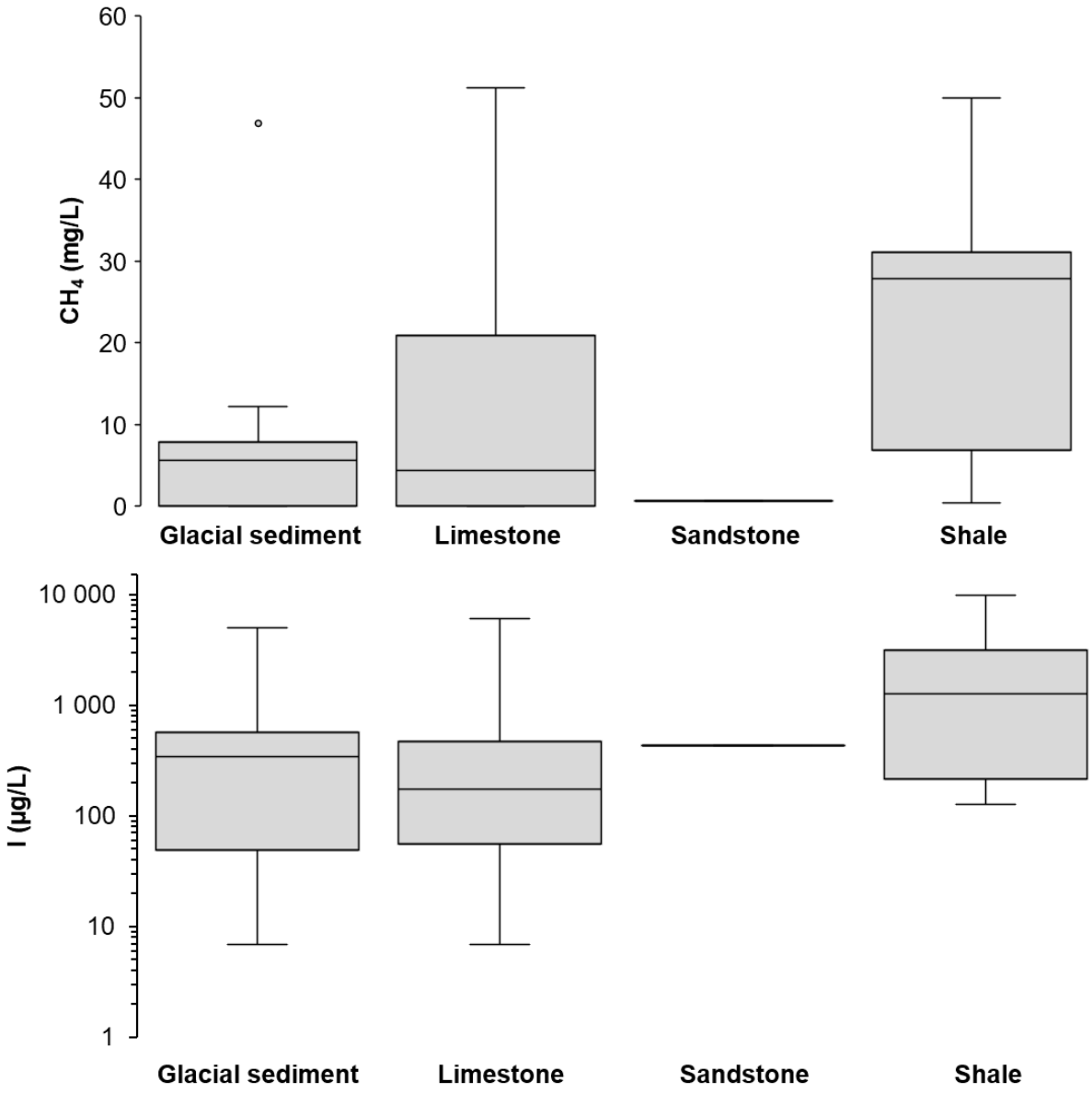

Figure 2-6. Box-and-whisker plots of I and CH_4 concentrations with respect to the geological unit sampled.

2.2.4 Redox-sensitive elements

In closed systems with an excess of organic C, O_2, NO_3^-, Mn^{4+}, Fe^{3+}, SO_4^{2-}, and C compounds are utilized as terminal electron acceptors for the oxidation of organic matter by microorganisms in the order presented here, based on the relative energy yield from reduction. As oxidants are consumed and reduced to a different oxidation state, their concentration in groundwater will decrease, with the notable exception of Mn and Fe, which are insoluble in their oxidized forms (Mn^{4+} and Fe^{3+}), but soluble in their reduced state (Mn^{2+}, Fe^{2+}). More mature systems will present a depletion in oxidants.

Figure 2-7 represents I and CH_4 concentrations vs. redox-sensitive dissolved species and indicate that higher proportions of I and CH_4 are prevalent in environments where reducing conditions dominate, exhibiting high concentrations in environments where both NO_3 and SO_4 are depleted, and where dissolved metal concentrations are high. The trends for NO_3 and SO_4 are similar for both I and CH_4, indicating that they are both sensitive to redox conditions. The trends observed for CH_4 are logical, as it is unstable (i.e. will be oxidized) in environments where significant quantities of NO_3 and SO_4 are present. Similar trends for I are interesting and demonstrate that I is enriched in environments depleted in redox-sensitive species, suggesting a link with microbial decomposition of organic matter. This will be further discussed in Chapter 3. However, the trends observed for Fe are different for I and CH_4. Whereas I concentrations appear to increase concurrently with Fe, CH_4 concentrations are high at both low and high proportions of Fe, again suggesting that the factors influencing CH_4 enrichment differ slightly from those affecting I enrichment. Additionally, this could be attributed to the inherent error associated with the headspace gas measurement method that was used to estimate CH_4 concentrations (McIntosh et al., 2014), as it does not represent a direct measurement of dissolved CH_4, but rather an estimation based on Henry's Law.

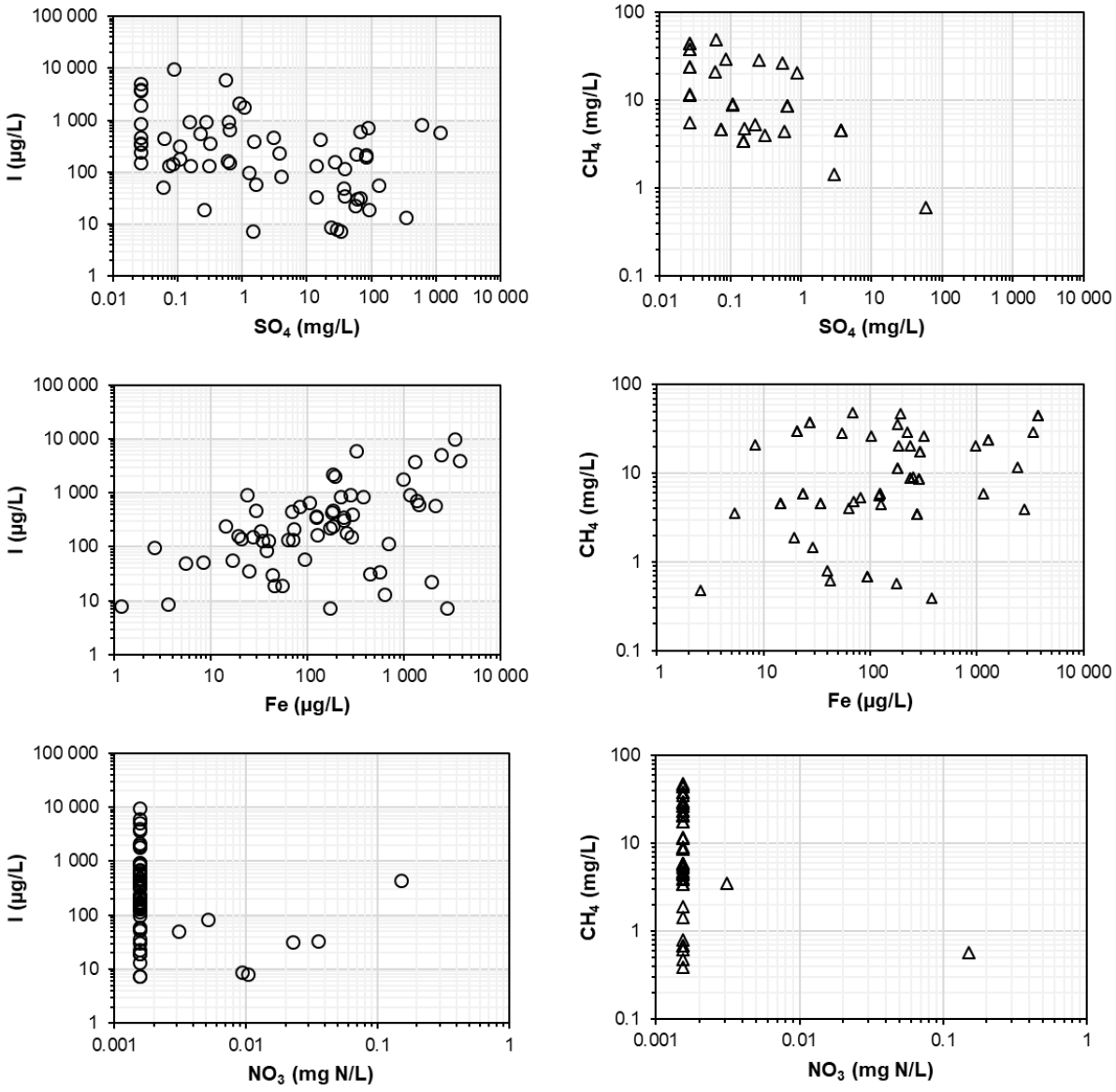

Figure 2-7. I and CH_4 concentrations vs. redox-sensitive dissolved species. I represented by open circles, CH_4 represented by open triangles. Values below detection limit for SO_4 and NO_3-N were replaced with a value of 50% of the detection limit (0.025 mg/L and 0.0015 mg/L, respectively)

2.3 Summary and Conclusions

The data presented in this section illuminates many features with respect to the hydrogeochemical characteristics of groundwater affected by I and CH_4 enrichment within the studied area in southeastern Ontario. Extreme proportions of I (> 1 000 µg/L) and CH_4 (> 28 mg/L) appear to be concentrated in areas of low bedrock elevation where aquifers are overlain by thick lenses of glaciomarine muds. The environment in these areas is highly reducing as evidenced by the prevalence of CH_4 and concurrent absence of terminal electron acceptors for microbial oxidation such as NO_3 and SO_4, and the geochemical facies of groundwater is predominantly of the Na-Cl type due to mixing with lenses of fossil Champlain Sea water and ion exchange with glaciomarine muds. Glaciomarine muds not only affect the hydrogeological conditions of the interface aquifer (unconfined, semi-confined, confined) through their varying permeabilities, but can also affect groundwater geochemistry through ion exchange, diffusion, and porewater leaching. It appears that the same processes driving the geochemical evolution and changing redox conditions of groundwater are at least partly responsible for the enrichment of I and CH_4 within the present system. However, the relationships observed for CH_4 are of less significance, and the apparent importance of bedrock lithology suggests that there may be a thermogenic CH_4 component in groundwater unrelated to the glaciomarine muds. The next section will explore this problem in depth to evaluate the hypothesis that the distribution of I and CH_4 in the study area is related.

2.4 References

Charron, J.E. (1975). A study of groundwater flow in Russell County, Ontario. Environment Canada, Inland Waters Dir. Sci. Ser. No. 40, 26 pp.

Christiansen, T.R., Cox, P., 1995. Response of methane emission from arctic tundra to climatic change: results from a model stimulation. *Tellus Series B: Chemical and Physical Meteorology* 47(B): 301–309.

Cloutier, V., Lefebvre, R., Savard, M., Bourque, E., and Therrien, R. (2006). Hydrogeochemistry and groundwater origin of the Basses-Laurentides sedimentary rock aquifer system, St. Lawrence Lowlands, Québec, Canada. *Hydrogeology Journal*, 14(4): 573-590.

Cloutier, V., Lefebvre, R., Savard, M., and Therrien, R. (2008). Multivariate statistical analysis of geochemical data as indicative of the hydrogeochemical evolution of groundwater in a sedimentary rock aquifer system. *Journal of Hydrology*, 353(3-4): 294-313.

Cloutier, V., Lefebvre, R., Savard, M. M., & Therrien, R. (2010). Desalination of a sedimentary rock aquifer system invaded by Pleistocene Champlain Sea water and processes controlling groundwater geochemistry. *Environmental Earth Sciences*, 59(5): 977–994.

Fabryka-Martin, J., Whittemore, D. O., Davis, S. N., Kubik, P. W., & Sharma, P. (1991). Geochemistry of halogens in the Milk River aquifer, Alberta, Canada. *Applied Geochemistry*, 6(4): 447–464.

Fuge, R., Johnson, C.C., 1986. The geochemistry of iodine—a review. *Environmental Geochemistry and Health* 8(2): 31–54.

Fuge, R. (2005). Soils and Iodine Deficiency. In O. Selinus, B. J. Alloway, J. A. Centeno, R. B. Finkelman, R. Fuge, U. Lindh, et al. (Eds.), *Essentials of medical geology: Impacts of the natural environment on public health* (pp. 417–433). Amsterdam: Elsevier.

Gao, C., Shirota, J., Kelly, R. I., Brunton, F.R. and van Haaften, S. 2006. Bedrock topography and overburden thickness mapping, southern Ontario; Ontario Geological Survey, Miscellaneous Release—Data 207. ISBN 1-4249-2550-9.

Goldschmidt, V.M. 1958. Geochemistry. Clarendon Press, University of California.

Hamilton, S. M., Grasby, S. E., McIntosh, J. C., & Osborn, S. G. (2015). The effect of long-term regional pumping on hydrochemistry and dissolved gas content in an undeveloped shale-gas-bearing aquifer in southwestern Ontario, Canada. *Hydrogeology Journal*, *23*(4), 719–739.

IPCC AR5 WG1 (2013). "Climate Change 2013: The Physical Science Basis - Summary for Policymakers". Retrieved online from http://www.climatechange2013.org/images/report/WG1AR5_SPM_FINAL.pdf on May 14th, 2018.

Lu, Z., Hummel, S. T., Lautz, L. K., Hoke, G. D., Zhou, X., Leone, J., & Siegel, D. I. (2015). Iodine as a sensitive tracer for detecting influence of organic-rich shale in shallow groundwater. *Applied Geochemistry, 60*, 29–36.

McIntosh, J. C., Grasby, S. E., Hamilton, S. M., & Osborn, S. G. (2014). Origin, distribution and hydrogeochemical controls on methane occurrences in shallow aquifers, southwestern Ontario, Canada. *Applied Geochemistry*, 50: 37–52.

Montcoudiol, N., Molson, J., and Lemieux, J.-M. (2014). Groundwater geochemistry of the Outaouais Region (québec, Canada): a regional scale study. *Hydrogeology Journal* 23: 377-396.

Montcoudiol, N., Molson, J., Lemieux, J. M., & Cloutier, V. (2015). A conceptual model for groundwater flow and geochemical evolution in the southern Outaouais Region, Québec, Canada. *Applied Geochemistry*, 58: 62–77.

Natural Resources Canada (NRCAN). "Ontario's shale and tight gas resources". Consulted April 2, 2018. Retrieved from https://www.nrcan.gc.ca/energy/sources/shale-tight-resources/17709

Rice, D.D., 1993. ''Biogenic'' gas: controls, habitats, and resource potential. In: Howell, D.G. (Ed.), *The Future of Energy Gases*. United States government printing office, Washington, pp. 583–606.

Voutchkova, D. D., Kristiansen, S. M., Hansen, B., Ernstsen, V., Sørensen, B. L., & Esbensen, K. H. (2014). Iodine concentrations in Danish groundwater: historical data assessment 1933–2011. *Environmental Geochemistry and Health*, *36*(6), 1151–1164.

3 Mechanisms for component enrichment

3.1 Introduction

Drawing on assertions from Chapter 2, this section explores the mechanisms for I and CH_4 enrichment using multivariate statistical analysis, descriptive statistics and isotopic data. The goal for this section is to determine which geochemical processes are responsible for the release of I and CH_4 into solution, to identify areas in which these processes would be prevalent, and finally to evaluate if these mechanisms explain the apparent relationship between I and CH_4 in groundwater.

3.2 I

The phenomenon of I enrichment in groundwater affects many regions in the world such as Japan (Kashiwagi et al., 2006; Togo et al., 2016), Denmark (Andersen et al., 2002; Voutchkova et al., 2014), China (Li et al., 2013; Zhang et al., 2013; Duan et al., 2016), and Canada (Fabryka-Martin et al., 1991; Hamilton et al., 2015). In these areas, decomposition of organic matter within marine sediments is typically one of the mechanisms invoked to explain I enrichment in groundwater (Kashiwagi et al., 2006; Li et al., 2013; Zhang et al., 2013; Hamilton et al., 2015; Duan et al., 2016). In marine or estuarine environments, I is concentrated into phytoplankton or other plants (Moisan et al., 1994) and correlates with organic matter in marine sediments (Fuge and Johnson, 1986; Malcolm and Price, 1984).

3.2.1 Principal Component Analysis

Principal Component Analysis (PCA) has previously been used to understand the correlation between chemical variables and I to infer the geochemical processes responsible for its spatial variation in groundwater in Denmark (Voutchkova et al., 2014) and China (Zhang et al., 2013; Duan et al., 2016), and was applied to the current dataset using version 3.3.1 of the programming language R (R, 2016). The procedure used to prepare the dataset for analysis resembles that of Cloutier et al. (2008) and Montcoudiol et al. (2015). Parameters were excluded

based on recommendations from Güler et al. (2002). For example, chemical parameters that were additive, redundant, measured in the field, exhibited little regional variation, and that had many (over 15% of samples) values below the detection limit or no result available were excluded. Samples exhibiting a charge balance error > ± 10% were excluded from analysis.

From the current dataset, 19 chemical parameters were retained for analysis: B, Ba, Br, Ca, Cl, DOC, F, Fe HCO_3, I, K, Li, Mg, Mn, Na, NH_4, Si, SO_4 and Sr. In total, the results from 49 of the 59 collected samples were retained for PCA. Eight samples were rejected upon the basis of charge balance error and two for multiple missing values or values below detection limit. In instances where the value of a retained chemical parameter for a given sample was below the detection limit, this value was replaced with 55% the detection limit (Sanford et al., 1993).

All variables were log-transformed. The variables were then standardized, which results in a new set of values (Z_i) with a mean of zero and is measured in units of standard deviation. This is done by subtracting the values for a given chemical parameter (x_i) of a selected sample by the mean for that set of values ($\bar{x}$), and subsequently dividing by the standard deviation (s), $Z_i = (x_i - \bar{x})/s$, where i represents the sample ID. Four principal components were retained based on the Kaiser criterion (Eigenvalue > 1), and a Varimax normalized rotation was applied to maximize perceived variance between the retained components.

3.2.2 Results and discussion

Principal components were then extracted using the Kaiser criterion, which discriminates against components that have an eigenvalue < 1. Eigenvalues are a measure of the variance explained by a component, and the Kaiser criterion is meant to distinguish the factors that significantly affect variance within the dataset from those that do not. For the current analysis, four factors were retained based on this criterion (see Table 2), accounting for 83% (36%, 18%, 15%, and 13%, respectively) of the variance for the considered dataset. Finally, a varimax normalized rotation was applied to the four retained factors to maximize the perceived variance between them.

Table 3 presents the factor loadings for the four retained parameters. Factor loadings are the correlation coefficients between variables and factors (principal components) which can vary from -1 and 1. Positive relationships are represented by positive factor loadings, and the inverse

is also true for negative relationships. Significant factor loadings (± 0.7) are highlighted in bold. Factor loadings for the first two components are presented in a bi-plot in Figure 3-1.

The first component is characterized by positive factor loadings for Na, K, HCO_3, NH_4, I, DOC, and B. These variables are either major or minor constituents of seawater, which would suggest that component 1 represents fossil Champlain Sea water. Although not significant, factor loadings > 0.60 suggest relationships with Cl, Br, and Ba, which are also constituents of seawater. Significant positive loadings for I, NH_4, K, DOC, and HCO_3 are representative of bacterial decomposition of organic matter. Decomposition in an anaerobic environment would generate CO_2, causing a corresponding rise in HCO_3 and DOC levels. The almost significant negative loading for SO_4 (-0.68), a major constituent of seawater, is suggestive of its reduction to S^{2-} by microbial respiration and precipitation along with Fe^{2+} in sediments. The positive loading for K can be explained through K release during decomposition of organic matter, as suggested by average K concentrations that exceed what would be expected with normal Cl/K ratios for seawater. Additionally, Champlain Sea muds have been found by others to have high contents of exchangeable K (Laventure and Warkentin, 1965). Anaerobic respiration would also result in the conversion of organic N to NH_4, and the conversion of organo-I to I^-, causing the enrichment of these elements in solution. Thus, component 1 can be interpreted as saline porewaters within the glaciomarine muds for which the geochemistry has been significantly influenced by anaerobic decomposition of marine organic matter enriched in I, such as phytoplankton. The high salinity of porewaters within the massive muds (Torrance, 1988), coupled with observations of hydrotroilite and evidence of bioturbation that are indicative bacterial reduction in the same massive muds (Cummings et al., 2011) suggests that I-rich saline porewater originates predominantly from the massive mud unit.

Table 2. PCA Eigenvalues, explained variance percentages, and Varimax-normalized factor loadings. Significant factor loadings (± 0.7) are highlighted in bold.

Parameter	Component 1	Component 2	Component 3	Component 4
Ca	-0.31	0.67	0.64	0.04
Mg	0.31	0.60	0.69	0.02
Na	**0.73**	0.19	0.26	0.48
K	**0.79**	0.39	0.38	0.20
HCO_3	**0.88**	-0.04	0.22	-0.15
SO_4	-0.68	0.45	0.02	-0.03
Cl	0.52	0.26	0.49	0.56
NH_4	**0.89**	0.30	0.01	0.15
Br	0.66	0.22	0.32	0.58
F	-0.04	-0.22	**-0.88**	-0.12
I	**0.84**	0.22	0.26	0.35
DOC	**0.82**	-0.17	-0.09	-0.24
B	**0.88**	0.16	-0.27	0.23
Fe	0.37	**0.76**	-0.05	-0.05
Sr	0.02	**0.79**	0.38	0.02
Si	0.19	0.18	0.01	**-0.86**
Ba	0.60	-0.01	0.55	-0.09
Li	0.30	0.43	-0.02	**0.70**
Mn	-0.04	**0.72**	0.20	0.22
Explained variance	6.86	3.51	2.92	2.51
Explained variance (%)	36	18	15	13
Cumulative variance (%)	36	55	70	83

The second component exhibits positive factor loadings for Fe, Sr, and Mn. Additionally, there are less significant positive relationships with Ca and Mg (loadings of 0.67 and 0.60, respectively). These components are likely related to the dissolution of carbonate minerals such as calcite and dolomite that are abundant in the study area due to the prevalence of carbonate bedrock formations, as well as the reductive dissolution of metal oxides. Ca, Mg, and Sr are major components of carbonate minerals. Carbonate dissolution would be exacerbated not only through ion exchange with glaciomarine muds, but also through microbial oxidation of organic matter, which would generate CO_2. Furthermore, microbial respiration would also establish the reducing conditions conducive to the dissolution of metal oxides.

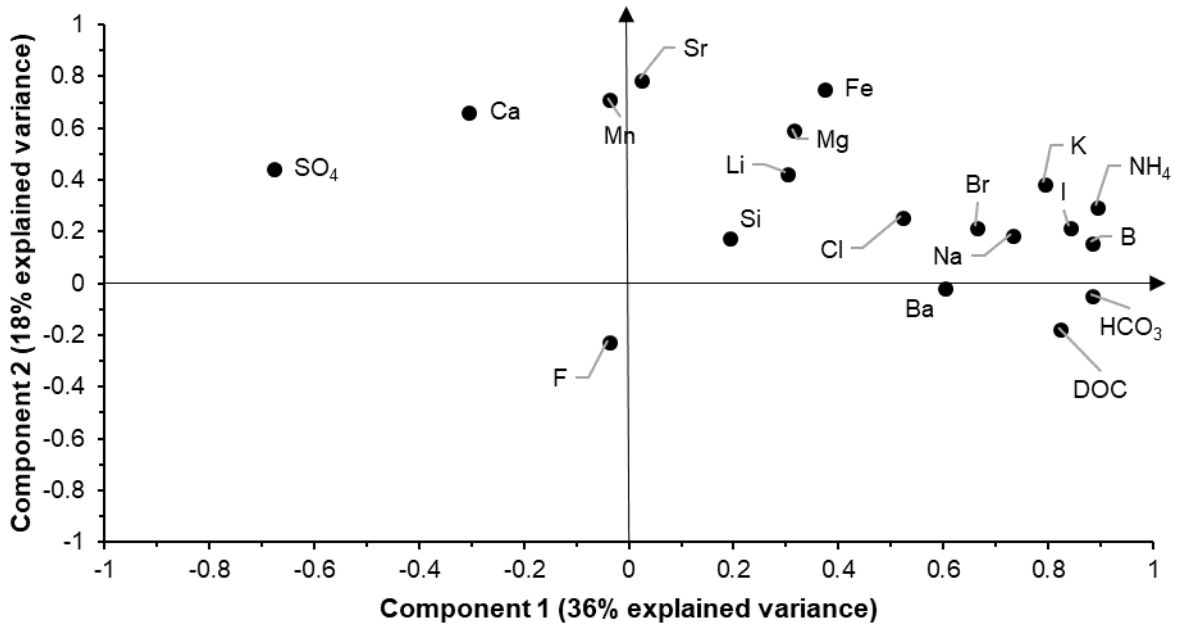

Figure 3-1. Factor loadings (after Varimax normalized rotation) for the first two components.

The third component shows a negative loading for F. The fourth component shows a negative loading for Si, and a positive loading for Li. These components do not present any significant loading for I. Coupled with the low proportion of variation within the dataset explained by these components (<15%), they were regarded as unimportant for the analysis of I enrichment.

Results from the spatial and multivariate statistical analysis demonstrate that variations in I concentrations can be attributed to the intrusion of porewater (likely through advection) from massive muds enriched with I through the decomposition of marine organic matter such as marine phytoplankton. The importance of this mechanism for I enrichment in groundwater is reported by Fuge and Johnson (1986), in a review of the geochemistry of I. These authors also reported mean I contents from 5 – 200 mg/kg sediment for recent marine sediments, which they recognized as the most enriched sedimentary reservoir for I.

3.3 CH_4

Abnormally elevated levels of CH_4 in regional aquifers has been widely studied in North America due to the recent development of the shale-gas industry. CH_4 in groundwater is primarily associated with the anaerobic decomposition of organic matter, either through biological activity ("biogenic" CH_4), or through inorganic decomposition ("thermogenic" CH_4). Biogenic, or microbial CH_4 is typically produced at shallow depths and low temperatures due to bacterial reactions in organic-rich environments. Studies have attributed CH_4 contamination in groundwater aquifers to microbial decomposition of organic matter in shallow bedrock formations, particularly shales (Osborn and McIntosh, 2010; McIntosh et al., 2014; Andrews et al., 1991, Martini et al., 1998), surficial deposits of alluvium or glacial sediment with high amounts of sedimentary organic matter (Aravena et al., 1995, Hackley et al., 1999; Ward et al., 2004; Woltemate et al., 1984), and landfills (Hughes et al., 1971; El-Fadel et al., 1997). In environments where more than one of these organic substrates are available, the sources of biogenic CH_4 has been shown to overlap. Coleman et al. (1988) provided geochemical evidence for simultaneous biogenic CH_4 contributions from the decomposition of organic matter in both shales and overlying glacial sediments.

Thermogenic CH_4 is produced at high temperatures associated with catagenetic processes in sedimentary formations, usually in deeper subsurface environments, and will migrate upwards into groundwater aquifers. Thermogenic CH_4 has been known to permeate into regional aquifers either naturally by diffusion through bedrock or by exploiting fault and fracture systems (Osborn and McIntosh, 2010; Lu et al., 2015).

In the context of regional aquifer contamination, the two formation pathways for CH_4 (microbial, thermogenic) are not mutually exclusive. Depending on local geology, it is possible for CH_4 contamination to originate from more than a single point source. For example, in areas of North America where shales are overlain by sedimentary organic matter within glacial sediments, stable isotope analysis of CH_4 has attributed contamination to the mixing of both thermogenic and microbial CH_4 (Osborn and McIntosh, 2010; Moritz et al., 2015; Martini et al., 1998). Mixing of thermogenic and microbial CH_4 has also been reported in productive natural gas basins in Siberia (Cramer et al., 1999) and Italy (Mattavelli et al., 1992). For the considered

aquifer, either thermogenic or microbial processes may contribute to the observed CH_4 enrichment. Thermogenic CH_4 may be migrating upward from the underlying black shales (Billings formation) or organic-rich limestones (Lindsay formation) that underlie a large portion of the study area (NRCAN, 2017). Béland-Otis (2012) observed and characterized shale gas from the Lindsay formation in a borehole in Russell, Ontario, approximately 50 km southwest of the studied area. Microbial CH_4 may also be generated from the in-situ fermentation of Wisconsinian-age organic matter contained within glacial sediments, or organic matter within Paleozoic sedimentary strata.

3.3.1 Methodology

There are several ways in which the mechanism for methanogenesis within a groundwater system can be deduced. Isotopic analysis of CH_4 has been shown to be an extremely useful tool when it comes to discriminating methanogenic mechanisms, and can be effectively supported with gas composition data, as well as stable isotope analysis of water and dissolved C sources. Stable isotope analysis of CH_4 ($\delta^{13}C$ and $\delta^{2}H$) was carried out for selected gaseous phase samples (n = 13 out of 19 sampled sites, see Figure 1-8 for locations). In conjunction with other qualitative gas analyses (presented in % mol fraction), isotopic data for waters ($\delta^{2}H$) and dissolved C species ($\delta^{13}C$), the results are presented below in table 3. Geochemical data for redox-sensitive species can be found in the dataset in the Appendix. Sample 16-AG-749 is a duplicate of sample 16-AG-738.

Table 3 Isotopic dataset for collected gas samples. *represents a duplicate sample from site 16-AG-738

	DOC			DIC									CH$_4$		
Sample ID	ppm C	$\delta^{13}C$ (‰)	$\delta^{2}H$ H_2O (‰)	ppm C	$\delta^{13}C$ (‰)	$\%C_2H_6$	$\%C_3H_8$	$C_1/(C_a+C_3)$	$\%CO_2$	$\%CH_4$	$\%N_2$	$\%O_2$	mg l^{-1}	$\delta^{2}H$ (‰)	$\delta^{13}C$ (‰)
16-AG-514	7.8	-26.0	-62.7	485.6	-21.1	0.00	0.00	-	0.20	56.6	48.1	0.95	12.2	-287.9	-98.4
16-AG-516	1.9	-26.9	-67.3	454.0	-15.7	0.04	0.00	1620	2.81	68.9	27.2	0.55	27.7	-284.9	-84.6
16-AG-701	6.8	-26.5	-76.7	72.8	-8.8	0.01	0.00	6378	0.04	74.6	25.1	0.49	22.1	-297.0	-60.8
16-AG-703	5.0	-28.0	-68.6	140.7	-11.8	0.00	0.00	-	0.12	75.6	20.7	0.43	46.8	-302.0	-81.7
16-AG-716	21.4	-26.3	-71.8	250.6	-17.7	0.01	0.00	7306	0.45	46.6	58.3	0.85	9.2	-342.6	-91.0
16-AG-719	7.5	-26.8	-73.3	129.4	-8.0	0.02	0.00	2995	0.09	89.2	9.4	0.21	51.2	-255.9	-52.6
16-AG-720	3.0	-27.9	-80.4	41.8	-8.2	0.02	0.00	3449	0.01	77.0	19.3	0.41	30.1	-347.0	-44.8
16-AG-723	16.6	-26.0	-69.8	182.5	-15.6	-	-	-	-	-	-	-	4.8	-	-
16-AG-726	13.2	-26.9	-72.1	216.9	-14.6	-	-	-	-	-	-	-	4.2	-	-
16-AG-732	8.8	-25.9	-69.2	164.3	-15.8	-	-	-	-	-	-	-	4.8	-	-
16-AG-736	9.2	-26.1	-74.2	115.2	-9.0	0.02	0.00	5294	0.04	84.5	13.6	0.36	39.8	-264.2	-52.6
16-AG-738	3.9	-29.7	-62.0	159.3	-5.1	0.46	0.01	186	1.34	87.5	2.6	0.08	30.8	-267.2	-59.2
16-AG-745	25.8	-26.0	-71.8	411.3	-14.2	0.02	0.00	3691	0.45	78.5	12.3	0.54	37.4	-289.8	-66.3
16-AG-746	15.4	-26.4	-72.7	338.2	-20.9	0.01	0.00	6023	0.33	64.0	38.0	0.73	18.7	-259.3	-64.9
16-AG-748	2.4	-27.8	-83.4	19.0	-20.1	-	-	-	-	-	-	-	0.41	-	-
16-AG-749*	4.2	-29.2	-56.7	226.1	-6.2	0.28	0.00	308	1.68	85.3	2.9	0.22	24.6	-272.2	-61.8
16-AG-752	6.1	-26.1	-77.7	189.2	-15.0	0.06	0.00	1021	0.21	65.2	36.0	0.67	27.8	-279.0	-66.9
16-AG-754	18.9	-26.1	-71.0	365.5	-18.3	-	-	-	-	-	-	-	6.2	-	-
16-AG-755	11.2	-26.2	-75.1	374.1	-21.0	0.02	0.00	3480	1.13	74.1	23.2	0.62	21.6	-259.9	-63.3
16-AG-794	14.6	-26.5	-70.6	340.6	-17.8	-	-	-	-	-	-	-	49.9	-	-

3.3.2 Results and Discussion

Differentiating between thermogenic and microbial pathways for methanogenesis can be accomplished through analysis of stable C and H isotopes of CH_4, and in examining the gas composition of collected gas samples. Microbial CH_4 typically exhibits $\delta^{13}C$ values below -58 ± 5‰, whereas thermogenic CH_4 usually presents a $\delta^{13}C$ signature exceeding -58 ± 5‰, (Fuex, 1977). However, microbial CH_4 with a $\delta^{13}C$ value less negative than -55‰ has been reported in numerous environments, such as hemipelagic marine sediments (Jenden and Kaplan, 1986), lacustrine sediments (Woltemate et al., 1984), and marshes (Fuex, 1977). Microbial gas contains very little higher chain hydrocarbons such as ethane (C_2H_6) or propane (C_3H_8). The proportion of higher chain hydrocarbons is commonly evaluated using the Bernard ratio, where the mol% of CH_4 in a gas sample is divided by the sum of the mol% of ethane and propane. Microbial gas commonly has Bernard ratios exceeding 1000, whereas thermogenic gas exhibits ratios typically vary from 0 to 50 (Bernard, 1976). The gases sampled as part of this study demonstrated a wide range of $\delta^{13}C$ values from -98.4 to -44.8‰, with an average value of -67.8‰, and $\delta^{2}H$ values between -347 and -256‰, with an average of -286‰. The stable isotopic and geochemical dataset can be found in table 3. Bolded sample 16-AG-749 represents a duplicate of sample 16-AG-738. A cross plot of the isotopic composition ($\delta^{13}C$, $\delta^{2}H$) of CH_4 gas samples can be found in Figure 3-2.

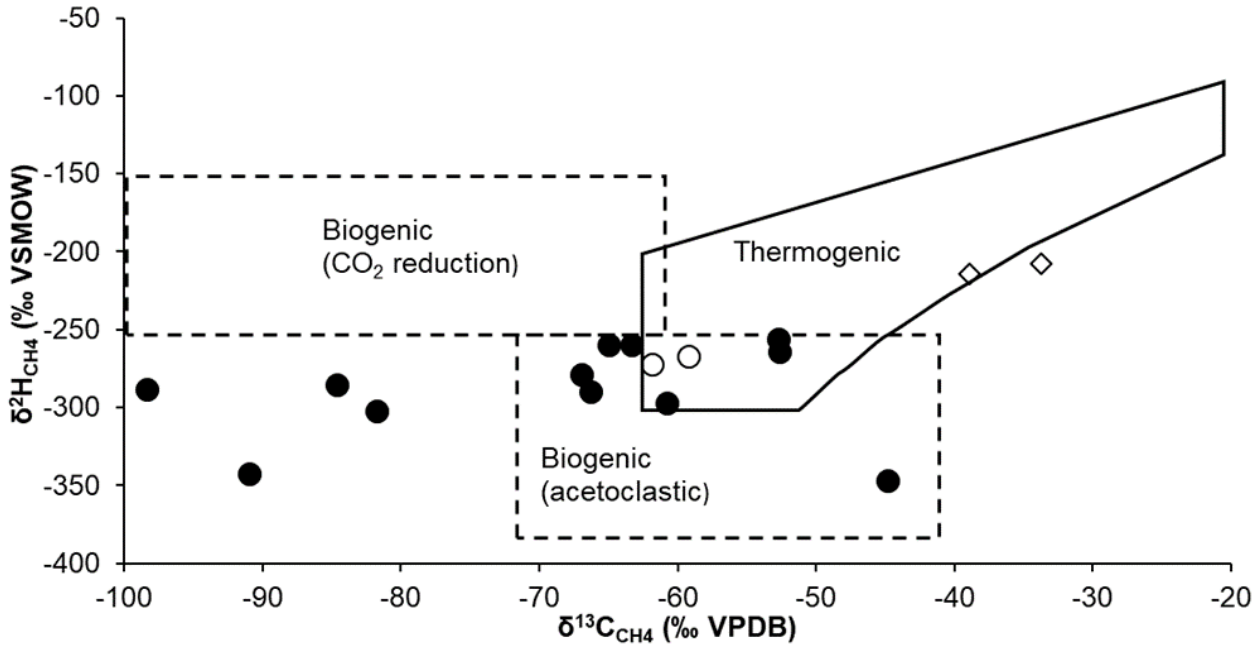

Figure 3-2. Cross plot of $\delta^{13}C_{CH4}$ vs. $\delta^{2}H_{CH4}$ for gaseous phase samples. Fields for microbial (acetoclastic and CO_2 reduction) and thermogenic CH_4 defined by Schoell (1988). Closed circles represent samples with a Bernard Ratio exceeding 10^3, whereas open circles represent a Bernard ratio between 10^2 and 10^3. Diamonds represent local thermogenic CH_4, as per Béland-Otis (2012).

Nine of thirteen collected CH_4 samples plot within the biogenic acetoclastic portion of the genetic diagram and exhibited significant overlap with the thermogenic portion. The remaining four samples show relatively depleted $\delta^{13}C$ signatures, and plot to the left of the biogenic acetoclastic area. Though the overlap with the thermogenic signature and apparent positive linear relationship between $\delta^{2}H$ and $\delta^{13}C$ values for CH_4 samples could be interpreted as potential mixing between microbial and thermogenic sources of CH_4, there are multiple lines of evidence indicating that the CH_4 is microbial in origin. Sulfate concentrations of < 10 µmol/L at sites where gaseous CH_4 samples were collected, and the presence of hydrotroilite in the massive glaciomarine mud facies (Cummings et al., 2011) suggests S in these sediments is mostly sequestered in solid form, resulting in reduced competition for methanogens. The Bernard ratios for all but one sample (16-AG-738 and its duplicate) exceeded 1000, and $\delta^{2}H$ values observed for all samples were below -250‰ – CH_4 with such an isotopic composition is rarely of thermogenic origin, and most likely microbial CH_4 (Schoell, 1980). Additionally, a two-tailed t-test revealed no significant difference ($p = 0.41$) in CH_4 concentrations for samples collected in

bedrock units with natural gas potential such as the Billings and Lindsay formations (n = 34) from other bedrock units (n = 25). However, it should be noted that only three samples were collected in wells underlain by the Billings formation, which all contained significant concentrations of CH_4 exceeding 5 mg/L. These results suggest that CH_4 concentrations are independent of bedrock lithology, with the potential exception of areas underlain by the Billings shale.

Local shale gas sampled from the Lindsay formation in Russell, Ontario (approximately 50 km southwest of the study site) by Béland-Otis (2012) exhibited $\delta^{13}C$ and $\delta^{2}H$ values between -38.9 to -33.7‰ and -214 to -208‰, respectively, with Bernard ratios close to 8. Comparing the results from Béland-Otis (2012) to the ones obtained from this study, it is possible to observe that the isotopic and quantitative compositions of the two gases are notably different. In systems where mixing between microbial and thermogenic gas is occurring, the proportion of C_2^+ gases typically exceeds 0.2 mol% and exhibits a positive relationship with the $\delta^{13}C$ signature of CH_4 (Schoell, 1983).

Considering the current data, the proportion of C_2^+ gases for collected samples was below 0.06 mol%, and no correlation between the $\delta^{13}C$ signature of CH_4 and C_2H_6 content was observed. One notable exception was sample 16-AG-738 and its duplicate, which is the only sample site underlain by the Billings shale for which gaseous phase samples were analyzed, exhibiting values of 0.46 and 0.28 mol% C_2H_6 gases, and 0.01 mol% for C_3H_8. The presence of detectable C_3H_8, in addition to the higher relative abundance of C_2H_6 to C_3H_8, is indicative of the presence of a thermogenic CH_4 component (Tissot and Welte, 1984). This suggests that mixing between microbial and thermogenic CH_4 is likely occurring in areas underlain by the Billings shale. Alternatively, the higher proportion of C_2H_6 could be attributed to diffusive loss of CH_4 by shallow migration processes in the unconsolidated sediments, resulting in an increase of the C_2^+ gas proportion in groundwater as higher-chain hydrocarbons are less mobile compared to CH_4 in the low-permeability glaciomarine mud matrix (Schoell, 1983) – however, this is much less likely. For all other collected samples, the lack of detectable C_3H_8, in addition to data presented above, indicate that CH_4 is microbial in origin.

There are two main pathways for microbial CH_4 generation: acetate fermentation (equation 3.1) and CO_2 reduction (equation 3.2).

(3.1) $CH_3COO^- + H^+ \rightarrow CH_4 + CO_2$

(3.2) $CO_2 + 4H_2 \rightarrow CH_4 + 2H_2O$

Typically, the isotopic signature for CH_4 generated via acetate fermentation is relatively depleted in δ^2H due to the fact that this pathway involves an intact transfer of the methyl group from acetate to CH_4, and thus only necessitates only one externally derived H atom, which most commonly originates from groundwater (Daniels et al., 1980). For this same reason, this also results in a more enriched $\delta^{13}C$ signature. Conversely, CO_2 reduction requires four externally derived H atoms, which would decrease the δ^2H fractionation observed between the isotopic signature for CH_4 samples and groundwater, with a relatively more depleted $\delta^{13}C$ signature. Figure 3-3 presents a comparison between the $\delta^{13}C$ signatures of CH_4 and groundwater, along with theoretical composition curves based on the C isotopic fractionation factor (α_c, see equation 3.3) associated with the two microbial CH_4 formation pathways.

(3.3) $\alpha_{DIC\text{-}CH4} = (\delta^{13}C_{DIC} + 10^3)/(\delta^{13}C_{CH4} + 10^3)$

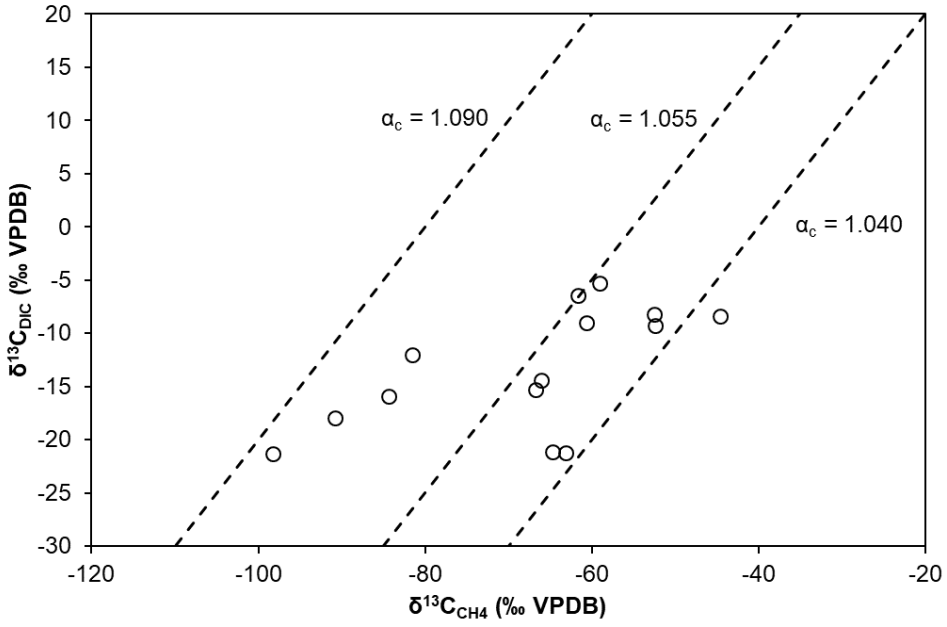

Figure 3-3. Cross plot of $\delta^{13}C_{CH4}$ and co-existing $\delta^{13}C_{DIC}$. The isotope fractionation factors (α_c) are shown for methanogenesis by CO_2 reduction ($1.090 < \alpha < 1.055$) and acetate fermentation ($1.055 < \alpha < 1.040$), derived from Whiticar and Faber (1986).

Whiticar and Faber (1986) defined the range for CO_2 reduction as $1.090 < \alpha_c < 1.055$, and the range for acetate fermentation as $1.055 < \alpha_c < 1.040$. The data in Figure 3-3 indicate that the four samples with depleted $\delta^{13}C$ signatures are generated through CO_2 reduction, and corroborates data from Figure 3-2 suggesting that the primary methanogenic pathway for the remaining 9 samples is acetate fermentation. Figure 3-4 presents $\delta^{13}C$ signatures of CH_4 and their respective N_2/CH_4 ratios. Samples affected by the presence of a hypothesized thermogenic mixing component (16-AG-738 and its duplicate) are circled and are obvious outliers to the left linear trend, due to the much lower N_2 proportions observed in thermogenic CH_4 relative to microbial CH_4. In closed groundwater systems, N_2 is most commonly derived from atmosphere and does not have any significant subsurface sources. Thus, as the system becomes more mature (i.e. more CH_4 is generated, and no more N_2 is being added), this ratio will decrease. There appears to be a transition from CO_2 reduction to acetate fermentation as the proportion of CH_4 in gaseous samples increases. The transition from the CO_2 reduction to acetoclastic methanogenic pathway in marine sediments following the SO_4-reducing phase was also observed by Alperin et al. (1992) in a laboratory microcosm. Additionally, these authors observed $\delta^{13}C_{CH4}$ signatures varying from -88 to -47‰ during the transition from CO_2 reduction to acetate fermentation phases, which roughly corresponds to the isotopic range observed for the current dataset. This, in addition to the group of samples plotting along the $\alpha_c = 1.055$ line, suggests that the wide range of isotopic signatures observed for collected CH_4 samples represents a mixture of gas from two different methanogenic pathways.

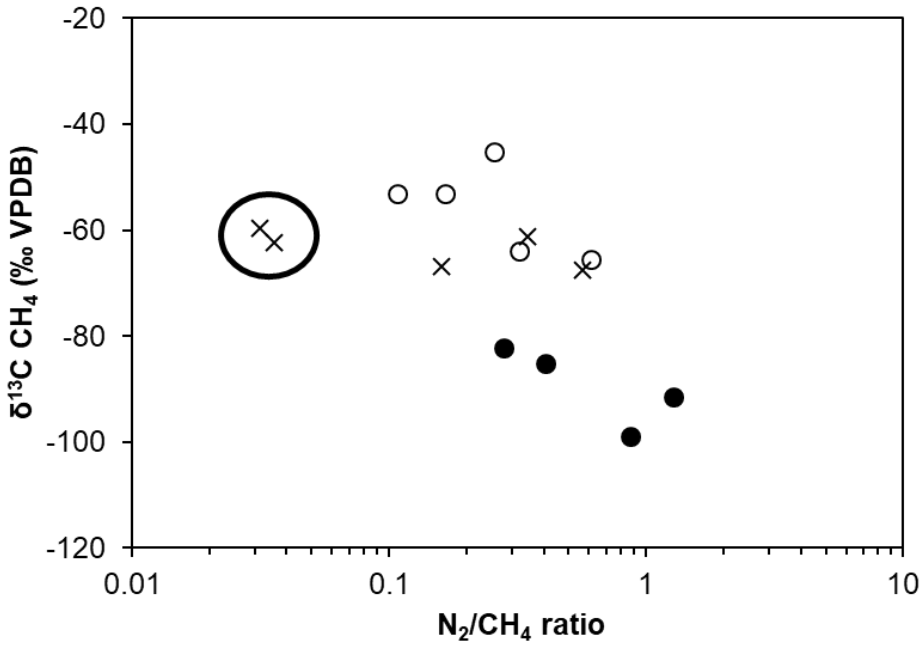

Figure 3.3-4. $\delta^{13}C_{CH4}$ vs. N_2/CH_4 molar ratios. Dominant methanogenic pathways are distinguished: acetate fermentation (open circles), CO_2 reduction (closed circles) or a mix between the two (x). Sample 16-AG-738 and its duplicate are circled.

It remains that the CH_4 generated through CO_2 reduction should plot in its corresponding portion of the genetic diagram – however, δ^2H signatures for these samples are more negative than was estimated by Schoell (1988). Sugimoto and Wada (1995) also noted depleted δ^2H signatures below -250‰ for CH_4 generated through CO_2 reduction similar to those for acetate fermentation, which they attributed to the higher H concentrations and H residence times in the freshwater environment from which the CH_4 samples were from. The negative δ^2H signatures for CH_4 samples in this data can be explained by the depletion in δ^2H for the Champlain Sea relative to the marine environment. Typical δ^2H values for marine waters vary from 0 to -20‰ (Schoell, 1980), whereas groundwaters for the studied area varied from -56.7 to -83.4‰ and are closer to modern freshwaters. This is attributed to dilution of the Champlain Sea by Pleistocene glacial meltwaters and precipitation (Cloutier et al., 2010). Thus, the isotopic similarity of the Champlain Sea to modern freshwaters would result in a more depleted δ^2H signatures for CH_4.

3.3 Conclusions

The goal of this chapter was to explore the mechanisms responsible for localized I and CH_4 enrichment in the study area. Results from a Principal Components Analysis (PCA) indicate that the proportion of I in groundwater is closely linked to mixing with fossil Champlain Sea water that has been affected by microbial decomposition of organic matter within the overlying massive glaciomarine muds. An isotopic and quantitative characterization of C pools demonstrated that CH_4 enrichment within the study area is associated predominantly with microbial processes, and also revealed evidence of a thermogenic CH_4 mixing component for sample sites underlain by the Billings shale. There is a transition from the CO_2 reduction to acetate fermentation methanogenic pathway as the relative proportion of CH_4 increases. Results presented in this section indicate that microbial decomposition of organic matter is the primary process driving the enrichment of both I and CH_4. This, in addition to a significant relationship between I and CH_4 concentrations (Spearman's coefficient of 0.62) suggests a positive monotonic relationship between the two parameters.

A particularly important question that remains unanswered is the nature of the substrate for methanogenesis: literature discussed in section 3.3 demonstrated that microbial CH_4 can originate from the fermentation of organic C from sedimentary rocks such as shales or limestones or from unconsolidated glaciomarine sediments, all of which are present in the study area. Similarly, literature discussed in section 3.2 established that I can be derived from a multitude of sources. Although PCA revealed that I enrichment is due to migration of porewater from within the massive glaciomarine muds, the source of I within these muds remains unclear. ^{14}C data for disseminated organic C within the mud matrix, DIC/DOC and CH_4 has been collected, in addition to ^{129}I analyses. Chapter 4 will aim to characterize the sources of I and CH_4 using the radioisotopic dataset.

3.4 References

Alperin, M.J., Blair, N.E., Albert, D.B., Hoehler, T.M., and Martens, C.S. (1992). Factors that control the stable carbon isotopic composition of methane produced in an anoxic marine sediment. *Global Biogeochemical Cycles,* 6(3): 271-291.

Andersen, S., Petersen, S.B., Laurberg, P., 2002. Iodine in drinking water in Denmark is bound in humic substances. *European Journal of Endocrinology* 147: 663–670.

Andrews, J. N., Drimmie, R. J., Loosli, H. H., & Hendry, M. J. (1991). Dissolved gases in the Milk River aquifer, Alberta, Canada. *Applied Geochemistry*, 6(4): 393–403.

Aravena, R., Wassenaar, L., and Barker, J. (1995). Distribution and isotopic characterization of methane in a confined aquifer in southern Ontario, Canada. *Journal of Hydrology*, 173: 51-70.

Béland-Otis, C. (2012). Potential Ordovician shale gas units in southern Ontario; *in* Summary of field work and other activities, 2012, Open file report 6280, p. 29-1 to 29-12. ISBN 978-1-4606-0489-2.

Bernard, B., Brooks, J., and Sackett, W. (1976). Natural gas seepage in the Gulf of Mexico. *Earth and Planetary Science Letters,* 31(1): 48-54.

Cloutier, V., Lefebvre, R., Savard, M., and Therrien, R. (2008). Multivariate statistical analysis of geochemical data as indicative of the hydrogeochemical evolution of groundwater in a sedimentary rock aquifer system. *Journal of Hydrology,* 353(3-4): 294-313.

Cloutier, V., Lefebvre, R., Savard, M. M., & Therrien, R. (2010). Desalination of a sedimentary rock aquifer system invaded by Pleistocene Champlain Sea water and processes controlling groundwater geochemistry. *Environmental Earth Sciences*, *59*(5), 977–994.

Coleman, D. D., Liu, C. L., & Riley, K. M. (1988). Microbial methane in the shallow Paleozoic sediments and glacial deposits of Illinois, U.S.A. *Chemical Geology*, 71(1–3): 23–40.

Cramer B., Poelchau, H.S., Gerling, P., Lopatin N. V., and Littke R. (1999). Methane released from groundwater: the source of natural gas accumulations in northern West Siberia. *Marine and Petroleum Geology*, 16(3): 225-244.

Cummings, D. I., Gorrell, G., Guilbault, J. P., Hunter, J. A., Logan, C., Ponomarenko, D., and Sharpe, D. R. (2011). Sequence stratigraphy of a glaciated basin fill, with a focus on esker sedimentation. *Bulletin of the Geological Society of America*, *123*(7–8), 1478–1496.

Daniels, L., Fulton, G., Spencer, R.W., and Orme-Johnson, W.H., 1980. Origin of hydrogen in methane produced by mehano-bacterium thermoautotrophicum. *Journal of Bacteriology,* 141: 694-698.

Duan, L., Wang, W., Sun, Y., and Zhang, C. (2016). Iodine in groundwater of the Guanzhong Basin, China: sources and hydrogeochemical controls on its distribution. *Environmental Earth Sciences*, 75:790.

El-Fadel, M., Findikakis, A. N., & Leckie, J. O. (1997). Environmental Impacts of Solid Waste Landfilling. *Journal of Environmental Management*, 50(1): 1–25.

Fabryka-Martin, J., Whittemore, D. O., Davis, S. N., Kubik, P. W., & Sharma, P. (1991). Geochemistry of halogens in the Milk River aquifer, Alberta, Canada. *Applied Geochemistry*, 6(4): 447–464.

Fuex, A.D. (1977). The use of stable carbon isotopes in hydrocarbon exploration. *Journal of Geochemical Exploration*, 7: 155-188.

Fuge, R., and Johnson, C.C. (1986). The geochemistry of iodine – a review. *Environ. Geochem. Health*. 8: 31-54.

Güler, C., Thyne, G., McCray, J., and Turner, A. (2002). Evaluation of graphical and multivariate statistical methods for classification of water chemistry data. *Hydrogeology Journal* 10(4): 455-474.

Hackley, K. C., Liu, C. L., & Trainor, D. (1999). Isotopic identification of the source of methane in subsurface sediments of an area surrounded by waste disposal facilities. *Applied Geochemistry*, 14: 119–131.

Hamilton, S. M., Grasby, S. E., McIntosh, J. C., & Osborn, S. G. (2015). The effect of long-term regional pumping on hydrochemistry and dissolved gas content in an undeveloped shale-gas-bearing aquifer in southwestern Ontario, Canada. *Hydrogeology Journal*, *23*(4), 719–739.

Hughes, G.M., Landon, R.A. and Farvolden, R.N., 1971. Hydrogeology of solid waste disposal sites in northern Illinois. Rep. SW-12D, US Environmental Protection Agency under Demonstration grant G06-EC-00006, 154 pp.

Jenden, P., and Kaplan, I. (1986). Comparison of microbial gases from the Middle America Trench and Scripps Submarine Canyon: Implications for the origin of natural gas. *Applied Geochemistry*, 1(6), 631-646.

Kashiwagi, H., Shikazono, N., Ogawa, Y., Higuchi, Y., Takahashi, M., & Tanaka, Y. (2006). Mineralogical and biological influences on groundwater chemistry of the Boso Peninsula, Chiba, central Japan: Implications for the origin of groundwater in sedimentary basins. *Geochemical Journal*, 40(4): 345–361.

Laventure, B, and Warkentin, R.S. (1965). Chemical properties of Champlain Sea sediments. *Canadian Geotechnical Journal*, 2: 299-308

Li, J., Wang, Y., Xie, X., and Gao, W. (2013). Hydrogeochemistry of high iodine groundwater: a case study at the Datong Basin, northern China. *Environmental Science Processes & Impacts*. 15(4): 848-859.

Lu, Z., Hummel, S. T., Lautz, L. K., Hoke, G. D., Zhou, X., Leone, J., & Siegel, D. I. (2015). Iodine as a sensitive tracer for detecting influence of organic-rich shale in shallow groundwater. *Applied Geochemistry*, 60: 29–36.

Malcolm, S. J., & Price, N. B. (1984). The behaviour of iodine and bromine in estuarine surface sediments. *Marine Chemistry*, *15*(3), 263–271.

Martini, A. M., Walter, L. M., Budat, J. M., Ku, T. C. W., Kaiser, C. J., & Schoell, M. (1998). Genetic and temporal relations between formation waters and biogenic methane: Upper Devonian Antrim shale, Michigan Basin, USA. *Geochimica et Cosmochimica Acta*, 62(10): 1699–1720.

Mattavelli L., Ricchiuto T., and Martinenghi C. (1992) Deep Isotopic light methane in northern Italy. *In* Bacterial Gas: Proceedings of the conference held in Milan, September 25-26, 1989 (ed. R. Vially), Editions Technip, Paris. pp. 121–132. ISBN 9782710806202

McIntosh, J. C., Grasby, S. E., Hamilton, S. M., & Osborn, S. G. (2014). Origin, distribution and hydrogeochemical controls on methane occurrences in shallow aquifers, southwestern Ontario, Canada. *Applied Geochemistry*, 50: 37–52.

Moisan TA, Dunstan WM, Udomkit A, Wong GTF. (1994). The uptake of iodate by marine phytoplankton. *Journal of Phycology*, 30:580–587.

Montcoudiol, N., Molson, J., Lemieux, J. M., & Cloutier, V. (2015). A conceptual model for groundwater flow and geochemical evolution in the southern Outaouais Region, Québec, Canada. *Applied Geochemistry*, 58: 62–77.

Moritz, A., Hélie, J. F., Pinti, D. L., Larocque, M., Barnetche, D., Retailleau, S., … Gélinas, Y. (2015). Methane baseline concentrations and sources in shallow aquifers from the shale gas-prone region of the St. Lawrence lowlands (Quebec, Canada). *Environmental Science and Technology*, 49(7): 4765–4771.

Natural Resources Canada (NRCAN). "Ontario's shale and tight gas resources". Consulted April 2, 2018. Retrieved from https://www.nrcan.gc.ca/energy/sources/shale-tight-resources/17709

Osborn, S. G., and McIntosh, J. C. (2010). Chemical and isotopic tracers of the contribution of microbial gas in Devonian organic-rich shales and reservoir sandstones, northern Appalachian Basin. *Applied Geochemistry*, 25(3): 456–471.

Sanford, R.F., Pierson, C.T., and Crovelli, R.A. (1993). An objective replacement method for censored geochemical data. *Mathematical Geology* 25: 59–80.

Schoell, M. (1980). The hydrogen and carbon isotopic composition of methane from natural gases of various origins. *Geochimica et Cosmochimica Acta.* 44(5): 649-661.

Schoell, M. (1983). Genetic characteristics of natural gases. *The AAPG Bulletin*, 67: 2225–2238.

Schoell, M. (1988). Multiple origins of methane in the Earth. *Chemical Geology,* 71(1-3): 1-10.

Sugimoto, A., and Wada, E., (1995). Hydrogen isotopic composition of bacterial methane: CO_2/H_2 reduction and acetate fermentation. *Geochimica et Cosmochimica Acta*, 59: 1329–1337.

Tissot, B., and Welte, D. (1984). Petroleum Formation and Occurrence. Springer, Berlin. ISBN 978-3-642-87813-8.

Togo, Y. S., Takahashi, Y., Amano, Y., Matsuzaki, H., Suzuki, Y., Terada, Y., Iwatsuki, T. (2016). Age and speciation of iodine in groundwater and mudstones of the Horonobe area, Hokkaido, Japan: Implications for the origin and migration of iodine during basin evolution. *Geochimica et Cosmochimica Acta, 191*, 165–186.

Torrance, J.K., 1988, Mineralogy, pore-water chemistry, and geotechnical behaviour of Champlain Sea and related sediments, p. 259–275, *in* Gadd, N.R., ed., The Late Quaternary Development of the Champlain Sea Basin: Geological Association of Canada Special Paper 35, 312 p. ISBN 0-919216-35-8.

Ward, J. A., Slater, G. F., Moser, D. P., Lin, L. H., Lacrampe-Couloume, G., Bonin, A. S., and Sherwood Lollar, B. (2004). Microbial hydrocarbon gases in the Witwatersrand Basin, South Africa: Implications for the deep biosphere. *Geochimica et Cosmochimica Acta*, 68(15): 3239–3250.

Voutchkova, D. D., Kristiansen, S. M., Hansen, B., Ernstsen, V., Sørensen, B. L., & Esbensen, K. H. (2014). Iodine concentrations in Danish groundwater: historical data assessment 1933–2011. *Environmental Geochemistry and Health*, *36*(6), 1151–1164.

Whiticar, M., and Faber, E. (1986). Methane oxidation in sediment and water column environments – Isotope evidence. *Organic Geochemistry*, 10(4-6): 759-768.

Woltemate, I., Whiticar, M., & Schoell, M. (1984). Carbon and hydrogen isotopic composition of bacterial methane in a shallow freshwater lake. *Limnology and Oceanography*, 29(5): 985–992.

Zhang, E., Wang, Y., Qian, Y., Ma, T., Zhang, D., Zhan, H., and Wang, S. (2013). Iodine in groundwater of the North China Plain: Spatial patterns and hydrogeochemical processes of enrichment. *Journal of Geochemical Exploration*, 135: 40–53.

4 Source tracing of I and CH_4

4.1 Introduction

In Chapters 2 and 3, the distribution of I and CH_4 was characterized, and the predominant geochemical mechanisms responsible for their enrichment were investigated. However, it remains to determine their origin: CH_4 could be derived from fermentation of organic matter found within the glaciomarine muds or within the shales/carbonates, and the source of I within the massive muds is poorly understood. This chapter aims to answer these questions, with the aid of compound-specific radiocarbon (^{14}C) and iodine-129 (^{129}I) data.

4.2 ^{129}I

There are two isotopes of I in the natural environment: stable ^{127}I and ^{129}I, the only long-lived radioactive isotope, which has a decay half-life on the order of 15.7 Ma. ^{129}I is produced through 3 different pathways: cosmic spallation of Xe atoms in the upper atmosphere ("cosmogenic"), from the spontaneous fission of ^{238}U ("geogenic"), and finally through nuclear activities such as nuclear power generation and nuclear bomb testing ("anthropogenic"). Since 1950, anthropogenic activities have been the dominant source of ^{129}I in the environment (Englund et al., 2008). The long half-life, in conjunction with its long residence time in the marine environment (40 000 years), would suggest that the pre-anthropogenic $^{129}I/^{127}I$ ratio would have been fairly constant, and has been estimated to be between $30 – 300 \times 10^{-14}$ based on fissiogenic and atmospheric inputs (Fabryka-Martin et al., 1985), and more recently $\sim 150 \times 10^{-14}$ based on measurements of recent marine sediments with no anthropogenic contamination (Fehn et al., 2000). Given the long half-life of ^{129}I (15.7 Ma) and the timing of the postglacial marine incursion in the study area (12 ka BP), it is expected that I derived from seawater during the Champlain Sea incursion would exhibit a $^{129}I/^{127}I$ ratio close to 150×10^{-14}.

Ages for samples from the marine environment can be calculated from measured $^{129}I/^{127}I$ ratios, using the following equation:

$$t = \ln(R_m/R_i)/-\lambda_{129}$$

Where R_m is the measured ratio, R_i is 150×10^{-14}, and λ_{129} is the decay constant of 4.41×10^{-8} y^{-1}. This equation represents a minimum age, as it does not account for geogenic inputs after the sample has been isolated from the atmosphere. Studies have used this equation to date geothermal waters (Fehn and Snyder, 2003; Fehn et al., 1992), oilfield brines (Fehn, 1990; Chen et al., 2016), and marine sediments (Fehn et al., 2000; Fehn et al., 2003).

In geological formations exceeding 100 Mya in age, the quantity of ^{129}I typically remains constant because the production rate from ^{238}U fission in the host rock is equal to the decay rate, which is referred to as secular equilibrium. Fabryka-Martin et al. (1985) calculated the estimated secular equilibrium $^{129}I/^{127}I$ ratios for I in groundwater derived from different bedrock types, which depend largely on the ^{129}I production rate (a function of the fractional ^{238}U concentration in the rock) and the leaching efficiency of produced ^{129}I from the host formation. Estimated groundwater $^{129}I/^{127}I$ values for samples derived from geological units relevant to the studied area vary from approximately 3×10^{-14} for limestones, 13×10^{-14} for clay shales, 63×10^{-14} for black shales, 320×10^{-14} for sandstones and 470×10^{-14} for crystalline granite. $^{129}I/^{127}I$ ratios for modern surface and recharge waters in North America are much higher, estimated to be on the order of 10^{-8} (Rao and Fehn, 1999; Rädlinger and Heumann, 2000) due to significant ^{129}I releases associated with nuclear activities.

4.2.1 Methodology

^{129}I analysis was carried out on n = 55 samples, the results for which can be found in Appendix F, and the locations in Figure 1-10. The results are presented as $^{129}I/^{127}I$ ratios $\times 10^{-14}$, for which error varies from ±0.1 to 2.6×10^{-14}. These results were compared to stable I concentrations and groundwater chemistry in an effort to explain the behaviour of ^{129}I in groundwater and the glaciomarine sediments within the studied aquifer.

4.2.2 Results

In Chapter 3, I in groundwater was attributed to leaching of saline porewaters enriched in by-products of organic matter decomposition within the unconsolidated massive glaciomarine muds. Figure 4-1 presents the $^{129}I/^{127}I$ ratios for collected groundwater samples relative to the expected secular equilibrium value based on the sampled geological unit. The ratios observed do

not correspond to the expected secular equilibrium values from Fabryka-Martin et al. (1985) and exhibit wide ranges regardless the samples geological unit. This would confirm that, similarly to stable I concentrations, ^{129}I values are independent of bedrock lithology.

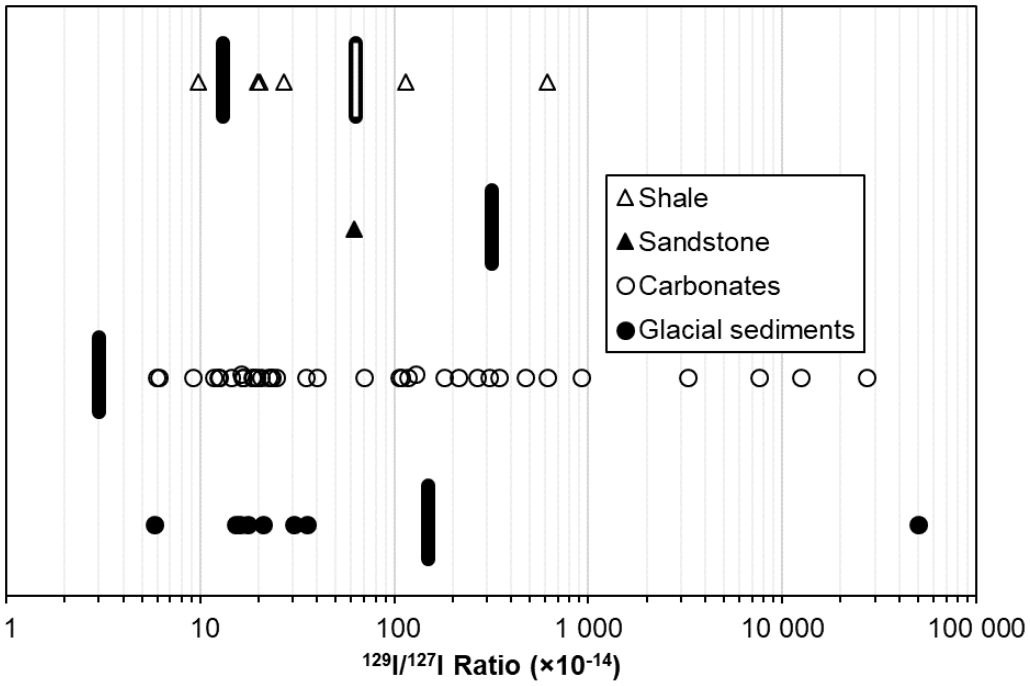

Figure 4-1. I^{129}/I^{127} ratio vs. sampled geological unit. Expected secular equilibrium values from Fabryka-Martin et al. (1985) indicated by vertical black bars for each bedrock unit. Values for shale represent both clay (13×10^{-14}) and black (63×10^{-14}) shales.

Samples were separated into two groups based on ^{3}H content, to qualitatively establish the presence of anthropogenic ^{129}I (Figure 4-2). As per Clark and Fritz (1997), groundwaters lacking detectable proportions of ^{3}H (< 0.8 T.U.) represent waters recharged prior to 1952, also referred to as "pre-modern" groundwaters, which are unaffected by anthropogenic sources of radionuclides such as ^{129}I. Conversely, samples containing detectable proportions of ^{3}H (> 0.8 T.U.) represent either recharge water dating after 1952 ("modern" groundwater) or a mix between pre-modern and modern groundwaters and would be affected by modern inputs of ^{129}I. Based on the classification from ^{3}H data, 21 samples analyzed for ^{129}I represent modern groundwater, whereas 34 represent pre-modern groundwaters.

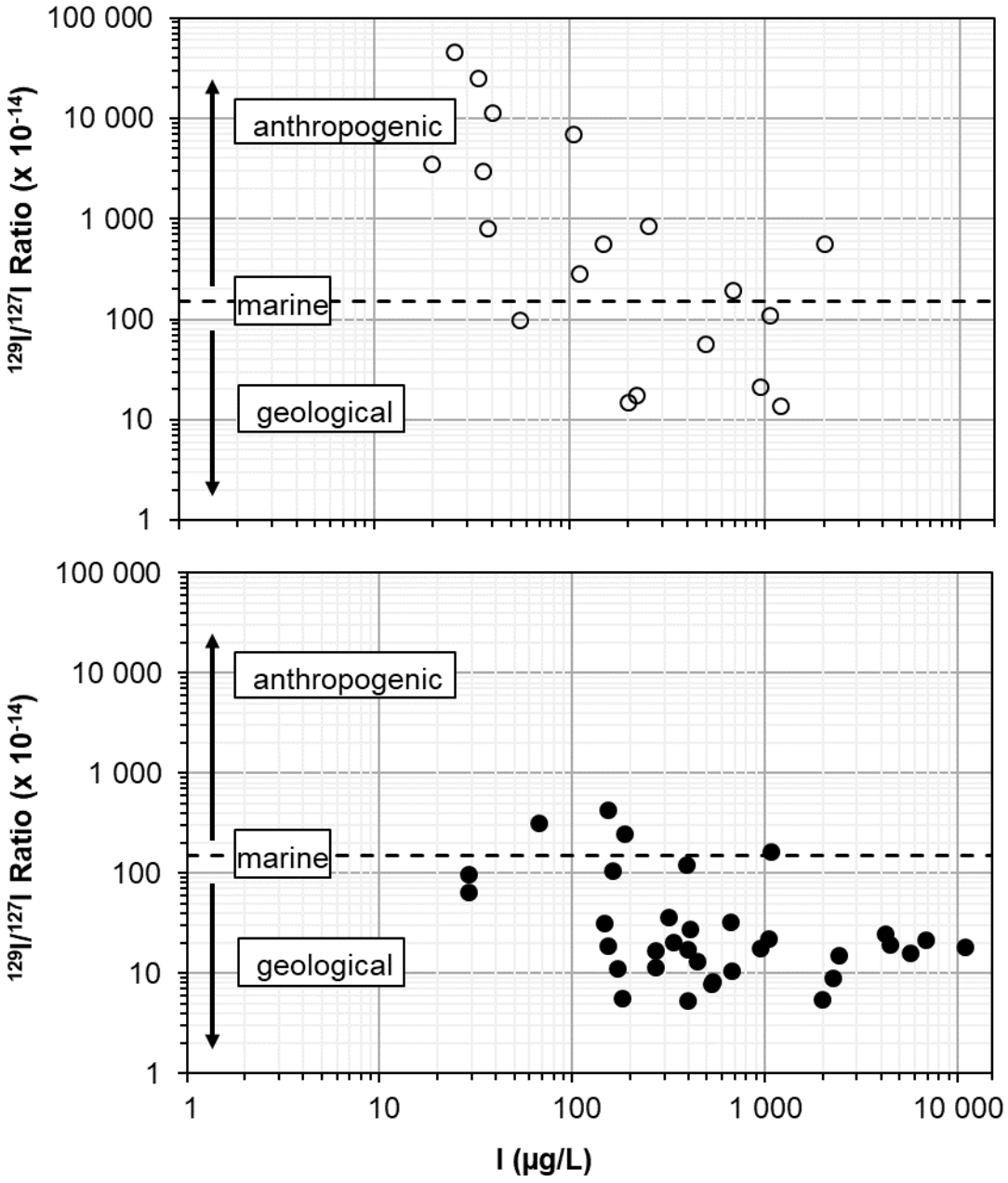

Figure 4-2. I^{129}/I^{127} ratio vs. stable I concentrations. Pre-anthropogenic I^{129}/I^{127} ratio of 150×10^{-14} indicated by the dashed line. Effect of influences from anthropogenic or geological sources of I indicated by arrows. Open circles represent samples containing ^{3}H (T.U. > 0.8), whereas closed circles represent samples that do not (T.U. < 0.8).

The data presented in Figure 4-2 demonstrate a relative decrease of the I^{129}/I^{127} ratio as I concentrations in a sample increase. Additionally, modern samples exhibited I^{129}/I^{127} ratios

which mostly exceeded the pre-anthropogenic ratio of 150×10^{-14}, whereas the I^{129}/I^{127} ratios for pre-modern samples were mostly inferior to this ratio. The higher I^{129}/I^{127} ratios for modern samples can be attributed to the contribution of anthropogenic ^{129}I from modern meteoric waters.

As I concentrations increase, the $^{129}I/^{127}I$ ratio decreases, and appears to remain constant around 20×10^{-14} after I concentrations surpass 500 µg/L, a value inferior to the pre-anthropogenic marine ratio of 150×10^{-14} expected for I in the Champlain Sea. For samples lacking ^{3}H, the $^{129}I/^{127}I$ ratio ranges from 5 to 460×10^{-14}. The range observed for $^{129}I/^{127}I$ ratios corresponds to those estimated local geological units.

The depleted isotopic signature observed for ^{129}I in groundwaters where I is derived from massive glaciomarine muds would most likely be due to the introduction of allochthonous sources of geogenic I during the Champlain Sea incursion via glacial meltwater. Cloutier et al. (2006) demonstrated that glacial meltwater was a significant component of the Champlain Sea. Modern-day analyses of glacial meltwater show that it can furnish the marine environment with important micronutrients such as Fe, DOC, NO_3, PO_4, and SiO_2, which would fertilize primary productivity (Hawkings et al., 2015; Bhatia et al., 2013; Slemmons and Saros, 2012; Hodson et al., 2004). No significant research has been conducted with respect to I loading in glacial meltwater.

PO_4 may serve as an analogue to interpret I transport in glacial meltwater. Hodson et al. (2004) remarked that PO_4 concentrations in glacial meltwater closely reflected the concentrations of underlying sedimentary units. Similarly, in an analysis of the sources of ^{127}I and ^{129}I in coastal watersheds of North America and Europe, Moran et al. (2002) demonstrated that rivers surrounded by marine shale or carbonate sedimentary terrain show higher relative I concentrations when compared to rivers surround by igneous or metamorphic bedrock. For rivers unaffected by anthropogenic point sources of ^{129}I, they observed a depletion in the $^{129}I/^{127}I$ ratio as I concentrations increased, which they attributed to the input of I derived from surrounding bedrock or soils. This is in line with conclusions from Cohen (1985) postulating that I in fresh surface waters is mainly derived from the weathering of sedimentary rocks. Sedimentary rocks such as carbonates and marine shales exhibit I concentrations with an average I content in the vicinity of 3 mg/kg (Fuge and Johnson, 1986), where most I is bound to organic matter, and contain relatively high proportions of I compared to sandstone (0.8 mg/kg) or metamorphic rocks

(0.3 mg/kg). The stable $^{129}I/^{127}I$ ratio of approximately 20×10^{-14} observed for higher proportions of I exceeding 500 µg/L suggests a significant proportion of I derived from limestone and/or shale units. I is released into solution both in its dissolved form as organic matter oxidation occurs, or as particulate organic matter during physical weathering of the rock. Conversely, the $^{129}I/^{127}I$ values exceeding the pre-anthropogenic ratio of 150×10^{-14} in the non-tritiated (pre-modern) group can be attributed to the presence of I derived from the weathering of sandstone of crystalline bedrock units.

As deglaciation proceeds, rock flour, typically of the clay and silt size fraction, is evacuated from the subglacial environment by increasing meltwater flows. In the context of the Champlain Sea, this rock flour would originate predominantly from weathering of local carbonate and shale bedrock units underlying the ice sheet. This would represent a significant input of particulate matter and limiting micronutrients into the Champlain Sea, resulting in an increase in primary production and subsequent I uptake as phytoplankton biomass increases. The ^{129}I and ^{127}I pools in massive muds containing marine organic matter would reflect the mixing of allochthonous geogenic sources exhibiting low $^{129}I/^{127}I$ ratios derived from surrounding sedimentary units with autochthonous marine sources having a pre-anthropogenic ratio of approximately 150×10^{-14}. This is also observable for modern groundwater samples, which present $^{129}I/^{127}I$ ratios as low as 10×10^{-14}. Estimating mixing proportions from each source in this instance is difficult, due to the lack of data regarding glacial meltwater fluxes and their relative I concentrations in the Pleistocene.

4.3 ^{14}C

Radiocarbon (^{14}C) is a weakly radioactive isotope of C with a half-life of 5730 years. It is naturally produced in the upper atmosphere via cosmic radiation as a ^{14}N nuclide absorbs a neutron and ejects a proton. It is then oxidized to $^{14}CO_2$ and incorporated into the global C cycle. However, nuclear testing in the modern era (post-1950) has released significant amounts of anthropogenically produced ^{14}C, increasing the total ^{14}C inventory of the atmosphere. Between 1963 and 1965, ^{14}C levels in the atmosphere were twice as high as natural levels (Nydal and Lövseth, 1965). For this reason, ^{14}C dates for organic material are reported as ^{14}C yBP (radiocarbon years before present), where t = 0 is defined as the year 1950 AD.

There are many methods to report ^{14}C data, either using the standard reporting convention for stable isotopes ($\delta^{14}C$, reported in ‰ relative to a standard), as percent modern carbon (pMC), where a measured ratio for a given sample ($^{14}C/^{12}C$) is compared to the measured ratio for a modern standard (usually oxalic acid), or as a ^{14}C age, which is obtained using the following equation:

$$\text{Age} = -8033 \times \ln(\text{pMC}/100) \text{ OR Age} = -8033 \times \ln(\delta^{14}C_{sample}/\delta^{14}C_{modern})$$

Generally, the detection limit for ^{14}C does not allow for age-dating samples older than 50 000 years. Due to varying degrees of isotopic fractionation in different organic matter substrates, ^{14}C measurements are converted to the $^{14}C/^{12}C$ ratio that would have been observed if the sample had a $\delta^{13}C$ signature of -25‰ (Aitken, 1990). While primarily used as a tool for archaeological dating, there are a multitude of applications for ^{14}C in the context of regional hydrogeology, groundwater dating, and contaminant source tracing.

4.3.1 Methodology

^{14}C analyses were carried out for n = 19 CH_4, DOC and DIC samples (see Appendix G), and n = 5 mud samples. The ^{14}C data were used to discern multiple characteristics of the groundwater system. DIC, DOC and mud ^{14}C data can be used to determine the components of their respective C pools, and CH_4 data can be used to confirm whether it is derived from decomposition of either organic matter within the glaciomarine muds or in sedimentary bedrock. Comparison of the ^{14}C data for each parameter can determine if a relationship exists between each C pool.

4.3.2 Dissolved inorganic carbon (DIC), dissolved organic carbon (DOC), and sedimentary organic C pools

Potential sources for DIC in the groundwater aquifer include: (1) dissolved CO_2 soil gases from recharge waters, (2) CO_2 derived from the decomposition of dissolved or sedimentary organic C sources within the glacial and glaciomarine sediments, and (3) HCO_3 derived from dissolution of carbonate bedrock. The DIC pool in groundwater represents the sum of CO_2, HCO_3, and CO_3 species, the proportions of which vary based on pH. Given the range of pH values observed for collected samples (see Figure 2-1), the DIC pool is expected to be predominantly comprised of the HCO_3 species. The relationship between ^{14}C ages for DIC and DOC with Cl and their respective $\delta^{13}C$ signatures is presented in Figure 4-3. Uncorrected ^{14}C ages for DIC were between 7.1 and 16.1 ka BP, with an average of 12.9 ka BP. $\delta^{13}C_{DIC}$ values range from -21.2 to -5.1‰, and do not exhibit a significant relationship with uncorrected ^{14}C ages for DIC. A lack of correlation also exists between uncorrected DOC ages with their respective $\delta^{13}C$ signatures. Uncorrected ^{14}C ages for DIC are youngest in low-salinity groundwaters, and increase to an age of approximately 15 ka BP at Cl concentrations exceeding 1000 mg/L. The same trend is observable for uncorrected DOC ages, although the average age for samples with Cl concentrations > 1000 mg/L is approximately 16 ka BP. The similarity of the trends for the DIC and DOC pools relative to Cl concentrations suggest a relationship between the two, and a prevalence of older C sources in more saline waters.

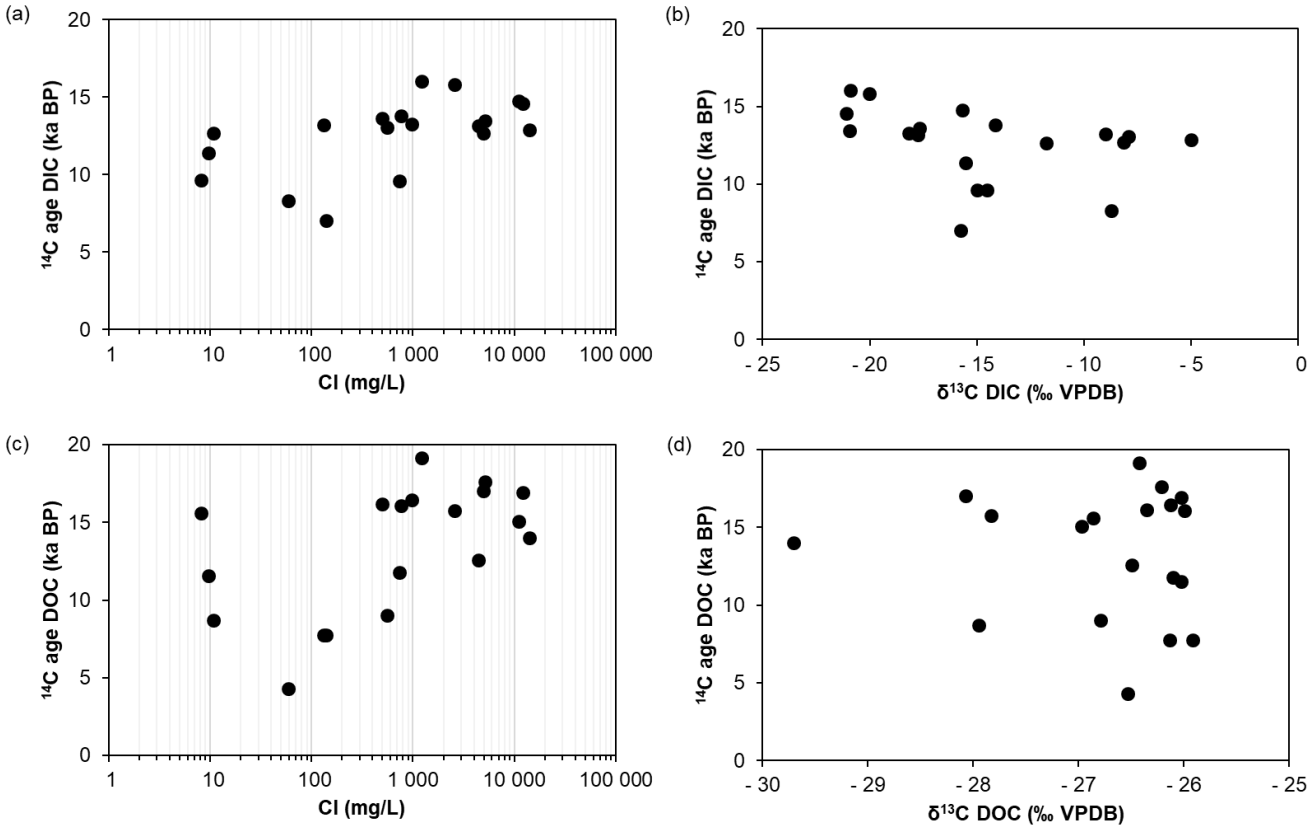

Figure 4-3. Uncorrected ^{14}C ages of DIC and DOC vs. Cl content and their respective δ^{13}C signatures. Closed circles represent DIC samples, whereas open circles represent DOC samples.

Potential sources for DOC in the aquifer include: (1) soil organic C sources from recharge waters, (2) organic matter from the Champlain Sea incursion, (3) organic matter from Early to Mid-Wisconsinian interstadial periods, and (4) ancient organic matter from Ordovician bedrock. The first two components would present detectable proportions of ^{14}C, whereas the last two would not. DOC ^{14}C ages from the current dataset vary from 4.4 – 19.3 ka BP, with an average of 13.5 ka BP. The average age corresponds to a time when the study area was still ice-covered, indicating mixing with a source of organic C which predates the Champlain Sea incursion. ^{14}C data for the disseminated organic matter within the glaciomarine muds presented in table 4 is also indicative of the presence of older organic C sources, as these ages range from 17.1 – 23.6 ka BP.

Table 4. Dataset for disseminated organic matter within glaciomarine mud. GC represents samples collected from Green's Creek, whereas EME/EMW represents samples collected in Embrun. pMC = % modern carbon

Sample ID	C:N	$\delta^{13}C$	pMC	^{14}C age	Error
	atomic ratio	‰ VPDB	%	^{14}C ka BP	± years
GC-2	8.8	-26.3	5.3	23.6	209
GC-3	8.1	-26.5	5.7	22.9	136
GC-4	8.9	-26.4	6.6	21.7	151
EME	9.4	-27.5	11.9	17.1	76
EMW	9.2	-27.2	7.8	20.5	115

The $\delta^{13}C$ signature for disseminated organic C within the mud varies between -27.5 to -26.3‰, and averages -26.7‰. Additionally, the $\delta^{13}C$ signatures for DOC in groundwater vary from -29.7 to -25.8‰, with an average value of -26.8‰.

Potential inorganic C sources within the aquifer were characterized using isotopic analyses of ^{14}C and $\delta^{13}C$. When considering the mixing dynamics of dissolved inorganic C, soil gas (or CO_2 generated from organic matter decomposition) is assumed to have a $\delta^{13}C$ signature of -25‰ with a ^{14}C content corresponding to the age of the organic matter, while carbonate is assumed to have a $\delta^{13}C$ signature of 0‰, with a negligible ^{14}C content of pMC = 0 (Pearson and Hanshaw, 1970). Groundwaters in closed systems where the two sources of DIC are at equilibrium commonly present $\delta^{13}C$ values around -12‰ for DIC.

The stable observed ^{14}C age of 15 ka BP for the DIC roughly corresponds to the Champlain Sea incursion. However, the study area was ice-covered until approximately 12 ka BP before glacial retreat (Parent and Ochietti, 1988), which would imply that ages exceeding 12 ka BP represent samples where older C sources have been added to the DIC pool. As observed in Figure 4-4, depleted $\delta^{13}C$ signatures of DIC (< -12‰) as HCO_3 concentrations increase suggests that the DIC pool is predominantly influenced by decomposition of organics (most likely in the glaciomarine sediments) rather than carbonate dissolution. Additionally, the proximity of the

uncorrected DIC ^{14}C ages to the timing of the Champlain Sea incursion indicate that DIC derived from the decomposition of contemporaneous autochthonous marine organic matter is the primary C source in the DIC pool, with minor contributions from decomposition of older sources of organic matter in saline waters (> 1000 mg/L Cl) with longer residence times.

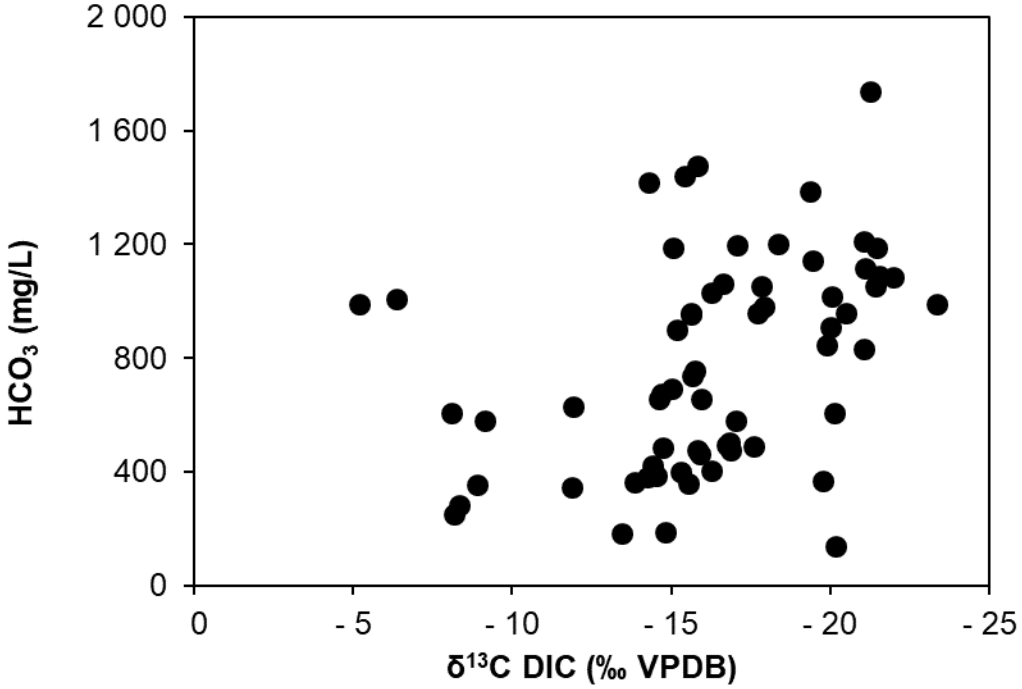

Figure 4-4. HCO_3 vs. $\delta^{13}C_{DIC}$

Following the retreat of the Champlain Sea ~10 ka BP (Parent and Ochietti, 1988) was a period of high flow for the Ottawa River as it established its main basin, lasting from 10 - 4.7 ka BP (Fulton, 1987). Evidence for these high flows is present in the study area in the form of anastomosed river valleys incised in the glaciomarine sediments. During this period of high flow, infiltration of freshwater into the interface aquifer and mixing with remnant Champlain Sea water would have occurred. No samples analyzed for ^{14}C contained any detectable proportion of ^{3}H (< 0.8 T.U.), which would preclude post-bomb sources of modern freshwater C. Thus, infiltration of freshwater from the paleo Ottawa River could potentially explain the prevalence of uncorrected ^{14}C ages < 10 ka BP in both the DIC and DOC at low proportions of Cl, as the

infiltrating freshwater would contain younger (but still sub-modern) sources of organic and inorganic C.

Stable isotopic and ^{14}C evidence for the introduction of older, allochthonous sources of organic C through glacial meltwater was presented. The average uncorrected ^{14}C ages for both DOC (13.5 ka BP) and disseminated organic C (21.1 ka BP) correspond to a time when the study area was glaciated, and the large range of observed ^{14}C ages suggest mixing between sources with varying ages. Additionally, these ages exceed ones found for local freshwater shells in Bourget, Ontario (10.2 ± 0.1 ka BP; Gadd, 1980) and a marine algal bed in Ottawa (10.8 ± 0.2 ka BP; Mott, 1968).

While C:N atomic ratios below 10 for disseminated organic C within the mud suggest that the primary source of organic matter within the glaciomarine sediments is marine phytoplankton, the $\delta^{13}C$ signatures for this organic matter and DOC are relatively depleted compared to what would be expected if organic C were derived solely from marine or estuarine phytoplankton, and overlap with the range for terrestrial C_3 vegetation (Meyers, 1994). This would suggest that mixing is occurring with an older C_3 vegetation source, most likely introduced into the marine basin through glacial meltwater following abrasion of proximal interstadial deposits (e.g. St. Pierre sediment), which would present a negligible ^{14}C signature. The presence of ancient, terrestrial organic matter in marine sediments has also been noted by Griffith et al. (2010). It is also interesting to note that the ^{14}C ages for disseminated organic matter observed here are similar to results from Silliman et al. (1996) for a sediment core in Lake Ontario, who also reported significantly older ^{14}C ages for disseminated organic matter (up to 36 ka BP) relative to ostracod shells, which they attributed to allochthonous sources of older detrital terrestrial C in the disseminated organic C pool introduced through streams and rivers. These authors also noted a trend of increasing ^{14}C ages for disseminated organic matter with depth in the sediment column. Given that the mud samples were collected at a depth of six mBGS, older ^{14}C ages of disseminated organic C would be expected as depth in the sediments increases toward the interface aquifer.

4.3.3 CH_4

Uncalibrated ^{14}C ages for CH_4 vary from 10.7 to 36.2 ka BP, with an average of 20.5 ka BP. This age range exceeds the Champlain Sea invasion (10 – 12 ka BP), and corresponds to a time when the study area was still ice-covered, and thus it is not particularly instructive because it artificially mixes CH_4 ages generated from two different pools of organic matter from during and before the Champlain Sea incursion. Considering the predominantly microbial nature of CH_4 as indicated by the stable isotopic dataset, potential organic matter sources for CH_4 include (1) the Champlain Sea incursion, (2) interstadial deposits predating the Champlain Sea, and (3) Paleozoic bedrock. The potential for production of biogenic CH_4 in Paleozoic bedrock in the study area would be restricted to the organic-rich Lindsay and Billings formations. However, the lack of a relationship between bedrock lithology and CH_4 concentrations, in conjunction with detectable proportions of ^{14}C for the CH_4 and dissolved inorganic and organic C pools and a wide range of uncalibrated ^{14}C ages of CH_4 regardless of bedrock lithology (see Figure 4-5) suggest that kerogen is an unlikely substrate for microbial methanogenesis.

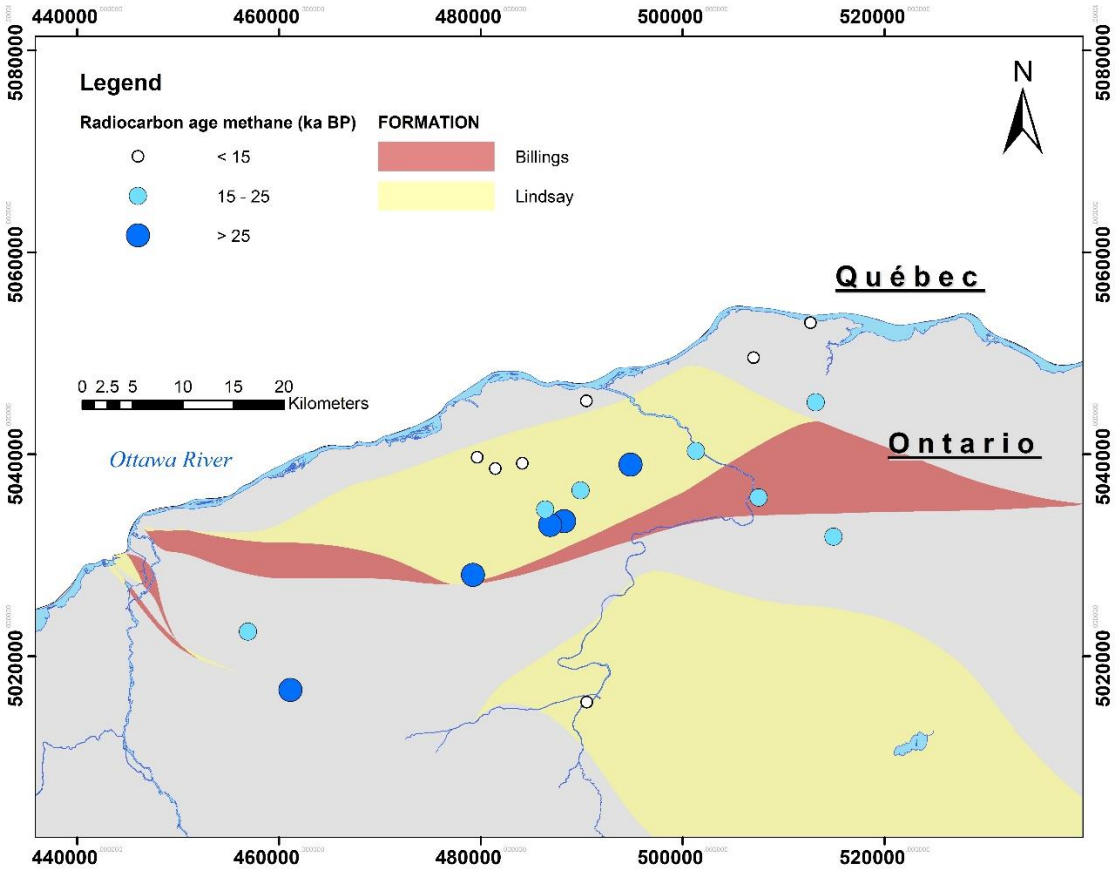

Figure 4-5. ^{14}C ages of CH_4 gas relative to spatial distribution of organic-rich bedrock units. Universal Transverse Mercator (UTM) co-ordinates provided using North American Datum 1983 (NAD83) in Zone 18N. *Map data acquired from OGS MRD 219.*

The ^{14}C ages of CH_4 and DIC/DOC are compared in Figure 4-6, in an effort to elucidate a relationship between the two. A linear relationship (as demonstrated by the dashed line in the diagram) between ^{14}C ages for DIC and CH_4 is observable for the CH_4 samples generated via CO_2 reduction (n = 4), whereas CH_4 samples generated predominantly through acetate fermentation or a mixture of both pathways (n = 9) exhibit ^{14}C ages that far exceed those of their corresponding DIC and DOC pools. This phenomenon could be a result of the fermentation of older, allochthonous organic matter within the glaciomarine muds, as it appears that samples for which the main methanogenic pathway is acetate fermentation reflect older terrestrial C sources, whereas samples for which CO_2 dominates do not.

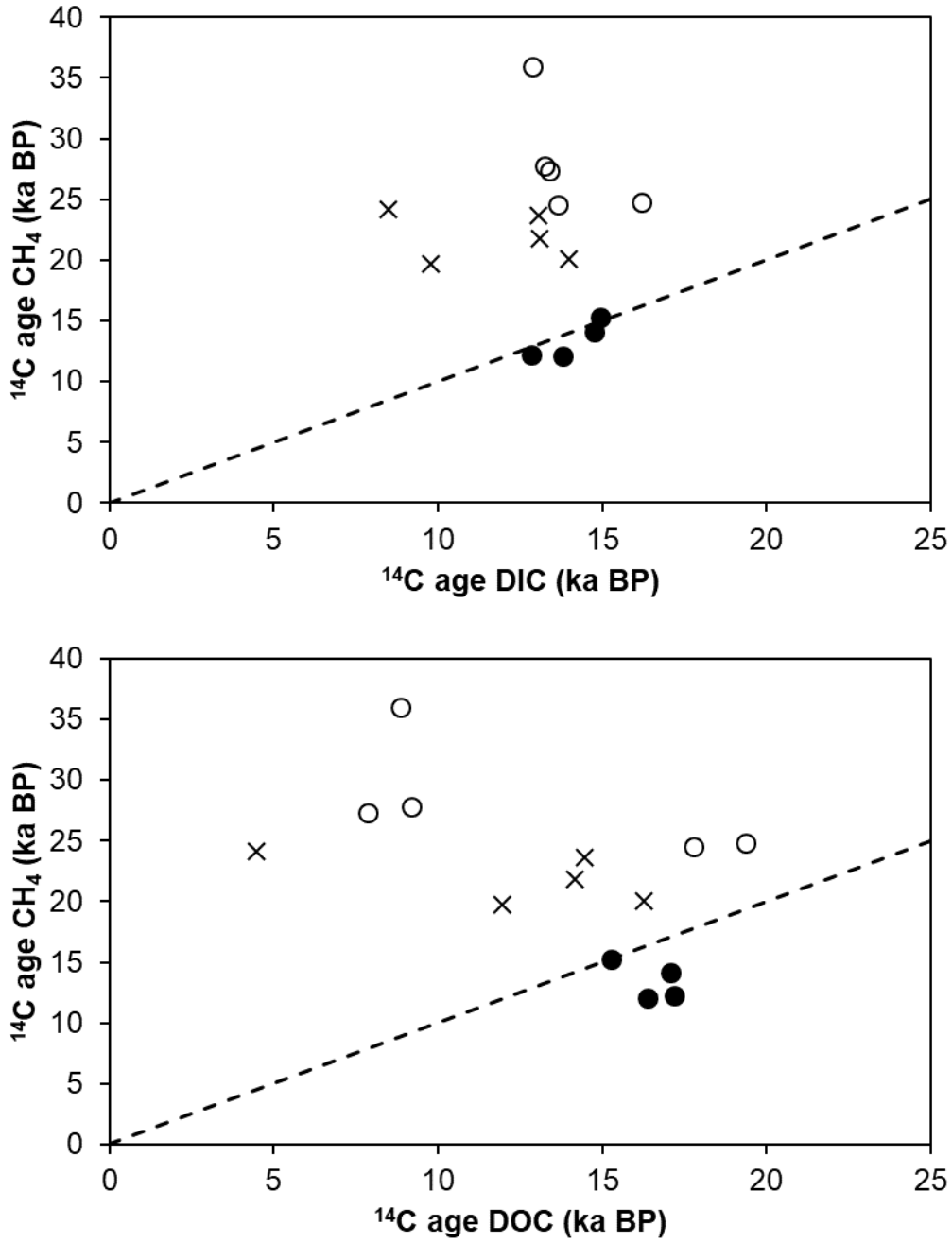

Figure 4-6. Uncorrected ^{14}C ages for DIC, DOC and CH_4 based on dominant methanogenic pathway(n = 13): acetate fermentation (open circles), CO_2 reduction (closed circles), or a mixture (x). Dashed black line represents 1:1 age line.

Decomposition rates of organic matter typically increase as N and P proportions increase, and total organic carbon (TOC): total nitrogen (TN) and TOC: total phosphorus (TP) ratios

decrease (Enriquez et al., 1993). “Labile” organic matter with low TOC/TN ratios such as marine phytoplankton breaks down more readily than “refractory” organic matter with high TOC/TN ratios, such as terrestrial plant matter (Middleburg & Nieuwenhuize, 1998). Considering the organic C pool within the glaciomarine muds, this implies that the marine phytoplankton dating from the Champlain Sea incursion would decompose preferentially, and at a faster rate, than the ancient terrestrial organic matter. Figure 4-7 presents a positive relationship between uncalibrated ^{14}C ages of CH_4 vs. concentrations. While this positive relationship could also be interpreted as representing mixing between a younger microbial end-member (~12 ka BP) and isotopically dead thermogenic CH_4, it should be noted that for all samples excluding 16-AG-738 (which overlies the Billings shale), there is no observable relationship between C_2H_6 (mol %) and ^{14}C age, indicating that mixing with a thermogenic end-member is unlikely.

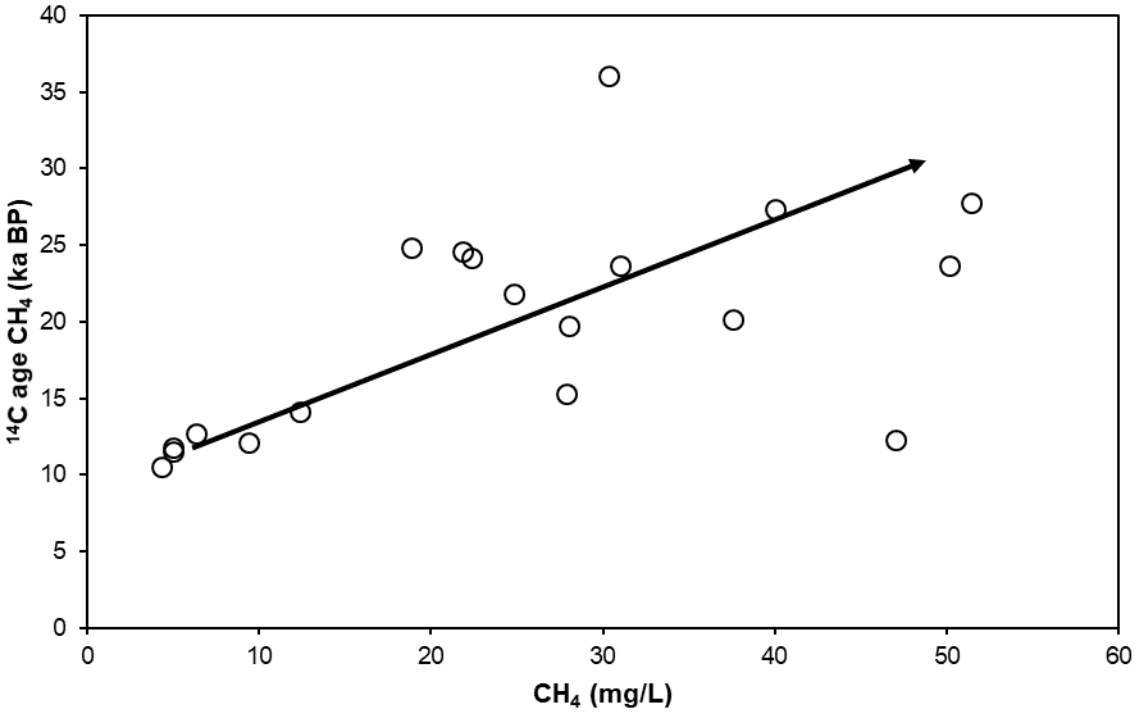

Figure 4-7. Uncalibrated ^{14}C ages for CH_4 vs. concentrations (n = 19).

These data demonstrate that as methanogenesis proceeds, there in an increased proportion of CH_4 reflecting older sources of organic matter. This suggests that during the early stages of methanogenesis in the glaciomarine sediments (i.e. at higher N_2/CH_4 ratios – see Figure 3-4), the

dominant substrate is CO_2 derived from the preferential decomposition of labile marine organic matter dating from the Champlain Sea incursion, most likely generated during the SO_4-reducing phase of organic matter decomposition, which is reflected by the ^{14}C and $\delta^{13}C$ signatures for the DIC pool. During later stages of methanogenesis (lower N_2/CH_4) as the CO_2 pool is depleted, there is a transition to acetate as the primary substrate for methanogenesis, likely derived from the fermentation of refractory ancient terrestrial organic matter within the glaciomarine muds occurring after, and at a slower rate than, decomposition of marine organic matter. This transition to the decomposition of older organic matter is also reflected in the DIC/DOC pools as Cl concentrations (and residence times) increase. Evidence for CH_4 enrichment from decomposition of early to mid-Wisconsinian buried terrestrial organic matter in an aquifer in the Great Lakes area influenced by the Laurentide glacial episode has been observed by Aravena et al. (1995) in the Alliston aquifer in southern Ontario.

4.4 Conclusions

Radioisotopic analyses were applied to the I and C pools in the studied aquifer, to elucidate the sources of these components. A trend of $^{129}I/^{127}I$ ratios for collected groundwater samples to approximately 20×10^{-14} as I concentrations increase, coupled with a range of $5 – 460 \times 10^{-14}$ for premodern samples reveal that the I pool in the Champlain Sea basin not only represents autochthonous marine I but is indicative of important influences from allochthonous I sources derived from the erosion of surrounding bedrock units and introduced by glacial meltwater flows. Evidence for allochthonous nutrient input by glacial meltwaters was also apparent from ^{14}C data of disseminated organic C within the glaciomarine muds. In tandem with stable C isotopes ($\delta^{13}C$), these analyses indicate that while the primary source of organic C within the mud is marine phytoplankton contemporaneous with the Champlain Sea incursion 10 – 12 ka BP, there is clearly an ancient C_3 terrestrial organic matter component, derived from the abrasion of Early Wisconsinian interstadial units. The presence of this ancient organic matter is also reflected in the DOC pool, albeit in smaller proportions.

Average uncalibrated ^{14}C ages of 20.5 ka BP, and a range of 10.7 – 36.2 ka BP for CH_4 gas suggest a change in substrate as methanogenesis proceeds, beginning with CO_2 derived from the decomposition of younger, labile marine phytoplankton within the glaciomarine muds during the

SO_4-reducing phase of organic matter decomposition, which is reflected by ^{14}C ages that roughly correspond to the Champlain Sea incursion in the DIC pool. This is followed by a transition to acetate derived from the fermentation of refractory, ancient terrestrial C sources in the latter stages of methanogenesis. This data also suggests that microbial CH_4 derived from the fermentation of kerogen and thermogenic CH_4 do not represent significant components of the CH_4 pool in the studied area.

4.5 References

Armstrong, D.K. and Dodge, J.E.P. (2007). Paleozoic geology of southern Ontario. *Ontario Geological Survey*, Miscellaneous Release—Data 219. ISBN 978-1-4249-4526-9.

Aitken, M.J. (1990). *Science-based Dating in Archaeology*. London: Longman. ISBN 9780582493094

Aravena, R., Wassenaar, L., and Barker, J. (1995). Distribution and isotopic characterization of methane in a confined aquifer in southern Ontario, Canada. *Journal of Hydrology*, 173: 51-70.

Bhatia, M.P., Kujawinski, E.B., Das, S.B., Breier, C.F., Henderson, P.B., and Charette, M.A. (2013). Greenland meltwater as a significant and potentially bioavailable source of iron to the ocean. *Nature Geoscience* 6: 274-278.

Chen, J., Liu, D., Peng, P., Ning, C., Xiaolin, H., Zhang, B., and Zhongyao, X. (2016). Iodine-129 chronological study of brines from an Ordovician paleokarst reservoir in the Lunnan oilfield, Tarim Basin. *Applied Geochemistry,* 65: 14-21.

Clark, I., and Fritz, P. (1997). Environmental Isotopes in Hydrogeology. Boca Raton, FL, CRC Press.

Cloutier, V., Lefebvre, R., Savard, M., Bourque, E., and Therrien, R. (2006). Hydrogeochemistry and groundwater origin of the Basses-Laurentides sedimentary rock aquifer system, St. Lawrence Lowlands, Quebec, Canada. *Hydrogeology Journal*, 14(4): 573-590.

Cohen, B. L. (1985). The origin of I in soil and the 129I problem, *Health Physical*, 49(2): 279–285.

Englund, E., A. Aldahan, G. Possnert, E. Haltia-Hovi, X. Hou, I. Renberg, and T. Saarinen. (2008). Modeling fallout of anthropogenic 129I, *Environmental Science Technologies*, 42(24): 9225–30.

Enriquez, S. Duarte, C.M. and Sand-Jensen, K. 1993. Patterns in decomposition rates among photosynthetic organisms: the importance of detritus C:N:P content. *Oecologia* 94, 457-471.

Fabryka-Martin, J., H. Bentley, D. Elmore, and P. Airey (1985), Natural iodine-129 as an environmental tracer, *Geochimica et Cosmochimica Acta*, 49(2): 337–347.

Fehn, U., S. Tullaifitzpatrick, R. Teng, H. Gove, P. Kubik, P. Sharma, and D. Elmore (1990), Dating of oil field brines using 129I, *Nucl. Instruments Methods Phys. Res. Sect. B Beam Interact. with Mater. Atoms*, 52(3-4): 446–450.

Fehn, U., Peters, E.K., Tullai-Fitzpatrick, S., Kubik, P.W., Sharma, P., Teng, R., Gove, H., and Elmore, D. (1992). 129I and 36Cl concentrations in waters of the eastern Clear Lake area, California: Residence times and source ages of hydrothermal fluids. *Geochimica et Cosmochimica Acta.* 56(5): 2069-2079.

Fehn., U. (2000). Dating of pore waters with 129I: Relevance for the origin of marine gas hydrates. *Science*, 289(5488): 2332-2335.

Fehn, U., Snyder, G.T., 2003. Origin of volatile elements in subduction zones: iodine and 129I in volcanic fluids from the North Island of New Zealand. *Economic Geology, Special Publication* 10: 159–170.

Fuge, R., and Johnson, C.C. (1986). The geochemistry of iodine – a review. *Environ. Geochem. Health*. 8:31-54.

Fulton, R. 1987. Quaternary Geology of the Ottawa Region, Ontario and Quebec. *Geological Survey of Canada,* Paper 86-23. https://doi.org/10.4095/122374

Gadd, N. (1980). Maximum age for a concretion at Green Creek, Ontario. *Geographie Physique et Quaternaire* 34(2): 229-238.

Griffith, D.R., Martin, W.R., and Eglinton, T.I. (2010). The radiocarbon age of organic carbon in marine surface sediments. *Geochimica et Cosmochimica Acta*, 74: 6788-6800.

Hawkings, J., Wadham, J., Tranter, M., Lawson, E., Sole, A., Cowton, T., Tedstone, A.J., Bartholomew, I., Nienow, P., Chandler, D., and Telling, J. (2015). The effect of warming climate on nutrient and solute export from the Greenland Ice Sheet. *Geochemical Perspectives Letters*, I: 94-104.

Hodson, A.J., Mumford, P., and Lister, D. (2004) Suspended sediment and phosphorus in proglacial rivers: bioavailability and potential impacts upon the P status of ice-marginal receiving waters. *Hydrological Processes* 18: 2409-2422.

Meyers, P.A. (1994). Preservation of elemental and isotopic source identification of sedimentary organic matter, *Chemical Geology*, 114: 289-302.

Middelburg, J. J., & Nieuwenhuize, J. (1998). Carbon and nitrogen stable isotopes in suspended matter and sediments from the Schelde Estuary. *Marine Chemistry*, 60(3–4): 217–225.

Moran, J., Oktay, S., and Santschi, R. (2002). Sources of iodine and iodine 129 in rivers. *Water Resources Research*, 38(8): 24-1 to 24-10.

Mott, R.J. (1968). A radiocarbon-dated marine algal bed of the Champlain Sea episode near Ottawa, Ontario. *Canadian Journal of Earth Sciences*, 5(2): 319-324.

Nydal, R., and Lövseth, K. (1965). Distribution of radiocarbon from nuclear tests. *Nature,* 206(4988): 1029-1031.

Ochietti, S. 1989. Quaternary geology of St. Lawrence Valley and adjacent Appalachian subregion. In: Fulton, R.J. (Ed.), Quaternary Geology of Canada and Greenland. Geology of Canada Series, No 1, pp. 350-389. ISBN 0-660-13114-5.

Parent, M., and Occhietti, S. (1988). Late Wisconsinian deglaciation and Champlain Sea invasion in the St. Lawrence Valley, Quebec. *Géographie physique et Quaternaire*, 42(3): 215-246.

Pearson, F.J., Hanshaw Jr., B.B., 1970. Sources of dissolved carbonate species in groundwater and their effects on carbon-14 dating. Isotope Hydrology 1970. IAEA, Vienna, pp. 271–286

Rädlinger,G., Heumann, K. G. (2000). Transformation of iodide in natural and wastewater systems by fixation on humic substances. *Environ. Sci. Technol*. 34(18), 3932.

Rao, U., and Fehn, U. (1999). Sources and reservoirs of anthropogenic Iodine-129 in western New York. *Geochimica et Cosmochimica Acta*, 63: 1927-1938.

Silliman, J., Meyers, P., and Bourbonniere, R. (1996). Record of postglacial organic matter delivery and burial in sediments of Lake Ontario. *Organic Geochemistry*, 24(4): 463-472.

Slemmons K.E.H., and Saros J.E. (2012). Implications of nitrogen-rich glacial meltwater for phytoplankton diversity and productivity in alpine lakes. *Limnology and Oceanography* 57: 1651–1663.

5 Conclusions and Future Work

I and CH_4 exceedances in a 1 500 km^2 sedimentary rock interface aquifer overlain by glaciomarine muds originating from the Champlain Sea incursion 12 – 10 ka BP were characterized using hydrogeological, geochemical, and isotopic datasets. In the studied area, CH_4 concentrations regularly exceeded Province of Ontario drinking water guidelines, and I proportions were significantly higher than the recommended drinking water limit of 150 µg/L in China. Major objectives for this thesis included a characterization of component distribution, analysis of the mechanisms leading to I and CH_4 enrichment, source tracing, and evaluating the potential relationship between the two components. A summary of the results from these analyses are presented below in an effort to synthesize the findings from this study and their implications.

The flow system for the interface aquifer is dependent on bedrock topography, which is reflected by the water table: recharge occurs in topographically high areas, where highly permeable tills and subaqueous outwash sands are the dominant surficial deposits, and travels through a layer of till, subglacial outwash deposits and heavily fractured bedrock that separates Paleozoic sedimentary rocks from glaciomarine muds into depressions in the bedrock surface, where there is salinization due to mixing with stagnant lenses of Champlain Sea waters and leaching of saline porewaters from the overlying mud.

Characterization of the distribution of I and CH_4 in the study area revealed that the highest proportions of these components were typically found in bedrock depressions in conjunction with highly reducing, Na-Cl type groundwaters. Cl/Br ratios of the saline groundwaters were similar to that of seawater, but Br/I and Cl/I ratios, which were lower than expected, indicate that I enrichment had taken place. Additionally, box-and-whisker plots revealed that groundwaters were enriched in I and CH_4 as they progressed from a Ca-HCO_3 to Na-Cl geochemical facies, although the trends were less obvious with CH_4, suggesting that other factors also control its enrichment. CH_4 was observed to be present in higher proportions in areas underlain by carbonate and shale units, suggesting a thermogenic component in the CH_4 pool. These results indicate that I and, in part, CH_4, are associated with glacial sediments. Results from the characterization of component distribution are representative of a system where the microbial

decomposition of organic matter in an anaerobic environment is the driving factor for I and CH_4 enrichment. The presence of low-permeability muds overlying the aquifer appears to exhibit a significant influence on both hydrogeological conditions of the aquifer (unconfined vs. confined conditions) and groundwater geochemistry through multiple processes such as ion exchange, diffusion, and porewater leaching.

Results from multivariate statistical analysis identified significant relationships between I, salinity, and indicators of microbial activity. These relationships, in conjunction with high porewater salinities and observed hydrotroilite and bioturbation in massive glaciomarine muds, suggest that I is derived from microbial decomposition of marine phytoplankton found within this unit.

Depleted $^{129}I/^{127}I$ ratios below the accepted pre-anthropogenic value of 150×10^{-14} for marine sediments are indicative of a mixture between autochthonous marine and allochthonous geogenic I sources in the Champlain Sea basin. The geogenic I would be derived from mechanical abrasion of the surrounding Paleozoic sedimentary terrain (particularly shale and carbonate bedrock) and transported into the Champlain Sea basin by glacial meltwaters. Similarly, C/N ratios, as well as $\delta^{13}C$ and ^{14}C analyses of disseminated organic matter within the glaciomarine muds indicated the presence of older, allochthonous sources of detrital C_3 terrestrial vegetation, most likely derived from the abrasion organic-rich Early Wisconsinian interstadial deposits, which would have also been transported into the Champlain Sea basin through glacial meltwaters.

Stable isotope and quantitative analysis of collected CH_4 gases indicate that they are microbial in origin, with the exception of areas underlain by the Billings shale, where evidence of a thermogenic component was observable. The absence of a relationship between bedrock lithology and ^{14}C age of CH_4 indicate that CH_4 generated by the microbial fermentation of kerogen is likely not a significant component of the CH_4 pool. Fractionation factors between DIC and CH_4 demonstrate that there is a transition of C substrate from CO_2 to acetate as methanogenesis proceeds, as indicated by a decreasing N_2/CH_4 ratio. In the glaciomarine muds, labile marine phytoplankton contemporaneous with the Champlain Sea incursion is preferentially decomposed by bacterial processes relative to the more refractory terrestrial organic C corresponding to the St. Pierre sediment that is Early Wisconsinian (60 – 75 ka BP) in age. This

is reflected by older uncalibrated ^{14}C ages of CH_4 as it becomes enriched in the groundwater system. The prevalence of older C sources in saline, mature portions of the groundwater system is also observed for the DIC/DOC pools. The transition in substrate for methanogenesis reflects the relative reactivity of the two sources of organic C within the mud matrix: initially, the CO_2 reduction pathway would utilize dissolved CO_2 generated from the decomposition of marine phytoplankton in the SO_4-reducing phase of the marine sediments. Upon depletion of available CO_2 to methanogens, acetate generated from the fermentation of ancient terrestrial organic C within the glaciomarine muds would become the dominant substrate, resulting in a transition to the acetate fermentation methanogenic pathway.

The link between decomposition of organic matter in marine sediments with high concentrations of biophilic elements (such as I) and CH_4 in fore arc fluids discussed in the introduction led to the initial hypothesis that I and CH_4 enrichment would be concurrent. This was confirmed by a moderately significant positive Spearman's rank correlation coefficient of 0.62 and supported by a multitude of observations in the hydrogeochemical dataset. I and CH_4 are enriched in groundwater as it travels from recharge zones to depressions in the bedrock surface. The sources for each component differ slightly in that I originates predominantly from marine phytoplankton within the massive glaciomarine muds, whereas marine phytoplankton and ancient terrestrial matter from the Early Wisconsinian are shown to be C sources for microbial CH_4, and the presence of thermogenic CH_4 cannot be precluded for areas underlain by the Billings shale. Marine phytoplankton contains significantly higher proportions of I compared to terrestrial organic matter which could explain why the relationships exhibited for CH_4 and various parameters related to mud porewater were less significant than those of I, and why the Spearman's coefficient for I and CH_4 was not more strongly significant. However, both components are associated with similar factors as they become enriched in groundwater, such as salinity, long groundwater residence times, and highly reducing environments. Thus, it would be more apt to attribute the relationship between I and CH_4 not only to similar sources, but also to similar hydrogeological controls for enrichment. These results differ slightly from studies of fore arc fluids in the marine environment because, in such an environment, all organic matter is derived from the marine environment, and the marine sediments are underlain by an organic-poor basalt crust, whereas continental aquifers (such as the one considered for this thesis)

typically exhibit multiple sources of organic matter and are underlain by various sedimentary bedrock lithologies.

Future work should endeavour to analyze the distribution of I and CH_4 and their respective isotopes in a sediment core taken above a depression in the bedrock surface, with particular attention paid to redox conditions. Analysis of the types and concentrations of geolipids such as hydrocarbons and fatty acids within the glaciomarine sediments would greatly aid in characterizing the sources of organic C and confirming the presence of ancient terrestrial organic matter. Additionally, the lack of provincial or federal regulation with regards to high I concentrations in groundwater in regions affected by the Champlain Sea incursion is of concern and future legislative work should investigate the potential health risks associated with the hydrogeological environment of the St. Lawrence Lowlands. Results from this thesis could be used to create an Aquifer Capacity Screening Tool (ACST), a predictive model which would indicate the regions of anticipated exceedances for I and CH_4. This would greatly aid developers, city planners and well drillers in evaluating whether potable groundwater would be available for a particular site within the studied area.

Appendices

Appendix A: Station Parameters

Sample ID	Sample Type	Subcropping Unit	Aquifer type	Elevation	Drift Thickness	Well Depth	Hydraulic Head
				mASL	m	m	mASL
16-AG-513	FS	Bobcaygeon	Bedrock	53.8	33.5	37.5	51.4
16-AG-514	FS	Rockcliffe	Overburden	52.5	61.0	60.4	36.7
16-AG-515	FS	Bobcaygeon	Bedrock	48.5	27.1	30.5	49.0
16-AG-516	FS	Bobcaygeon	Bedrock	49.7	39.6	45.3	45.7
16-AG-700	FS	Bobcaygeon	Overburden	81.0	44.5	44.5	19.3
16-AG-701	FS	Lindsay	Bedrock	66.8	21.0	31.1	38.3
16-AG-702	Standard	-		-	-	-	-
16-AG-703	FS	Precambrian	Overburden	49.9	144.8	137.2	2.5
16-AG-704	FS	Bobcaygeon	Bedrock	62.7	0.9	42.7	42.2
16-AG-705	FS	Billings	Bedrock	49.7	21.9	21.9	31.0
16-AG-706	FS	Lindsay	Bedrock	53.2	0.0	20.4	52.7
16-AG-707	FS	Lindsay	Bedrock	86.6	45.1	61.0	32.7
16-AG-708	FS	Gull River	Bedrock	51.1	41.8	42.7	2.5
16-AG-709	FS	Lindsay	Bedrock	47.6	6.1	17.4	36.0
16-AG-710	Duplicate of 709	Lindsay	Bedrock	47.6	6.1	17.4	28.3
16-AG-711	FS	Lindsay	Bedrock	58.6	47.5	73.0	17.8
16-AG-712	Blank	-	-	-	-	-	-
16-AG-713	FS	Lindsay	Bedrock	54.4	6.2	11.6	32.6
16-AG-714	FS	Lindsay	Overburden	55.5	6.8	23.5	29.7
16-AG-715	FS	Lindsay	Bedrock	54.5	5.7	21.3	32.8
16-AG-716	FS	Lindsay	Bedrock	54.3	25.0	29.4	40.4
16-AG-717	FS	Lindsay	Bedrock	62.5	12.2	15.2	33.7
16-AG-718	FS	Lindsay	Bedrock	63.6	6.5	14.0	39.3
16-AG-719	FS	Lindsay	Bedrock	52.6	7.6	33.5	9.8
16-AG-720	FS	Lindsay	Bedrock	67.4	33.5	33.5	18.2
16-AG-721	FS	Lindsay	Bedrock	79.8	44.5	47.2	25.0
16-AG-722	FS	Bobcaygeon	Bedrock	64.0	16.5	30.5	40.5
16-AG-723	FS	Lindsay	Overburden	85.2	41.8	45.7	7.9
16-AG-725	Standard	-	-	-	-	-	-
16-AG-726	FS	Lindsay	Bedrock	86.3	35.4	40.9	13.0
16-AG-727	FS	Billings	Overburden	62.3	42.1	27.8	20.5
16-AG-728	FS	Lindsay	Bedrock	76.5	28.0	30.5	36.6
16-AG-729	Standard	-	-	-	-	-	-
16-AG-730	Duplicate of 731	Lindsay	Bedrock	55.1	18.3	27.4	34.0
16-AG-731	FS	Lindsay	Bedrock	55.1	18.3	27.4	33.1
16-AG-732	FS	Lindsay	Bedrock	63.4	4.9	24.4	36.3

Sample ID	Sample Type	Subcropping Unit	Aquifer type	Elevation	Drift Thickness	Well Depth	Hydraulic Head
				mASL	m	m	mASL
16-AG-733	FS	Lindsay	Overburden	59.7	11.0	38.1	16.5
16-AG-734	FS	Carlsbad	Overburden	55.9	8.8	6.1	33.6
16-AG-735	FS	Lindsay	Bedrock	56.5	1.5	77.1	39.8
16-AG-736	FS	Lindsay	Bedrock	61.2	26.8	27.5	37.3
16-AG-737	FS	Carlsbad	Overburden	53.8	31.0	20.9	15.3
16-AG-738	FS	Billings	Bedrock	50.2	12.8	76.2	4.6
16-AG-740	FS	Lindsay	Bedrock	66.6	24.4	26.2	27.2
16-AG-741	FS	Gull River	Bedrock	73.7	16.2	18.5	43.3
16-AG-742	FS	Lindsay	Bedrock	63.0	18.3	19.5	41.2
16-AG-744	FS	Rockcliffe	Bedrock	53.3	9.8	4.6	16.0
16-AG-745	FS	Lindsay	Bedrock	59.8	24.2	40.0	26.7
16-AG-746	FS	Lindsay	Overburden	84.0	33.9	42.1	52.6
16-AG-747	FS	Bobcaygeon	Bedrock	53.1	18.9	23.5	46.4
16-AG-748	FS	Queenston	Bedrock	77.7	22.9	27.4	58.0
16-AG-749	Duplicate of 738	Billings	Bedrock	50.2	12.8	76.2	6.0
16-AG-750	FS	Gull River	Bedrock	62.0	29.9	33.2	34.8
16-AG-751	FS	Lindsay	Bedrock	87.8	6.1	23.5	60.3
16-AG-752	FS	Bobcaygeon	Overburden	64.0	32.0	35.2	33.1
16-AG-753	FS	Bobcaygeon	Overburden	65.7	17.4	21.8	42.5
16-AG-754	FS	Gull River	Bedrock	57.5	38.1	42.7	14.3
16-AG-755	FS	Lindsay	Bedrock	52.0	9.8	13.4	36.5
16-AG-756	FS	Lindsay	Bedrock	72.7	26.5	83.2	37.2
16-AG-757	FS	Lindsay	Bedrock	66.3	15.2	19.8	43.6
16-AG-758	FS	Carlsbad	Bedrock	77.1	24.7	25.9	45.4
16-AG-759	Standard	-	-	-	-	-	-
16-AG-760	Standard	-	-	-	-	-	-
16-AG-761	FS	Rockcliffe	Bedrock	53.8	21.3	36.3	12.8
16-AG-792	FS	Queenston	Bedrock	73.7	18.3	42.7	67.1
16-AG-793	FS	Gull River	Bedrock	67.7	12.2	13.7	64.5
16-AG-794	FS	Carlsbad	Bedrock	80.8	60.0	61.0	79.3
16-AG-795	FS	Lindsay	Bedrock	83.7	38.1	48.8	69.0
16-AG-796	FS	Lindsay	Bedrock	64.2	17.7	18.3	58.9

FS = Full Sample

0* = Artesian Well

Appendix B: Field Parameters

Sample ID	Date	Temperature	Conductivity	pH	ORP	H_2S	Alkalinity
		˚C	µs/cm		mV (Ag-AgCl)	mg/L	ppm HCO3
16-AG-513	2016-08-05	12.34	5463	7.67	-218.9	0.00	966
16-AG-514	2016-08-05	10.15	30329	7.49	-196.8	<0.01	1746
16-AG-515	2016-08-06	8.32	13780	7.66	-149.1	0.00	1197
16-AG-516	2016-08-06	9.86	27511	7.02	-220.5	12.00	1487
16-AG-700	2016-07-19	9.99	1069	7.98	-92.5	0.35	764
16-AG-701	2016-07-19	10.39	666	8.18	-10.6	0.00	363
16-AG-702	2016-07-19	-	-	-	-	-	-
16-AG-703	2016-07-20	9.29	13728	8.55	-283.9	0.00	640
16-AG-704	2016-07-20	N/A	1110	7.59	-20.1	<0.01	540
16-AG-705	2016-07-20	10.98	17622	7.52	-54	<0.01	1450
16-AG-706	2016-07-21	11.02	813	7.44	-175.7	0.33	505
16-AG-707	2016-07-22	9.55	1183	8.28	-227.6	0.19	1069
16-AG-708	2016-07-22	10.42	5212	7.87	-179.2	0.00	1024
16-AG-709	2016-07-22	-	-	-	-	-	-
16-AG-710	2016-07-22	9.22	9651	6.94	103	<0.01	430
16-AG-711	2016-07-22	9.83	7965	7.99	-227.1	0.00	1095
16-AG-712	2016-07-22	-	-	-	-	-	-
16-AG-713	2016-07-23	9.87	458	8.06	-273.3	1.15	194
16-AG-714	2016-07-23	10.33	2057	8.62	-206.2	0.09	841
16-AG-715	2016-07-23	9.97	3370	8.16	-113.2	0.00	1394
16-AG-716	2016-07-23	10.4	2823	8.05	-218.7	<0.01	1064
16-AG-717	2016-07-24	9.87	1001	7.75	-192	0.35	500
16-AG-718	2016-07-24	9.53	971	8.14	-228.8	0.20	666
16-AG-719	2016-07-24	9.94	2361	8.56	-264.3	<0.01	614
16-AG-720	2016-07-24	9.18	424	9.31	-219.9	<0.01	293
16-AG-721	2016-07-26	9.71	1432	8.09	-223.2	0.00	964
16-AG-722	2016-07-26	10.41	1929	8.2	-180.7	0.00	415
16-AG-723	2016-07-26	10.31	1085	8.42	-200.8	0.25	745
16-AG-725	2016-07-26	-	-	-	-	-	-
16-AG-726	2016-07-26	10.76	1003	8.22	-191.1	0.13	683
16-AG-727	2016-07-27	9.76	2782	8.2	-229.1	0.00	853
16-AG-728	2016-07-27	9.22	1091	8.28	-199.8	0.12	703
16-AG-729	2016-07-27	-	-	-	-	-	-
16-AG-730	2016-07-27	N/A	N/A	N/A	N/A	0.10	1064
16-AG-731	2016-07-27	10.08	3297	8.3	-185.4	0.20	1097
16-AG-732	2016-07-27	10.38	1328	8.29	-164	0.00	667
16-AG-733	2016-07-28	11.18	1325	7.69	-217.9	0.22	591
16-AG-734	2016-07-28	11.3	507	7.43	90	<0.01	369
16-AG-735	2016-07-28	9.37	905	7.83	-222.2	0.90	374

Sample ID	Date	Temperature	Conductivity	pH	ORP	H_2S	Alkalinity
		˚C	µs/cm		mV (Ag-AgCl)	mg/L	ppm HCO3
16-AG-736	2016-07-28	9.31	1109	8.86	-257.5	<0.01	591
16-AG-737	2016-07-29	12.45	6318	7.3	-193.7	0.00	999
16-AG-738	2016-07-29	9.66	36158	7.06	-134.4	<0.01	997
16-AG-740	2016-08-02	10.03	4906	8.02	-144.8	0.00	1153
16-AG-741	2016-08-02	10.75	1144	7.06	-86.6	<0.01	356
16-AG-742	2016-08-02	9.66	701	7.84	-179.8	0.10	514
16-AG-744	2016-08-02	N/A	520	6.49	-45.7	<0.01	258
16-AG-745	2016-08-02	10.44	3929	8.18	-223.7	0.00	1426
16-AG-746	2016-08-03	9.23	4963	8.15	-248.9	1.25	1219
16-AG-747	2016-08-03	9.37	3041	7.45	-231.9	1.00	917
16-AG-748	2016-08-03	N/A	7990	7.69	-163.5	<0.01	148
16-AG-749	2016-07-30	-	-	-	-	-	-
16-AG-750	2016-08-03	9.87	1886	8.22	-225.6	0.00	1039
16-AG-751	2016-08-03	9.84	893	7.05	-130.5	<0.01	472
16-AG-752	2016-08-04	9.79	3184	8.15	-200.1	<0.01	910
16-AG-753	2016-08-04	9.82	975	8.36	-243.6	1.15	614
16-AG-754	2016-08-04	10.29	4128	7.91	-239.5	0.00	1213
16-AG-755	2016-08-04	10.48	14294	7.53	-199.8	<0.01	1127
16-AG-756	2016-08-04	9.79	2288	8.49	-250.1	N/A	968
16-AG-757	2016-08-04	9.87	9421	7.78	-192.5	0.00	1207
16-AG-758	2016-08-04	11.93	931	8.3	-227.9	0.12	378
16-AG-759	2016-08-05	-	-	-	-	-	-
16-AG-760	2016-08-05	-	-	-	-	-	-
16-AG-761	2016-08-05	10.9	4719	7.97	-169.7	0.00	1198
16-AG-792	2016-08-09	10.01	1119	8.74	-127	<0.01	484
16-AG-793	2016-08-09	10.17	713	7.14	-119.1	0.00	390
16-AG-794	2016-08-09	10.08	12347	8.01	-167.3	<0.01	992
16-AG-795	2016-08-09	9.92	1431	8.67	-124.6	1.35	969
16-AG-796	2016-08-09	9.11	891	7.86	-211.5	1.15	484

“<” Symbolizes parameter below detection limit

“N/A” Symbolizes no data available

Appendix C: C parameters and isotopes

Sample	DIC	δ ^{13}C DIC	DOC	δ ^{13}C DOC	CH_4	CO_2
	mg C/L	‰ VPDB	mg C/L	‰ VPDB	mg/L	mg/L
16-AG-513	184.5	-20.4	9.5	-26.72	0.0	17.3
16-AG-514	485.6	-21.2	7.8	-26.04	12.3	29.1
16-AG-515	235.8	-15.0	3.6	-26.74	21.6	17.1
16-AG-516	454.1	-15.8	2.0	-26.99	27.8	57.6
16-AG-700	165.1	-15.7	22.6	-28.5	9.5	9.8
16-AG-701	72.9	-8.8	6.9	-26.55	22.2	9.8
16-AG-702	-	-	-	-	-	-
16-AG-703	140.7	-11.9	5.0	-28.09	46.9	4.6
16-AG-704	N/A	N/A	N/A	N/A	0.0	15.9
16-AG-705	330.4	-15.3	6.6	-26.56	25.0	23.9
16-AG-706	124.2	-16.7	3.6	-26.38	0.0	12.2
16-AG-707	215.2	-16.6	18.6	-25.99	9.0	6.4
16-AG-708	150.6	-20.0	4.9	-26.64	0.0	10.8
16-AG-709	84.6	-14.4	3.9	-27.52	0.0	26.7
16-AG-710	81.7	-14.3	3.7	-27.56	0.0	31.1
16-AG-711	265.0	-21.9	9.9	-26.36	3.6	11.4
16-AG-712	-	-	-	-	-	-
16-AG-713	25.0	-13.4	1.6	-27.17	0.0	0.0
16-AG-714	190.0	-21.0	18.6	-26.04	0.0	1.3
16-AG-715	310.1	-19.3	22.1	-26.19	5.6	9.9
16-AG-716	250.7	-17.7	21.5	-26.37	9.3	9.3
16-AG-717	84.7	-17.5	3.5	-27.21	0.0	1.9
16-AG-718	158.2	-14.5	8.1	-26.86	4.6	0.6
16-AG-719	129.4	-8.0	7.5	-26.81	51.3	0.0
16-AG-720	41.8	-8.2	3.1	-27.96	30.2	0.0
16-AG-721	221.0	-15.6	25.0	-26.24	12.2	2.6
16-AG-722	106.5	-16.2	3.9	-26.74	0.0	0.0
16-AG-723	182.5	-15.6	16.6	-26.04	4.9	3.9
16-AG-725	-	-	-	-	-	-
16-AG-726	217.0	-14.6	13.2	-26.88	4.2	5.1
16-AG-727	209.3	-19.8	18.4	-26.33	5.9	6.4
16-AG-728	227.8	-14.9	17.9	-26.16	5.1	3.9
16-AG-729	-	-	-	-	-	-
16-AG-730	245.3	-21.3	21.4	-26.25	1.7	7.7
16-AG-731	244.0	-21.5	21.6	-26.24	1.5	7.1
16-AG-732	164.4	-15.9	8.8	-25.93	4.8	3.9
16-AG-733	145.5	-16.9	7.9	-27.03	0.0	11.7
16-AG-734	47.2	-15.5	3.1	-27.04	0.0	7.2

Sample	DIC	δ^{13}C DIC	DOC	δ^{13}C DOC	CH_4	CO_2
	mg C/L	‰ VPDB	mg C/L	‰ VPDB	mg/L	mg/L
16-AG-735	90.4	-13.8	5.9	-27.07	0.6	7.8
16-AG-736	115.2	-9.1	9.2	-26.15	39.8	0.0
16-AG-737	236.0	-23.3	17.6	-26.18	0	49.7
16-AG-738	159.4	-5.1	3.9	-29.72	30.8	38.0
16-AG-740	248.7	-19.4	10.4	-26.13	6.2	12.8
16-AG-741	61.4	-11.8	2.5	-27.08	0.0	19.5
16-AG-742	99.0	-16.8	5.4	-26.77	0.7	5.4
16-AG-744	70.1	-8.1	28.4	-29.39	4.1	61.2
16-AG-745	411.4	-14.2	25.9	-26.01	37.4	9.4
16-AG-746	338.3	-21.0	15.5	-26.44	18.7	10.9
16-AG-747	177.6	-19.9	12.7	-26.36	0.0	21.2
16-AG-748	19.0	-20.1	2.4	-27.85	0.4	1.4
16-AG-749	226.1	-6.3	4.2	-29.26	24.7	37.3
16-AG-750	215.0	-16.2	20.9	-25.86	6.2	5.5
16-AG-751	106.3	-15.8	3.2	-26.91	0.0	32.8
16-AG-752	189.3	-15.1	6.2	-26.12	27.9	5.6
16-AG-753	106.1	-20.1	4.6	-28.52	3.7	2.1
16-AG-754	365.5	-18.3	18.9	-26.14	6.2	13.4
16-AG-755	374.1	-21.0	11.3	-26.23	21.7	21.1
16-AG-756	224.9	-15.6	16.4	-28.12	21.7	0.0
16-AG-757	280.3	-17.0	11.8	-26.45	31.0	14.1
16-AG-758	71.4	-19.7	3.6	-26.86	0.8	0.0
16-AG-759	-	-	-	-	-	-
16-AG-760	-	-	-	-	-	-
16-AG-761	363.0	-21.4	17.1	-26.3	0.6	11.1
16-AG-792	117.5	-15.7	7.3	-26.85	31.2	0.0
16-AG-793	91.9	-14.2	4.7	-27.15	0.0	19.4
16-AG-794	340.6	-17.8	14.6	-26.51	50.0	8.3
16-AG-795	130.5	-17.6	23.7	-26.39	2.0	0.7
16-AG-796	109.6	-16.8	7.2	-26.45	0.5	3.5

“N/A” Symbolizes no data available

Appendix D: Major Constituents

Sample	Ca	Mg	Na	K	SO_4	Cl	Br	F
	mg/L	mg/L	mg/L	mg/L	mg/L	mg/L	mg/L	mg/L
16-AG-513	50.2	53.0	1220.0	31.3	62.7	1550.3	5.3	0.2
16-AG-514	51.1	558.1	5649.1	116.3	<0.1	11682.6	39.2	0.0
16-AG-515	40.3	144.5	2569.8	67.1	0.8	4651.4	15.5	0.1
16-AG-516	98.9	481.1	5120.5	153.4	0.5	10614.2	35.7	0.0
16-AG-700	9.3	12.2	230.0	10.6	0.1	26.2	0.2	0.8
16-AG-701	1.8	2.9	184.1	5.5	0.1	57.1	0.6	1.2
16-AG-702	9.0	5.0	226.1	2.3	57.5	202.9	0.5	2.5
16-AG-703	47.9	137.8	2188.7	75.5	<0.1	4791.6	18.0	0.2
16-AG-704	44.8	21.7	211.5	7.1	35.6	103.0	0.5	0.3
16-AG-705	64.0	205.5	2754.8	112.0	<0.1	6251.7	22.5	0.0
16-AG-706	34.7	18.6	156.7	9.4	13.1	44.8	0.2	0.3
16-AG-707	5.6	8.1	301.2	10.4	0.6	32.3	0.2	1.0
16-AG-708	33.0	86.5	937.2	37.1	81.6	1499.3	5.4	0.1
16-AG-709	261.2	24.7	1675.5	5.2	122.4	3120.1	0.6	0.0
16-AG-710	260.2	24.5	1670.9	5.1	122.1	3142.6	0.6	0.0
16-AG-711	10.0	55.6	1589.5	45.0	0.1	2300.6	9.6	0.3
16-AG-712	0.0	0.0	0.1	0.0	0.0	0.0	0.0	0.0
16-AG-713	23.6	13.2	68.2	2.0	86.2	28.6	0.1	1.2
16-AG-714	2.6	7.6	442.5	7.8	77.5	250.3	0.9	3.5
16-AG-715	4.7	20.6	703.3	23.0	0.2	562.1	2.0	1.3
16-AG-716	6.1	20.6	574.9	17.7	0.1	480.6	1.8	1.0
16-AG-717	30.9	35.1	154.9	12.9	3.7	126.3	0.4	0.4
16-AG-718	10.4	22.7	177.1	11.9	0.5	38.5	0.3	0.7
16-AG-719	3.3	5.0	471.3	13.9	0.1	535.1	2.1	1.0
16-AG-720	0.6	0.1	113.1	1.2	0.2	10.4	0.1	2.2
16-AG-721	5.2	11.1	307.9	13.6	<0.1	52.4	0.3	1.0
16-AG-722	7.8	11.2	351.5	14.7	75.7	393.7	1.5	0.9
16-AG-723	3.4	5.0	246.1	8.2	0.1	9.2	0.1	1.7
16-AG-725	168.8	51.1	7.8	0.9	353.1	7.3	0.0	1.4
16-AG-726	6.6	6.2	219.0	8.4	0.3	7.8	0.1	1.3
16-AG-727	7.0	21.7	537.0	19.4	<0.1	562.3	2.0	0.7
16-AG-728	4.8	6.7	241.3	8.9	0.1	30.6	0.2	1.5
16-AG-729	11.1	2.4	5.4	0.9	56.5	201.5	5.5	7.6
16-AG-730	4.2	19.9	666.6	17.7	2.9	645.2	2.4	1.4
16-AG-731	4.3	19.5	657.1	18.2	2.8	645.6	2.3	1.4
16-AG-732	2.9	10.2	273.5	11.9	3.4	135.0	0.6	0.9
16-AG-733	27.1	31.2	204.5	13.3	36.0	150.9	0.5	0.8
16-AG-734	69.5	21.1	5.8	1.9	22.1	19.6	0.0	0.0
16-AG-735	14.9	8.5	160.5	4.2	55.6	83.4	0.2	0.9

Sample	Ca	Mg	Na	K	SO_4	Cl	Br	F
	mg/L	mg/L	mg/L	mg/L	mg/L	mg/L	mg/L	mg/L
16-AG-736	2.1	3.9	227.7	7.7	<0.1	126.0	0.5	0.9
16-AG-737	85.3	66.1	1113.4	29.5	1080.4	1000.6	3.4	0.5
16-AG-738	235.1	573.4	6807.0	170.0	0.1	13622.0	73.5	0.2
16-AG-740	8.1	35.2	1164.4	27.5	0.3	1265.0	5.1	0.4
16-AG-741	128.3	38.5	75.9	8.1	323.5	44.3	0.1	1.3
16-AG-742	20.4	41.8	82.3	15.5	1.5	8.6	0.1	0.3
16-AG-744	32.7	17.8	26.9	44.1	1.3	37.3	0.0	0.5
16-AG-745	4.6	14.5	1021.3	22.9	<0.1	741.6	2.7	0.7
16-AG-746	6.2	24.2	1227.2	21.8	1.4	1167.1	4.8	0.6
16-AG-747	51.9	27.1	627.7	14.1	54.2	692.7	2.3	0.5
16-AG-748	187.6	77.8	1662.8	16.3	557.6	2496.0	11.8	0.2
16-AG-749	220.1	577.0	6701.7	174.1	<0.1	13623.0	59.1	0.2
16-AG-750	6.0	11.8	437.4	15.5	0.3	242.9	0.8	1.3
16-AG-751	118.4	34.4	40.8	3.9	51.5	62.0	0.0	0.2
16-AG-752	9.4	19.7	610.7	23.5	0.6	705.8	2.6	0.5
16-AG-753	10.1	19.3	174.9	8.8	34.5	68.4	0.2	0.8
16-AG-754	9.1	23.0	979.9	31.4	0.6	941.9	3.4	0.4
16-AG-755	37.3	200.6	2267.8	70.2	1.0	4911.3	16.1	0.3
16-AG-756	2.9	6.3	571.2	10.7	<0.1	344.1	1.2	1.3
16-AG-757	18.9	88.4	2220.5	43.3	<0.1	2927.8	11.9	0.1
16-AG-758	5.5	5.8	168.4	9.3	12.8	131.3	0.4	0.7
16-AG-759	9.3	5.1	195.7	2.4	57.4	205.9	0.4	2.4
16-AG-760	11.1	2.4	4.9	0.9	56.3	201.8	5.4	7.5
16-AG-761	18.5	43.8	854.3	25.5	14.9	1138.4	3.9	0.4
16-AG-792	4.1	2.1	333.8	7.3	0.1	175.9	1.6	1.4
16-AG-793	82.3	27.2	33.1	6.8	63.0	18.4	0.0	0.5
16-AG-794	21.2	125.4	2698.3	65.9	<0.1	4255.0	15.1	0.2
16-AG-795	4.2	5.6	412.0	7.2	24.8	144.4	0.6	3.1
16-AG-796	19.4	11.6	193.2	10.3	1.2	75.4	0.1	0.2

"<" Symbolizes parameter below detection limit

Appendix E: Trace Constituents

Sample	NO_3	NH_4	I	Ba	B	Fe	Sr	Si	Li	Mn
	mg N/L	mg N/L	µg/L	µg/L	µg/L	µg/L	µg/L	µg/L	µg/L	µg/L
16-AG-513	<0.03	2.81	664	231	821	1347	4411	7041	23	31.3
16-AG-514	<0.3	15.60	5514	3756	2549	2310	5015	5406	9	57.3
16-AG-515	<0.03	5.01	2359	7533	1256	175	6829	6471	93	14.8
16-AG-516	<0.3	15.60	6621	2209	2767	306	24394	11329	96	16.4
16-AG-700	<0.003	1.04	194	722	534	243	1659	8952	9	1.5
16-AG-701	<0.003	0.47	57	39	454	8	171	4113	36	<0.2
16-AG-702	<0.03	<0.04	N/A	40	1893	501	569	3704	53	36367.3
16-AG-703	<0.03	10.90	4293	727	1858	3590	1861	5466	8	43.5
16-AG-704	<0.003	0.16	39	89	404	24	3209	5344	75	3.1
16-AG-705	<0.03	12.20	4066	6548	2221	1236	5608	5383	89	88.3
16-AG-706	0.034	0.48	37	180	312	534	2503	8293	13	13.5
16-AG-707	<0.003	1.53	168	223	764	272	403	7790	6	3.0
16-AG-708	<0.3	4.53	772	154	958	1298	28702	10976	24	56.6
16-AG-709	<0.3	0.04	62	452	19	16	1918	3860	6	0.8
16-AG-710	<0.3	0.04	62	449	18	16	1812	3827	4	0.9
16-AG-711	<0.3	2.73	1007	2006	1238	263	1988	7532	40	2.6
16-AG-712	<0.003	<0.04	N/A	0	<5.6	<0.93	0	<29	0	<0.2
16-AG-713	<0.003	0.07	21	40	138	43	3300	6322	9	1.9
16-AG-714	<0.003	0.64	231	50	893	68	2229	6304	8	<0.2
16-AG-715	<0.003	2.07	617	1139	1155	78	1761	8013	21	<0.2
16-AG-716	<0.003	1.64	347	962	939	227	1718	8490	25	<0.2
16-AG-717	0.005	0.86	92	463	309	36	1344	9132	24	9.0
16-AG-718	<0.003	1.45	183	248	668	120	850	10761	16	1.0
16-AG-719	<0.003	1.33	488	217	1076	65	318	4379	27	2.0
16-AG-720	<0.003	0.46	21	11	301	52	46	4631	30	1.9
16-AG-721	<0.003	1.36	262	432	702	173	585	8961	9	1.2
16-AG-722	<0.003	1.09	214	28	494	31	970	6539	39	2.6
16-AG-723	<0.003	1.05	143	282	637	33	595	7548	5	1.4
16-AG-725	<0.003	0.04	N/A	49	56	38	13004	4330	5	1.0
16-AG-726	<0.003	1.01	148	557	579	60	714	7760	6	2.0
16-AG-727	<0.003	1.62	387	537	728	117	469	6126	11	4.9
16-AG-728	<0.003	0.99	148	317	672	67	506	8025	8	1.8
16-AG-729	<0.003	4.90	N/A	13	7	94	60	2078	0	7.3
16-AG-730	<0.03	1.52	499	382	952	26	1842	7018	19	1.1
16-AG-731	<0.03	1.60	512	371	948	28	1859	6936	20	1.2
16-AG-732	<0.003	1.50	261	166	855	14	363	9072	14	0.3
16-AG-733	<0.003	1.27	126	1144	399	664	7060	10571	11	9.2
16-AG-734	0.009	<0.04	9	48	7	3	164	10408	4	2.0
16-AG-735	<0.003	0.31	33	49	311	41	8438	5219	33	4.6

Sample	NO_3	NH_4	I	Ba	B	Fe	Sr	Si	Li	Mn
	mg N/L	mg N/L	µg/L	µg/L	µg/L	µg/L	µg/L	µg/L	µg/L	µg/L
16-AG-736	<0.003	0.81	166	103	493	26	135	3484	21	2.4
16-AG-737	<0.03	1.73	643	8	1378	2012	5008	7964	70	21.8
16-AG-738	<0.3	20.80	10655	18860	1896	3230	29299	3695	1025	299.5
16-AG-740	<0.03	2.77	1021	487	1288	22	3641	7722	48	1.1
16-AG-741	<0.003	0.60	15	45	303	594	17345	6060	32	19.8
16-AG-742	<0.003	1.41	65	417	395	89	824	14861	15	7.2
16-AG-744	<0.003	1.49	8	23	36	2662	130	3662	1	335.3
16-AG-745	<0.003	2.04	521	292	1526	175	448	5400	54	7.6
16-AG-746	<0.03	1.71	433	1859	1163	278	729	4991	44	5.4
16-AG-747	<0.003	0.98	244	86	546	163	2134	5395	25	13.0
16-AG-748	<0.03	0.74	916	11	638	360	17455	3924	169	105.9
16-AG-749	<0.3	19.90	10966	18132	1891	3159	28268	3618	917	298.2
16-AG-750	<0.003	1.69	397	387	838	119	1049	8298	10	3.3
16-AG-751	<0.003	0.09	25	366	41	1831	1793	8777	7	111.1
16-AG-752	<0.003	2.62	728	392	1095	99	520	5297	40	9.2
16-AG-753	0.003	0.55	54	125	546	5	630	6421	29	1.7
16-AG-754	<0.03	2.81	1014	135	1352	1101	1753	5617	21	13.8
16-AG-755	<0.03	5.34	1945	4936	1551	936	4641	9008	59	24.6
16-AG-756	<0.003	0.78	379	226	1202	226	367	6625	25	62.2
16-AG-757	<0.03	3.08	922	3401	1013	213	2585	5485	71	10.1
16-AG-758	<0.003	0.52	143	528	477	38	531	3910	20	5.4
16-AG-759	<0.003	<0.04	N/A	40	1928	516	575	3811	48	37198.2
16-AG-760	<0.003	1.74	N/A	14	7	95	60	2122	0	8.1
16-AG-761	0.147	2.02	478	863	1103	171	1772	5051	11	12.9
16-AG-792	<0.003	0.46	156	208	784	20	306	3712	46	5.5
16-AG-793	0.022	0.32	35	264	147	427	14924	7400	13	27.7
16-AG-794	<0.03	7.99	2172	4881	1728	183	2898	6014	66	13.8
16-AG-795	<0.003	0.66	175	167	753	18	1198	5869	11	2.8
16-AG-796	<0.003	0.72	108	527	450	2	689	6016	23	5.3

“<” Symbolizes parameter below detection limit

“N/A” Symbolizes no data available

Appendix F: Isotopic Dataset

Sample	^{3}H	$\delta^{18}O$	$\delta^{2}H$	$^{129}I/^{127}I$	$^{129}I/^{127}I$ Error	$^{129}I/^{127}I$ Corrected Ratio
	TU	‰VSMOW	‰VSMOW	Ratio x 10^{-14}	SD	Ratio x 10^{-14}
16-AG-513	4.8	-11.49	-73.7	13.8	0.6	208.5
16-AG-514	<0.8	-9.29	-62.7	6.1	0.3	17.0
16-AG-515	<0.8	-10.76	-71.2	3.5	0.4	16.2
16-AG-516	<0.8	-10.00	-67.3	9.4	0.4	22.7
16-AG-700	1	-11.29	-71.3	0.7	0.2	15.7
16-AG-701	0.8	-12.00	-76.7	0.5	0.1	16.0
16-AG-702	<0.8	-11.61	-72.4	6.6	0.4	19.9
16-AG-703	**<0.8**	**-10.61**	**-68.6**	**20.5**	**1.0**	**20.5**
16-AG-704	7.8	-11.80	-75.3	50.2	1.3	12147.2
16-AG-705	<0.8	-10.49	-68.5	8.0	0.4	26.3
16-AG-706	5.6	-12.22	-77.2	3.6	0.3	853.1
16-AG-707	<0.8	-11.16	-70.2	1.6	0.3	38.9
16-AG-708	<0.8	-12.23	-78.0	N/A	N/A	N/A
16-AG-709	13	-11.82	-74.2	78.9	1.8	6897.5
16-AG-710	14.2	-11.85	-74.2	75.5	1.6	7363.1
16-AG-711	<0.8	-11.64	-74.6	1.3	0.2	5.8
16-AG-712	N/A	-9.44	-68.5	0.5	0.1	N/A
16-AG-713	<0.8	-12.86	-81.9	0.6	0.1	68.2
16-AG-714	<0.8	-11.69	-73.7	1.1	0.2	18.2
16-AG-715	50.1	-11.48	-72.4	2.0	0.2	14.7
16-AG-716	<0.8	-11.37	-71.8	1.1	0.2	11.3
16-AG-717	<0.8	-11.13	-70.1	5.3	0.4	260.0
16-AG-718	<0.8	-11.52	-73.2	1.1	0.2	22.0
16-AG-719	<0.8	-11.59	-73.3	17.4	0.6	176.0
16-AG-720	<0.8	-12.58	-80.4	0.7	0.1	103.0
16-AG-721	<0.8	-11.26	-70.9	0.9	0.2	17.9
16-AG-722	1.8	-12.68	-81.8	0.8	0.1	18.9
16-AG-723	<0.8	-11.08	-69.8	0.9	0.2	34.0
16-AG-725	**2.4**	**-12.50**	**-77.9**	**19.2**	**0.9**	**19.2**
16-AG-726	<0.8	-11.38	-72.1	0.7	0.2	20.0
16-AG-727	<0.8	-11.30	-72.1	0.6	0.1	5.7
16-AG-728	<0.8	-11.72	-74.4	7.7	0.5	460.7
16-AG-729	16.5	-11.62	-72.4	6.6	0.3	20.9
16-AG-730	<0.8	-11.57	-73.8	1.2	0.2	17.3
16-AG-731	<0.8	-11.57	-73.8	0.8	0.2	8.2
16-AG-732	<0.8	-10.86	-69.2	0.7	0.2	12.2
16-AG-733	3.5	-12.06	-77.0	104.1	2.1	8125.6
16-AG-734	10.5	-12.39	-78.6	108.0	2.1	116204.5

Sample	^{3}H	$\delta^{18}O$	$\delta^{2}H$	$^{129}I/^{127}I$	$^{129}I/^{127}I$ Error	$^{129}I/^{127}I$ Corrected Ratio
	TU	‰VSMOW	‰VSMOW	Ratio x 10^{-14}	SD	Ratio x 10^{-14}
16-AG-735	7.8	-11.46	-73.3	92.8	1.8	26620.3
16-AG-736	<0.8	-11.73	-74.2	0.6	0.2	12.0
16-AG-737	<0.8	-10.85	-68.9	2.5	0.3	34.4
16-AG-738	**<0.8**	**-9.20**	**-62.0**	**19.6**	**0.9**	**19.6**
16-AG-740	1.3	-10.56	-66.9	11.2	0.5	114.6
16-AG-741	2.9	-12.41	-79.4	N/A	N/A	N/A
16-AG-742	<0.8	-11.22	-71.6	2.8	0.4	338.0
16-AG-744	15.3	-8.11	-61.3	N/A	N/A	N/A
16-AG-745	<0.8	-11.22	-71.8	0.9	0.2	8.9
16-AG-746	<0.8	-11.41	-72.7	1.0	0.2	14.0
16-AG-747	7.6	-11.14	-70.6	24.3	0.9	901.8
16-AG-748	<0.8	-12.75	-83.4	2.1	0.2	19.2
16-AG-749	**N/A**	**-8.38**	**-56.7**	**11.1**	**0.5**	**19.9**
16-AG-750	<0.8	-11.36	-71.3	1.6	0.2	29.7
16-AG-751	5.8	-12.48	-79.3	140.0	2.6	48867.3
16-AG-752	N/A	-12.13	-77.7	1.6	0.2	16.4
16-AG-753	2.6	-11.97	-76.2	1.0	0.2	105.4
16-AG-754	<0.8	-11.30	-71.0	2.7	0.2	23.9
16-AG-755	1.1	-11.58	-75.1	100.0	1.9	599.3
16-AG-756	<0.8	-11.57	-72.6	5.6	0.3	129.8
16-AG-757	1.6	-11.19	-71.4	2.5	0.2	22.4
16-AG-758	2.9	-12.81	-81.5	9.5	0.5	595.6
16-AG-759	<0.8	-11.79	-72.7	N/A	N/A	N/A
16-AG-760	16	-11.70	-71.9	6.3	0.4	18.8
16-AG-761	0.9	-10.71	-67.5	3.2	0.4	60.3
16-AG-792	<0.8	-11.52	-73.9	2.2	0.3	111.4
16-AG-793	6.4	-12.55	-80.2	11.8	0.6	3174.6
16-AG-794	<0.8	-10.88	-70.6	2.3	0.3	9.5
16-AG-795	<0.8	-11.77	-74.8	0.5	0.1	5.9
16-AG-796	2.2	-12.36	-79.3	3.9	0.4	301.9

"<" Symbolizes parameter below detection limit

"N/A" Symbolizes no data available

"Corrected ratio" represents $^{129}I/^{127}I$ ratio corrected for carrier

Samples in bold were analyzed without the use of an I carrier

Appendix G: ^{14}C dataset

Sample	CH_4			DOC			DIC		
	pMC	Age (ka BP)	± age (yBP)	pMC	Age (ka BP)	± age (yBP)	pMC	Age (ka BP)	± age (yBP)
16-AG-514	16.8	14.3	50	12.0	17.0	459	16.1	14.7	67
16-AG-516	14.5	15.5	62	15.1	15.2	78	15.7	14.9	78
16-AG-701	4.8	24.4	106	57.9	4.4	121	35.1	8.4	41
16-AG-703	21.3	12.4	53	11.9	17.1	111	20.4	12.8	48
16-AG-716	21.6	12.3	51	13.2	16.3	47	18.1	13.7	47
16-AG-719	3.1	28.0	126	32.1	9.1	59	19.4	13.2	55
16-AG-720	1.1	36.2	215	33.5	8.8	77	20.4	12.8	77
16-AG-723	23.4	11.7	93	23.4	11.7	209	23.9	11.5	48
16-AG-726	26.5	10.7	175	14.2	15.7	344	29.8	9.7	43
16-AG-732	22.7	11.9	58	37.5	7.9	87	41.1	7.1	31
16-AG-736	3.3	27.5	128	37.7	7.8	81	19.0	13.3	44
16-AG-738	5.2	23.8	89	17.3	14.1	100	19.9	13.0	46
16-AG-745	8.0	20.3	70	13.4	16.2	50	17.7	13.9	61
16-AG-746	4.5	25.0	129	9.1	19.3	493	13.4	16.1	78
16-AG-748	1.6	33.3	1820	13.8	15.9	70	13.9	15.9	151
16-AG-749	6.5	22.0	94	17.3	14.1	98	19.8	13.0	66
16-AG-752	8.4	19.9	82	22.8	11.9	47	29.9	9.7	61
16-AG-754	20.2	12.9	68	12.8	16.5	54	18.9	13.4	127
16-AG-755	4.6	24.7	89	11.0	17.7	92	18.5	13.6	53
16-AG-794	5.2	23.8	94	20.6	12.7	59	19.2	13.3	61

"N/A" Symbolizes no data available

Appendix H: Compositional Ratios and Geochemical Facies

Sample	Geochemical Facies	Cl/Br	Cl/I	Br/I
16-AG-513	Na-HCO_3-Cl	293.1	2334.3	8.0
16-AG-514	Na-Cl	297.9	2118.8	7.1
16-AG-515	Na-Cl	299.1	1972.1	6.6
16-AG-516	Na-Cl	297.5	1603.2	5.4
16-AG-700	Na-HCO_3	137.7	134.5	1.0
16-AG-701	Na-HCO_3	103.3	999.8	9.7
16-AG-702	-	411.8	-	-
16-AG-703	Na-Cl	266.7	1116.1	4.2
16-AG-704	Na-HCO_3-Cl	224.0	2663.0	11.9
16-AG-705	Na-Cl	277.4	1537.7	5.5
16-AG-706	Na-HCO_3	286.0	1222.7	4.3
16-AG-707	Na-HCO_3	151.4	193.0	1.3
16-AG-708	Na-HCO_3-Cl	276.7	1942.8	7.0
16-AG-709	Na-Cl	4925.6	50268.9	10.2
16-AG-710	Na-Cl	5210.7	50630.5	9.7
16-AG-711	Na-HCO_3	240.1	2285.6	9.5
16-AG-712	-	2.0	-	-
16-AG-713	Ca-HCO_3	238.1	1380.4	5.8
16-AG-714	Na-HCO_3-Cl	265.4	1085.0	4.1
16-AG-715	Na-HCO_3-Cl	274.3	911.7	3.3
16-AG-716	Na-HCO_3-Cl	272.3	1386.7	5.1
16-AG-717	Na-HCO_3	291.6	1372.3	4.7
16-AG-718	Na-HCO_3	127.5	210.0	1.6
16-AG-719	Na-HCO_3-Cl	260.5	1095.9	4.2
16-AG-720	Na-HCO_3	142.3	501.1	3.5
16-AG-721	Na-HCO_3	165.7	200.3	1.2
16-AG-722	Na-HCO_3-Cl	265.6	1838.6	6.9
16-AG-723	Na-HCO_3	89.2	64.7	0.7
16-AG-725	-	-	-	-
16-AG-726	Na-HCO_3	80.3	53.0	0.7
16-AG-727	Na-HCO_3-Cl	285.2	1453.4	5.1
16-AG-728	Na-HCO_3	150.8	206.9	1.4
16-AG-729	-	-	-	-
16-AG-730	Na-Cl	269.0	1294.0	4.8
16-AG-731	Na-Cl	278.3	1260.7	4.5
16-AG-732	Na-HCO_3-Cl	240.4	518.0	2.2
16-AG-733	Na-HCO_3-Cl	274.7	1195.7	4.4
16-AG-734	Ca-HCO_3	644.3	2073.4	3.2
16-AG-735	Na-HCO_3-Cl	349.0	2494.9	7.1
16-AG-736	Na-HCO_3-Cl	233.5	761.1	3.3

Sample	Geochemical Facies	Cl/Br	Cl/I	Br/I
16-AG-737	Na-HCO_3-Cl	298.4	1555.0	5.2
16-AG-738	Na-Cl	185.3	1278.4	6.9
16-AG-740	Na-HCO_3-Cl	250.2	1238.9	5.0
16-AG-741	Ca-HCO_3	346.2	3037.4	8.8
16-AG-742	Na-HCO_3	130.7	132.7	1.0
16-AG-744	Ca-HCO_3	932.4	4682.6	5.0
16-AG-745	Na-HCO_3-Cl	276.2	1422.4	5.1
16-AG-746	Na-HCO_3-Cl	245.4	2692.5	11.0
16-AG-747	Na-HCO_3-Cl	302.5	2837.2	9.4
16-AG-748	Na-Cl	211.4	2726.3	12.9
16-AG-749	Na-Cl	230.6	1242.3	5.4
16-AG-750	Na-HCO_3-Cl	302.6	611.4	2.0
16-AG-751	Ca-HCO_3	1595.2	2476.1	1.6
16-AG-752	Na-HCO_3-Cl	272.6	969.2	3.6
16-AG-753	Na-HCO_3	280.4	1266.0	4.5
16-AG-754	Na-HCO_3-Cl	277.0	929.1	3.4
16-AG-755	Na-Cl	305.5	2525.3	8.3
16-AG-756	Na-HCO_3-Cl	285.2	908.7	3.2
16-AG-757	Na-Cl	245.1	3176.4	13.0
16-AG-758	Na-HCO_3-Cl	335.5	919.8	2.7
16-AG-759	-	563.3	-	-
16-AG-760	-	37.1	-	-
16-AG-761	Na-HCO_3-Cl	294.4	2381.9	8.1
16-AG-792	Na-HCO_3-Cl	108.3	1126.1	10.4
16-AG-793	Ca-HCO_3	-	526.4	-
16-AG-794	Na-Cl	281.3	1958.6	7.0
16-AG-795	Na-HCO_3-Cl	249.5	825.7	3.3
16-AG-796	Na-HCO_3-Cl	827.9	700.5	0.8